The Dissertation Committee for Juhoon Lee Certifies that this is the approved version of the following dissertation:

Syntheses of Calix[4]pyrrole Functionalized Extended Molecular Systems and Applications for Environmental Concerns

Committee:

Jonathan L. Sessler, Supervisor

Eric V. Anslyn

Hung-wen Liu

Simon M. Humphrey

Jennifer S. Brodbelt

Syntheses of Calix[4]pyrrole Functionalized Extended Molecular Systems and Applications for Environmental Concerns

by

Juhoon Lee

Dissertation

Presented to the Faculty of the Graduate School of

The University of Texas at Austin

in Partial Fulfillment

of the Requirements

for the Degree of

Doctor of Philosophy

The University of Texas at Austin

August 2017

Dedication

To my late father, Yang Han Lee

To my mother, Won Joong Yong

To my family

Acknowledgements

I would first like to thank my supervisor Professor Jonathan L. Sessler for having me in this group to pursue the Ph. D degree. His trust and encouragement led me to complete the program successfully.

I would also like to thank Prof. Cheal Kim of Seoul National University of Science and Technology. I cannot appreciate enough for his great support and guidance on my adventurous journey to the scientific field.

I would thank Prof. Simon M. Humphrey and Dr. Vincent M. Lynch for their collaborations and valuable advices about metal-organic frameworks and X-ray crystallography.

Special thanks would go to Prof. Sung Kuk Kim of Gyeongsang National University for the inspirations and all the chemistry advices he provided me.

I would also like to thank all group members, past and present, for their kindness and true friendship, especially: Aaron Lammer, Dr. Gregory Thiabaud, Dr. Huacheng Zhang, James Brewster, Dr. Gabriela Vargas-Zuniga, Dr. Byung Joon Lim, Dr. Min Hee Lee, Inhong Hwang, Ren-Tsung Wu, and Dr. Gonzalo Anguera.

I would also give particular thanks to Dr. Juhyeon Lee for her solicitude and motivational advices she bestowed upon me whenever I fall down.

And last but not least, my late father Yang Han Lee, my mother Won Joong Yong, my brother Ju Sang Lee, my sister in law Young Sun Lee, and my mentor Jung Hun Kim have my great thanks for their unconditional support and faith in me.

Syntheses of Calix[4]pyrrole Functionalized Extended Molecular Systems and Applications for Environmental Concerns

Juhoon Lee, Ph. D.

The University of Texas at Austin, 2017

Supervisor: Jonathan L. Sessler

Considerable efforts have been made to develop the supramolecular systems being capable of selectively binding and recognizing specific chemical species. Within this context, particular has been put towards nuclear waste remediation, environmental chemistry, and biology. Calix[4]pyrroles are non-conjugated tetrapyrrolic macrocycles capable of binding anions and neutral substrates via concerted and directional hydrogen bonding. Moreover, functionalization of the calix[4]pyrrole *meso* position allows the incorporation of additional binding sites for both cations and anions. Due to the ease of preparation and functionalization, elaborated calix[4]pyrroles have been employed as various anion and ion pair receptors as well as potential extractants for species present in high-level liquid waste (HLLW) and transporters for biological important ions in connection with therapeutic aims. These studies reported herein are primarily focused on the discovery in *meso*-substituted calix[4]pyrrole-functionalized extended molecular systems and applications for environmental concerns.

Chapter 1 provides a brief overview regarding the historical perspective and inherent properties of calix[4]pyrroles, as well as outlines recent contributions for capturing, extracting and sequestering chemical species with environmental concerns.

Chapter 2 describes the extraction of the sulfate anion via bipyrrole-strapped calix[4]pyrroles. Through these studies, we have discovered such cryptand-like receptors could extract the highly hydrophilic sulfate anion into an organic solvent from aqueous solutions when A336Cl was used as a coextractant. Chapter 3 depicts a novel *meso*-functionalized calix[4]pyrrole-based three dimensional networked molecular cage. Interestingly, upon treatment of fluoride, the resultant framework could be disassembled, which serves to release the inner molecules. Moreover, multiple lone pairs and hydrogen bonding donors provided by the calix[4]pyrrole building units allow for a highly selective adsorption for CO_2 over other gaseous guest, such as N_2, O_2, H_2 and CH_4. Chapter 4 describes two novel calix[4]pyrrole-based uranyl complex cages, **cage-1** and **-2**. The transformation from a tripodal cage (**cage-1**) to a tetrapodal system (**cage-2**) was achieved by a sunlight induced photochemical oxidation or via simple addition of hydrogen peroxide. Chapter 5 details the synthetic procedures and characterizations of all compounds used in these studies.

Table of Contents

List of Tables

List of Figures

List of Schemes

Chapter 1: Introduction

1.1 CALIX[4]PYRROLE

Calix[4]pyrroles (Figure 1.1) are non-aromatic tetrapyrrolic macrocyclic receptors capable of binding Lewis basic anions and neutral substrates in organic media through N-H hydrogen bonds. Baeyer first disclosed the synthesis of this nonplanar tetrapyrrole, originally referred to as pyrrole-acetone and subsequently as *meso*-octamethyl porphyrinogen. However, in his 1886 report, involving the condensation of pyrrole with acetone under acidic conditions, he claimed a 2 + 2, rather than 4 + 4 product was formed.[1a] Some 30 years later, the correct structure was proposed by Chelintzev.[1b] Since that time, despite significant interest in porphyrin and related congeners, so-called calix[4]pyrroles remained relatively unexplored.[1c-f] The inaugural report on calix[4]pyrrole by Sessler and coworkers in 1996,[2] served to focus attention on a propensity for anion binding. Since then, the anion recognition chemistry of calix[4]pyrroles has attracted considerable attention. Furthermore, due to its facile preparation synthesize, a variety of modified systems have been developed to modulate the selectivity and binding affinity for specific anions.[3]

Structural analysis via X-ray crystallography and computational energy minimization studies revealed that the parent form of calix[4]pyrrole is capable of interconverting between four possible conformations (1,3-alternate, 1,2-alternate, partial cone, and cone).

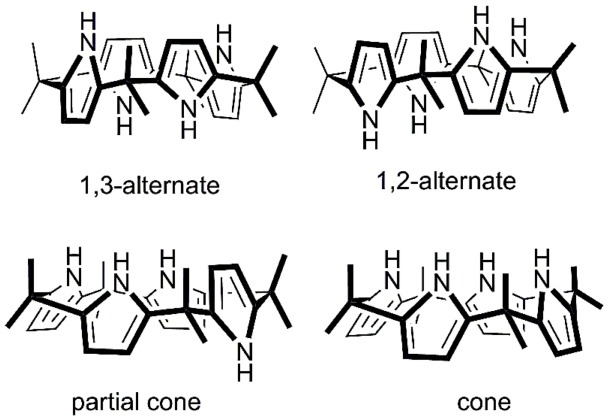

Figure 1.1 Representations of the four characteristic conformations of calix[4]pyrroles.

In the absence of coordinating anions, the parent form of calix[4]pyrrole adopts a 1,3-alternate conformation wherein four adjacent pyrroles are oriented in opposite directions to one another. However, in the presence of an anion (e.g., F^- and Cl^-), calix[4]pyrrole undergoes a conformational change and adopts a cone-like conformation wherein the four pyrrolic protons hydrogen bond to coordinating anion, as shown in Figure 1.2.[2] Moreover, this conversion affords a cup-like cavity allowing recognition of charge diffuse cations, such as cesium, small tetraalkylammonium, protonated triethylamine, imidazolium and pyridinium cations, through cation-π interactions.[4]

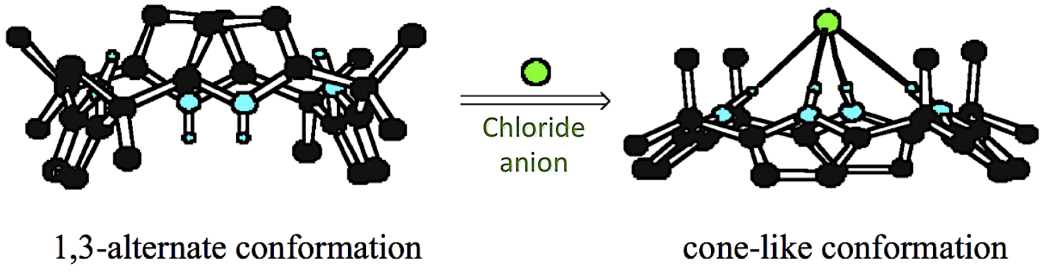

Figure 1.2 X-ray crystallographic analysis of calix[4]pyrrole in the absence (left) and presence of chloride anion (right).

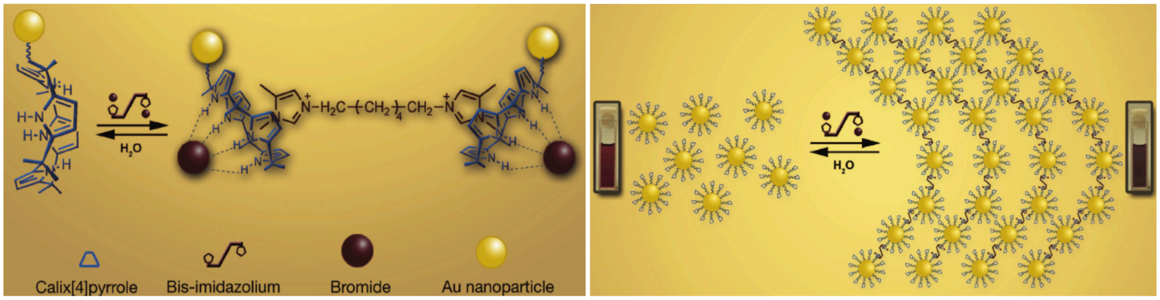

Figure 1.3 Schematic representations of calix[4]pyrrole-decorated gold nanoparticles incorporated with a bis(imidazolium) ditopic cation (left) and the illustration of the aggregation of the nanoparticles (right).

The anion binding-induced creation of a concave cation binding site and accommodation of the corresponding counter cation within the cavity was thought to give rise to an allosteric effect that enhances ion pair recognition.[4,5] Independent of any proposed synergy, it is now established that calix[4]pyrrole and its derivatives behave as ion-pair receptors.[4,5] Moreover, treatment with appropriately chosen ditopic cations can lead to the formation of extended structure systems (Figure 1.3).[4b]

Separate from its anion recognition capabilities, calix[4]pyrrole has also been explored for its ability to bind neutral substrates, including short-chain alcohols and simple monoamides.[6] As a general rule, the recognition of these substrates by synthetic receptors is particularly difficult because these molecules have few functionalized sites available for hydrogen bonding and they lack the large hydrocarbon surfaces necessary to participate in efficient hydrophobic or π-π stacking interactions. X-ray crystal analysis of a calix[4]pyrrole derivative complexed with DMF (*N,N'*-dimethylformamide), in particular, reveals each oxygen atom from the carbonyl group of DMF is hydrogen bonded to two adjacent pyrroles resulting in a 1,2-alternate conformation for the macrocycle. The unsaturated carbonyl portion of the amide lies above the plane of a pyrrole ring where it is presumably stabilized through π-π stacking interactions (Figure 1.4). This property has been taken advantage of to enforce a degree of for what is

normally flexible *meso*-functionalized calix[4]pyrrole. This was done by using a DMF abundant solvent system, as will be discussed in chapter 3 of this dissertation.

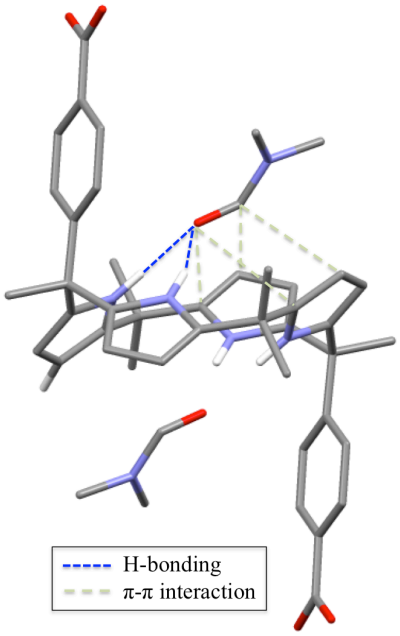

Figure 1.4 X-ray structure of the *N,N'*-dimethylformamide complex of *meso*-substituted calix[4]pyrrole dibenzoic acid.

Over the last two decades, considerable efforts have been devoted to developing efficient anion and ion pair receptors. Strategies pursued include the use of *meso*-substitution, *β*-functionalization, as well core-modifications of calix[4]pyrroles.[7] Functionalization of the calix[4]pyrrole *meso* position, in particular, allows the incorporation of additional binding sites for both cations and anions. In this dissertation, syntheses of *meso*-functionalized calix[4]pyrrole derivatives and applications for environmental concerns, including sulfate extraction, carbon dioxide adsorption, and uranyl sequestration will be discussed.

1.2 SULFATE ANION RECEPTORS

The selective recognition and extraction of sulfate (SO_4^{2-}) is of importance in terms of disposing of millions of gallons of sulfate-containing high-level liquid waste (HLLW). [8] The plans for disposal of this waste currently focus on pretreatment and vitrification prior to long-term storage. A borosilicate glass matrix is generally viewed as suitable for vitrification of HLLW. One of the limitations of this glass matrix is its limited solubility with respect to certain specific waste constituents. For instance, vitrification of sulfate-containing HLLW using this matrix is rendered challenging task since the solubility of sodium sulfate is low. At higher sulfate concentration, a separate phase of alkali sulfate is formed. Its presence in glass is not desirable as this phase has high solubility in water, which can lead to leaching of radioactive containments.[9] Furthermore, the presence of sulfate can facilitate erosion of the glass smelter, the constituent electrodes, and the superstructure components. This not only inhibits performance, but creates safety hazards, such as the explosive release of steam.[10] Unfortunately, the sulfate anion has a high hydration energy (-1080 kJ/mole). This makes its recognition and extraction from aqueous media particularly difficult.

In recent years, progress has been made in sulfate and hydrogen sulfate anion recognition. Moran and coworkers reported the use of a tris-urea receptor to recognize SO_4^{2-} in 1995.[11] Since then, similar tren-based tris-urea receptors have been extensively developed. In 2011, Wu *et al*. reported a tren-based tripodal hexaurea receptor **1.1** capable of encapsulating the sulfate anion in a complementary cavity. With this receptor, extraction of sulfate ions from an aqueous solution into a chloroform organic phase in a recyclable manner was accomplished.[12]

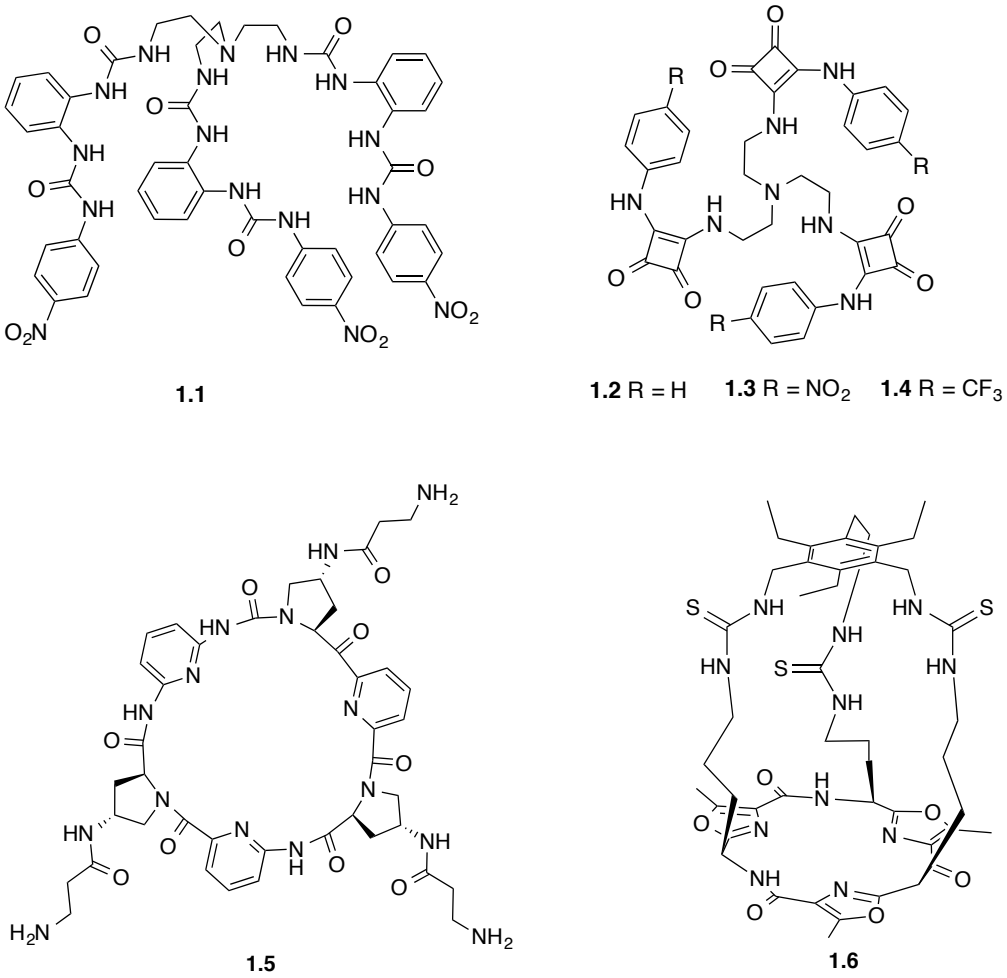

Figure 1.5 Various sulfate anion receptors based on multiple hydrogen bonding donors.

Another example of tren-based sulfate ion receptor was reported by Wang and co-workers in 2013.[13] They prepared squaramide-based tripodal receptors **1.2**-**1.4** and demonstrated that receptor **1.2** forms a dimeric complex with SO_4^{2-} in the solid state and a 1:1 complex in solvent solution. Jiang and coworkers further studied such receptors as carrier-based ion-selective electrodes (ISEs).[14] Their research suggested that the tripodal ionophore **1.3** incorporated into membranes contains tridodecylmethylammonium chloride (TDMACl) give rise to a Nernstian response toward sulfate with high selectivity over $H_2PO_4^-$, Cl^-, Br^-, NO_3^-, SCN^-, I^- and ClO_4^-. They were able to achieve the analysis of sulfate in the cellular lysates and drinking water. Cyclopeptide scaffolds have also been

exploited for the selective recognition of sulfate anions. In 2013, Kubik et al. reported a cyclic hexapeptide **1.5** with L-proline and 6-aminopicolinic acid subunits.[15] They demonstrated the high affinity and selectivity of **1.5** for sulfate anions in aqueous phosphate buffer solution. More recently, the groups of Gale and Jolliffe synthesized the tris-thiourea cyclopeptide receptor **1.6**, which is capable of efficiently and selectively transporting sulfate anions across a lipid bilayer.[16]

One approach to sulfate separation from aqueous solutions is based on crystallization. In 2016, Custelcean *et al*. reported the selective crystallization of sulfate using a simple insoluble imine-linked bis-guanidinium ligand **1.7**.[17] They also reported that the capture and release of sulfate can be achieved by neutralization with NaOH, with concomitant recovery of the ligand.

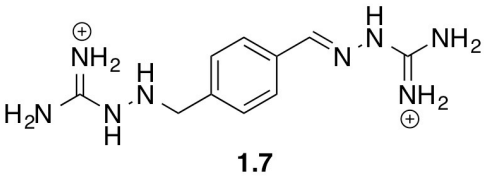

1.7

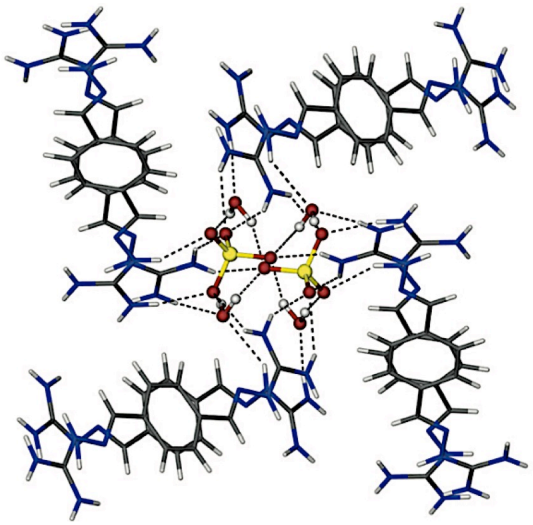

Figure 1.6 (Left) Structure of **1.7** and (Right) X-ray crystal structure of sulfate-water clusters surrounding by ligand **1.7**. Reprinted with permission from ref.[17] Copyright (2016) John Wiley and Sons.

Taking a more coordination chemistry approach, a recent report by Mezei and co-workers describes copper hydroxide pyrazolate complexes of formula [anion•Cu^{II}(μ-OH)(μ-pz)$_n$], also known as *nanojars*, can extract sulfate anion from water into organic solvents under neutral or alkaline conditions.[18] These researchers also emphasized that pH-dependent reversible assembly/disassembly of their nanojars allows the extraction and recycling of the sulfate anion.

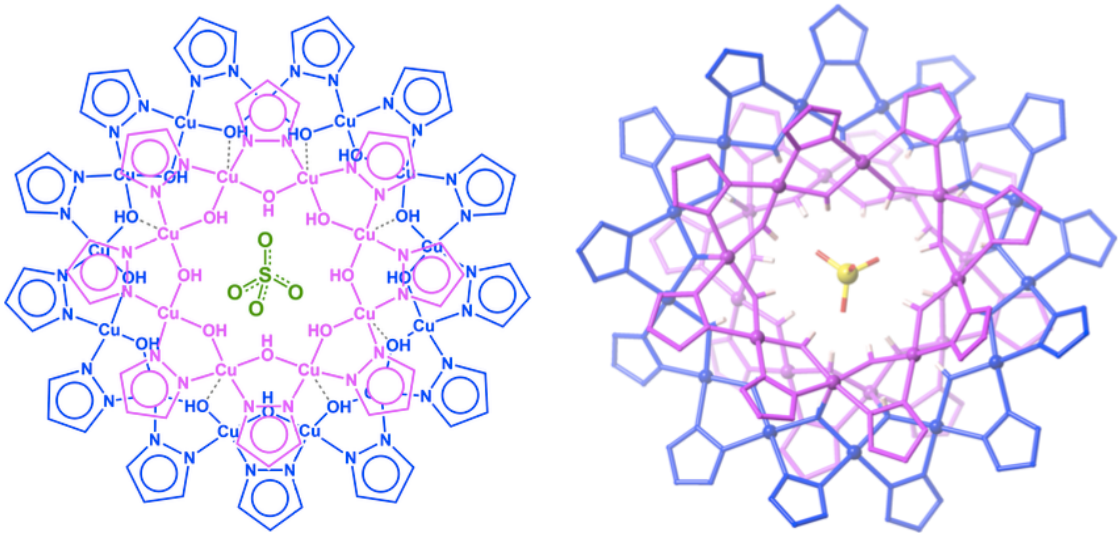

Figure 1.7 (Left) Schematic representation and (Right) the crystal sturucture of the Cu_{29} nanojar $[SO_4•\{Cu(\mu\text{-}OH)(\mu\text{-}pz)\}_{8+13+8}]^{2-}$. Reprinted with permission from ref.[18] Copyright (2016) American Chemical Society.

In addition to these examples, there has been increasing interest in utilizing positively charged moieties to detect sulfate anion by fluorescent spectroscopy.[19]

However, there still remains a need for a practical liquid-liquid extractant that can be used to remove the sulfate anion from aqueous waste streams. As part of the author's doctoral research, efforts were made to the design and synthesize receptors that bind the sulfate anion with sufficient affinity to overcome the high hydration energy associated with this particular hydrophilic tetrahedral oxoanion. This work is presented in chapter 2.

1.3 CARBON DIOXIDE CAPTURE

The rising level of atmospheric carbon dioxide stemming from anthropogenic emissions is one of the utmost environmental concerns confronting our society today. These emissions, which mostly result from the combustion of fossil fuel, are predicted to continuously increase in the future due to industrial development and economic growth.[20] The concentration of CO_2 in the atmosphere at the present time is greater than at any other time in modern history, exceeding 408 ppm in 2017.[21] The main existing CO_2 capture technologies are aqueous alkanolamine solutions[22] and solid porous adsorbent materials.

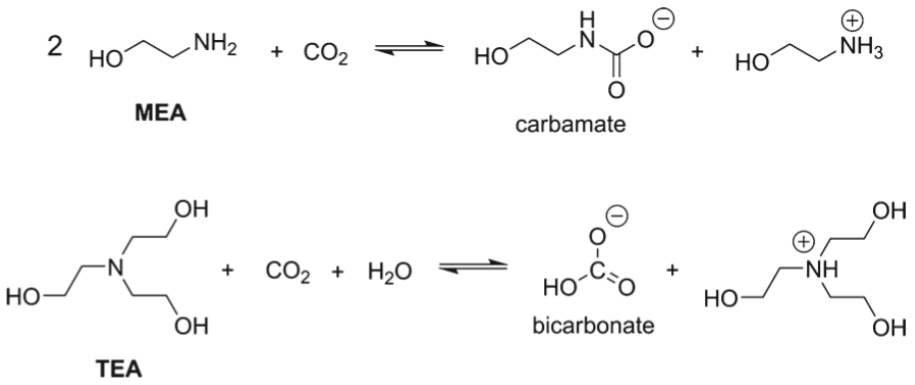

Scheme 1.1 Reaction of CO_2 with monoethanolamine (MEA) to give a carbamate product (upper), and the corresponding reaction with triethanolamine (TEA) resulting in a bicarbonate species (lower).

Monoethanolamine (MEA) is the most well-studied alkanolamine for CO_2 capture applications. Nucelophilic attack from the amine group to the carbon atom of CO_2 results in the formation of an anionic carbamate species. MEA is often used in mixtures with secondary or tertiary alkanolamines, such as diethnaolamine (DEA) and triethanolamine (TEA). Because of the bulky environment surrounding the nitrogen center present in tertiary amine, TEA leads to the formation of a bicarbonate species rather than a carbamate species. However, aqueous alkanolamine soultions have several limitations.

The lack of stability of the solutions towards heating constrains the regeneration temperatures available for full regeneration of the capture material. Degradation of the amine results in a decrease of the lifetime of the solutions. Moreover, the amine solutions are corrosive towards the vessels. Therefore, practical use requires the addition of corrosion inhibitors or reductions in the concentration of alkanolamine species used in the process.

Metal-organic frameworks (MOFs) are porous materials that are attractive for CO_2 capture.[23] This class of materials can overcome the shortcoming of more classic porous materials, such as zeolites that become readily saturated with water vapor, such as is present in the flue gas stream; consequently, the CO_2 adsorption capacity is reduced over time.[24] MOFs are made by linking inorganic nodes (single ions or clusters) and organic bridging groups to form infinite three dimensional structures with high porosity (Figure 1.8). The high surface areas, tunable pore size, and adaptable surface properties of MOFs have made them of particular interest in the context of gas capture.

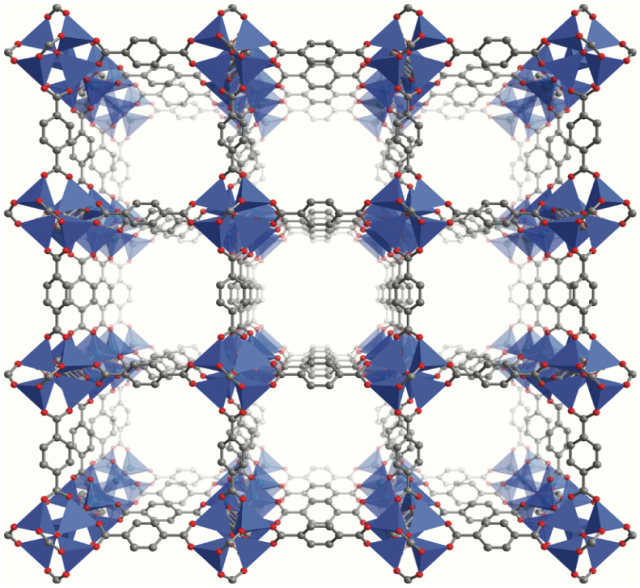

Figure 1.8 Crystal structure of $Zn_4O(BDC)_3$ (MOF-5). Reprinted with permission from ref.[23] Copyright (2012) American Chemical Society.

To date, efforts improve the CO_2 capture performance of MOFs have centered around the use of including utilizing N-rich ligands, amines to functionalize the MOF framework.[25,26] In 2014, Liu *et al*. reported an N-rich MOF with open Cu^{II} metal sites, Cu_3(TDPAH), based on 2,5,8-tris-(3,5-dicarboxylphenylamino)-s-heptazine ligand.[25a] Cu_3(TDPAH) exhibits an excellent CO_2 adsorption capacity of 5.2 mmol g^{-1} at 1 bar and 298 K. Grand canonical Monte Carlo (GCMC) calculations showed that the open metal sites, s-heptazine and NH groups within the framework are responsible for the high and selective CO_2 adsorption.

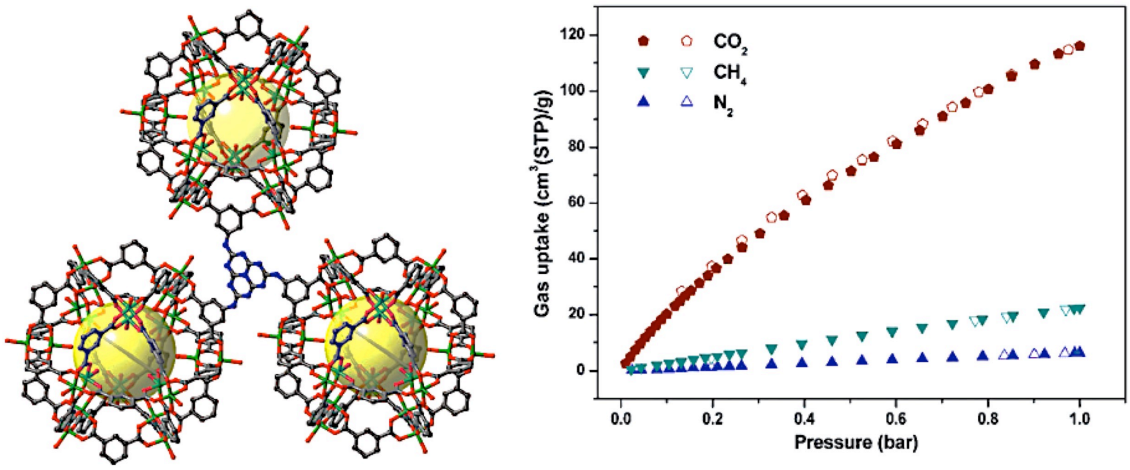

Figure 1.9 (left) Crystal structure of Cu_3(TDPAH) and (right) sorption isotherms at 298 K for CO_2, CH_4 and N_2 (adsorption: filled; desorption: open) Reprinted with permission from ref.[25a] Copyright (2014) Royal Society of Chemistry.

In 2016, Li et al. reported a triazole-containing MOF with exposed metal sites and N-rich triazole groups.[25c] It exhibits an excellent CO_2 adsorption capacity (up to 7.2 mmol g^{-1}) at 1 bar and 273 K. These favorable features were ascribed to the high affinity between the targeted CO_2 molecules and the uncoordinated N atoms/exposed metal sites in the frameworks. These researchers demonstrated catalytic activity for their system, in particular, high efficiency for the cycloadditon of CO_2 with small expoxides.

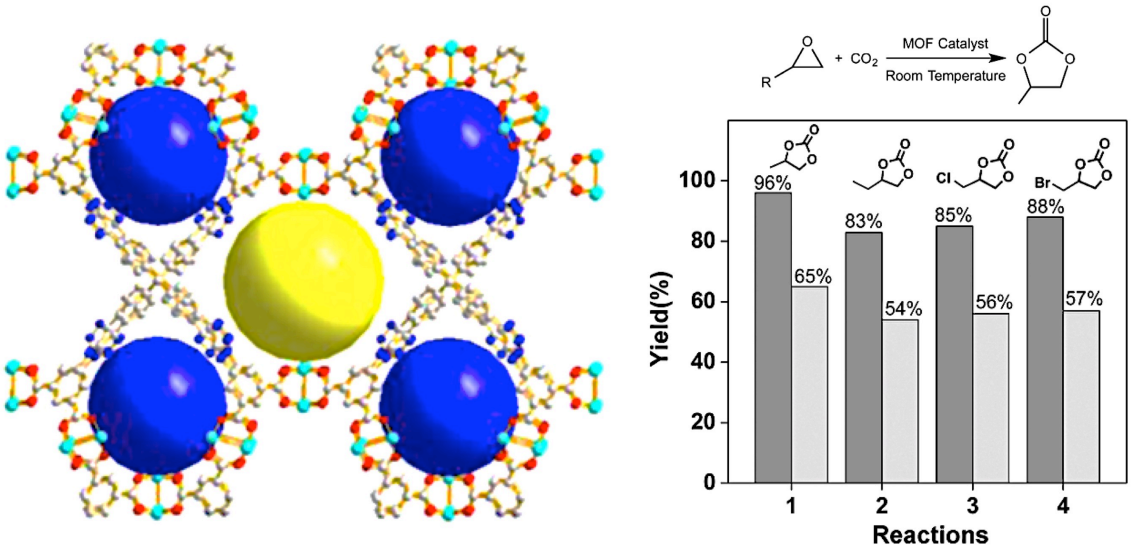

Figure 1.10 (left) 3D porous triazole-based framework and (right) yields of various cyclic carbonates prepared from the cycloaddtion of CO_2 with epoxides catalyzed by the triazole-based framework (black) and HKUST-1, a control benchmark MOF without triazole (gray). Reprinted with permission from ref.[25c] Copyright (2016) American Chemical Society.

Torrisi and co-workers investigated the intramolecular interactions between the CO_2 molecule and a range of functionalized aromatic molecules using density functional theory.[27] They found that lone pair donor atoms (N, O) and hydrogen bond donors can enhance the CO_2 binding energies of MOFs by up to 8 kJ mol^{-1} and 3-4 kJ mol^{-1}, respectively.

With such findings in mind, we proposed calix[4]pyrrole could act as a promising candidate for MOF preparation and the resulting systems could prove useful for CO_2 capture. The underlying thinking was calix[4]pyrrole would provide multiple pre-organized lone pairs and hydrogen bonding donor groups. As it turned out a first approach yielded a non-porous system that acted like a "ship in a breakable bottle". This work is discussed in chapter 3.

1.4 URANYL RECEPTORS

The continued use of uranium as an energy source has provided an incentive to develop methods to improve the separation of uranium from other actinides. It is also driving efforts to obtain uranium from nature (e.g., by extraction from seawater), as well as ways to detect and control the presence of uranium in the environment. The principal form of uranium on Earth is the uranyl dication (UO_2^{2+}), which is the most stable form found in oxidizing environments. Typical uranium ores and coal ash contain uranium at the ~1000 and 300 ppm levels, respectively.[28] The Dnieper River in Kiev is contaminated with uranium at the 11.5 ppm level and the concentration of uranium in of Bavarian drinking water has reached 10 ppb.[29] More than 99% of all global uranium resides in the Earth's oceans, where uranium is presented in the form of the uranyl cation (UO_2^{2+}) at a concentration of ~ 3 ppb.[30] The Fukushima disaster in 2011 has reemphasized the need for improved procedures for cleaning up nuclear waste and remmediating contaminated regions.[31]

While the uranyl cation has been extensively studied, it remains a challenging target, particularly in regard to detection and selective recognition in aqueous environments. The linear geometry and the short U-O bond lengths in the uranyl ion complicate receptor design efforts by limiting the approach of complementary anions at the equatorial positions.[32] Ligand design strategies for uranyl complexation are largely based on two traditional coordination chemistry concepts, namely the "hard and soft, acids and bases" (HSAB) principle[33] and matching the spatial array of donor group to the coordination sites on the metal ion.[34] Since the uranyl ion is classified as a hard ion, it has an enhanced affinity for oxygen atoms; accordingly, many uranyl ion receptors containing carboxylate, catechol, and hydroxypyridinone-amide moieties have been reported.[32,35]

One newer approach to sequestering the uranyl cation involves the creation of uranyl-based nanostructural cages. Burns and co-workers have reported such a system that consists of C_{60} fullerene-type, polyhedral that incorporate uranyl peroxide components with various sized anions, including nitrate, oxalate, and phosphate in a range of pH from 3.0 to 13.[36] In these nanoclusters, the peroxide anions serve to bridge two uranyl clusters to create overall pentagonal or hexagonal bipyramidal structures (Figure 1.11).

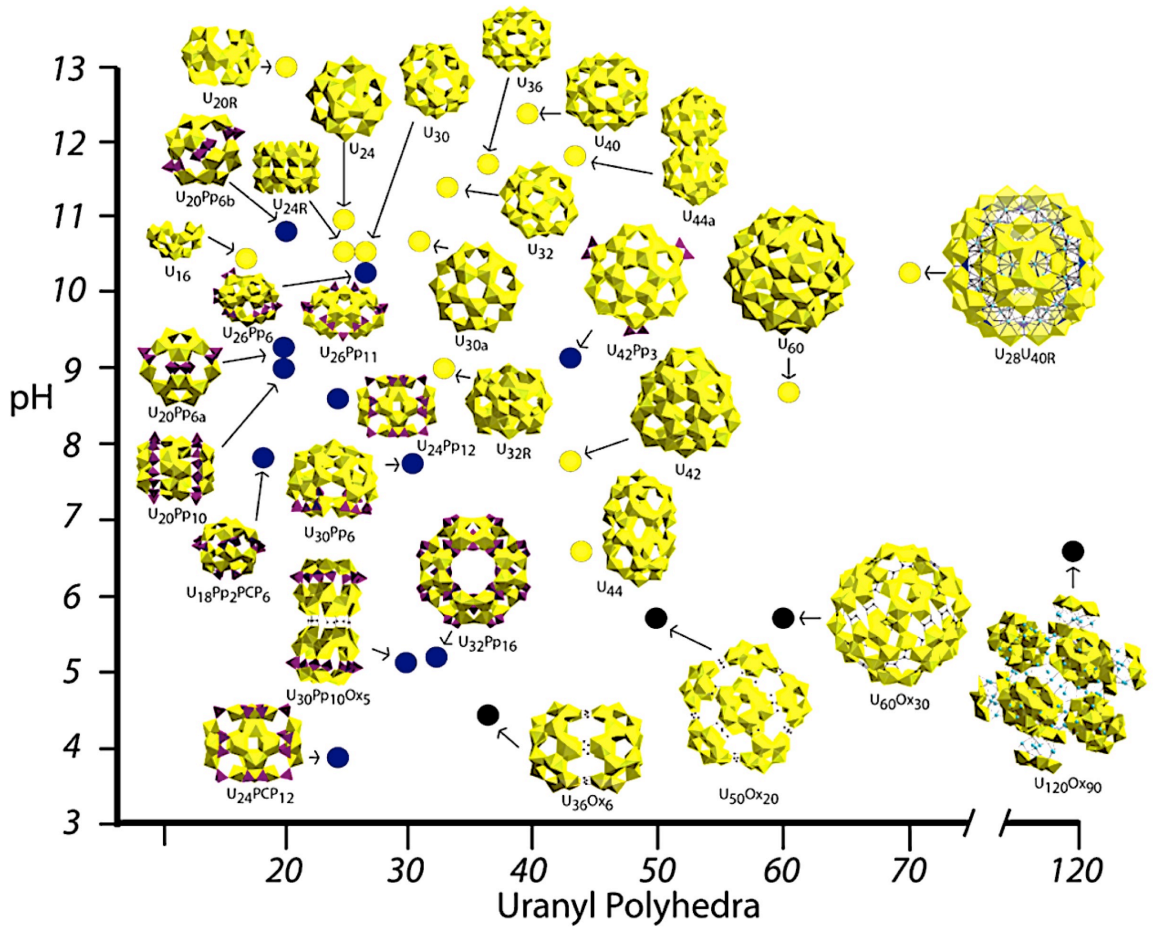

Figure 1.11 Various polyhedra and graphical representations of uranyl peroxide clusters and the relationship among the solution pH, composition, and number of uranyl ions; Pp = pyrophosphate, Ox = oxalate, Nt = nitrate, P = phosphate, and PCP = methylenediphosphonate. Reprinted with permission from ref.[36] Copyright (2013) American Chemical Society.

However, as a general rule, the lack of axial coordination (other than oxo ligands) favors formation of either one-dimensional chains or two-dimensional sheets. Formation of well-organized three-dimensional structures is particularly challenging when planar aromatic ligands are involved.[37] In 2012, giant regular polyhedral made up from calixarene carboxylates and the uranyl cation were described by Mendoza and co-workers.[38] These researchers showed the use of bowl-shaped calix-[4]- and -[5]-arenes carboxylic acids in conjunction with a uranyl cation source promotes self-assembly into hexameric cages and icosahedral structures, respectively, as shown in Figure 1.12.

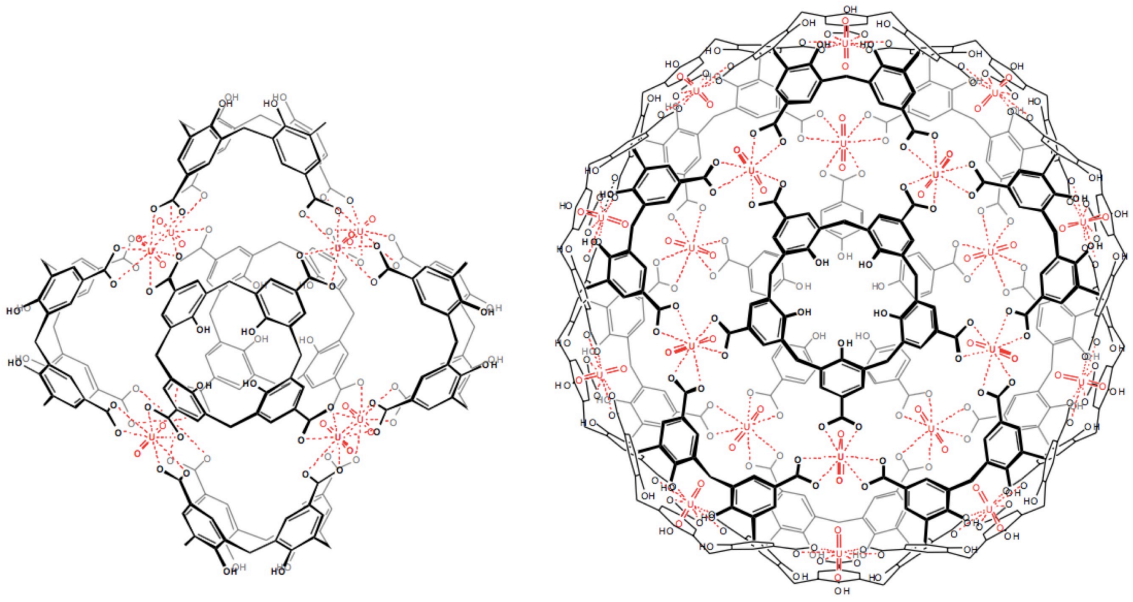

Figure 1.12 Chemical structures of (Left) hexameric cage from six calix[4]arene tetracarboxylates and eight uranyl cations and (Right) icosahedral cage from 12 calix[5]arene pentacarboxylate and 20 uranyl cations. Reprinted with permission from ref.[38] Copyright (2012) Nature Publishing Group.

In a more recent report, Thuery and Harrowfield showed racemic or enantiopure (1*R*, 2*R*) forms of *trans*-1,2-cyclohexanedicarboxylic acid (H_2chdc and *R*-H_2chdc, respectively) could be used to form pseudotetrahedral cluster cages.[39] The clusters in

question were obtained under solvohydrothermal conditions from the corresponding diacids in the presence of uranyl nitrate and guanidinium nitrate in a ratio of 4 : 3 (uranyl : diacid). These anionic clusters can incorporate alkali or alkaline-earth metal cations, such as Na^+, K^+, Ba^{2+}, Rb^+, and Cs^+, to form either higher dimensionality assemblies or heterometallic cuboidal clusters depending on the conditions (Figure 1.13).

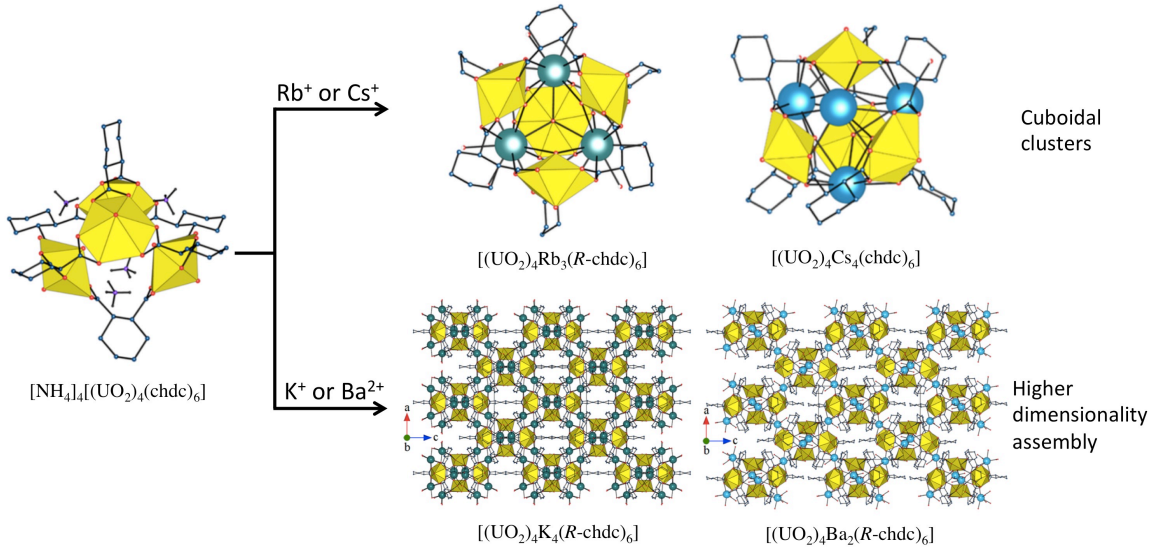

Figure 1.13 Crystal structures of pseudotetrahedral cluster cage $[NH_4]_4[(UO_2)_4(chdc)_6]$ and corresponding clusters incorporated with alkali or alkaline-earth cations, those with larger ionic radii (Rb^+, Cs^+) and smaller radii (K^+, Ba^{2+}). Reprinted with permission from ref.[39] Copyright (2017) American Chemical Society.

In chapter 4, a new set of uranyl-based cage complexes constructed from dibenzoic acid functionlized *cis*-calix[4]pyrrole will be described.

1.5 REFERENCES

1) (a) Baeyer, A.; *Ber. Dtsch. Chem. Ges.* **1886**, *19*, 2184–2185. (b) Chelintzev, V. V.; Tronov, B. V. *J. Russ. Phys. Chem. Soc.* **1916**, *48*, 105, 127. (c) Floriani, C. *Pure Appl. Chem.* **1996**, *68*, 1. (d) Jubb, J.; Floriani, C.; Chiesi-Villa, A.; Rizzoli, C. *J. Am. Chem. Soc.* **1992**, *114*, 6571. (e) Piarulli, U.; Floriani, C.; Chiesi-Villa, A.; Rizzoli, C. *J. Chem. Soc. Chem. Commun.* **1994**, 895. (f) De Angelis, S.; Solari, E.; Floriani, C.; Chiesi-Villa, A.; Rizzoli, C. *J. Am. Chem. Soc.* **1994**, *116*, 5691.

2) Gale, P. A.; Sessler, J. L.; Kral, V.; Lynch, V. *J. Am. Chem. Soc.* **1996**, *118*, 5140-5141.

3) (a) Gale, P. A.; Sessler, J. L.; Kral, V. *Chem. Commun.* **1998**, 1-8. (b) Gale, P. A.; Anzenbacher, P.; Sessler, J. L. *Coord. Chem. Rev.* **2001**, *222*, 57-102. (c) Gale, P. A.; Lee, C. -H. *Top. Heterocycl. Chem.* **2010**, *24*, 39-73. (d) Lee, C. –H.; Miyaji, H.; Yoon, D. –W.; Sessler, J. L. *Chem. Commun.* **2008**, 24-34. (e) Kim, D. S.; Sessler, J. L. *Chem. Soc. Rev.* **2015**, *44*, 532-546. (f) Adriaenssens, L.; Ballester, P. *Chem. Soc. Rev.* **2013**, *42*, 3261-3277.

4) (a) Custelcean, R.; Delmau, L. H.; Moyer, B. A.; Sessler, J. L.; Cho, W. –S.; Gross, D.; Bates, G. W.; Brooks, S. J.; Light, M. E.; Gale, P. A. *Angew. Chem. Int. Ed.* **2005**, *44*, 2537-2542. (b) Aydogan, A.; Lee, G.; Lee, C. –H.; Sessler, J. L. *Chem. Eur. J.* **2015**, *21*, 2368-2376. (c) Sessler, J. L.; Gross, D. E.; Cho, W. –S.; Lynch, V. M.; Schmidtchen, F. P.; Bates, G. W.; Light, M. E.; Gale, P. A. *J. Am. Chem. Soc.* **2006**, *128*, 12281-12288.

5) Kim, S. K.; Sessler, J. L. *Chem. Soc. Rev.* **2010**, *39*, 3784-3809.

6) Allen, W. E.; Gale, P. A.; Brown, C. T.; Lynch, V. M.; Sessler, J. L. *J. Am. Chem. Soc.* **1996**, *118*, 12471-12472.

7) Saha, I.; Lee, J. T.; Lee, C.-H. *Eur. J. Org. Chem.* **2015**, 3859-3885.

8) Ravikumar, I.; Ghosh, P. *Chem. Soc. Rev.* **2012**, *41*, 3077-3098.

9) (a) Ojovan, M. I.; Lee, W. E. An Introduction to Nuclear Waste Immobilization; Elsevier: Amsterdam, Netherlands, 2005; Chapter 17. (b) Das, D.; Bharadwaj, S. R. Thoria-based nuclear fuels: thermophysical and thermodynamic properties, fabrication, reprocessing, and waste management; Springer: London, 2013; Chapter 8.

10) Moyer, B. A.; Custelcean, R.; Hay, B. O.; Sessler, J. L.; Bowman-James, K.; Day, V. W.; Kang, S. *Inorg. Chem.* **2013**, *52*, 3473-3490.

11) Raposo, C.; Almaraz, M.; Martin, M.; Weinrich, V.; Mussons, M. L.; Alcazar, V.; Caballero, M. C.; Moran, J. R. *Chem. Lett.* **1995**, 759-760.

12) Jia, C.; Wu, B.; Li, S.; Huang, X.; Zhao, Q.; Li, Q. S.; Yang, X. J. *Angew. Chem. Int. Ed.* **2011**, *50*, 486-490.

13) Jin, C.; Zhang, M.; Wu, L.; Guan, Y.; Pan, Y.; Jiang, J.; Lin, C.; Wang, L. *Chem. Commun.* **2013**, *49*, 2025.

14) Liu, Y.; Qin, Y.; Jiang, D. Analyst **2015**, *140*, 5317-5323.

15) Schaly, A.; Belda, R.; Garcia-Espana, E.; Kubik, S. *Org. Lett.* **2013**, *15*, 6238-6241.

16) Busschaert, N.; Karagiannidis, L. E.; Wenzel, M.; Haynes, C. J. E.; Wells, N. J.; Young, P. G.; Makuc, D.; Plavec, J.; Jolliffe, K. A.; Gale, P. A. *Chem. Sci.* **2014**, *5*, 1118–1127.

17) Custelcean, R.; Williams, N. J.; Seipp, C. A.; Ivanov, A. S.; Bryantsev, V. S. *Chem. Eur. J.* **2016**, *22*, 1997-2003.

18) Ahmed, B. M.; Hartman, C. K.; Mezei, G. *Inorg. Chem.* **2016**, *55*, 10666-10679.

19) (a) Zhou, H.; Zhao, Y.; Gao, G.; Li, S.; Lan, J.; You, J. *J. Am. Chem. Soc.* **2013**, *135*, 14908-14911. 9 (b) Song, N. R.; Moon, J. H.; Choi, J.; Jun, E. J.; Kim, Y.; Kim, S.; Lee, J. Y.; Yoon, J. *Chem. Sci.* **2013**, *4*, 1765-1771. (c) Saini, R.; Kumar, S. *RSC Adv.* **2013**, *3*, 21856-21862.

20) Pachauri, R. K.; Reisinger, A. *IPCC Fourth Assessment Report*, Intergovernmental Panel on Climate Change, 2007.

21) Earth System Research Laboratory: http://www.esrl.noaa.gov/gmd/ccgg/trends/, 2017

22) Rochelle, G. T. *Science* **2009**, *325*, 1652.

23) Sumida, K.; Rogow, D. L.; Mason, J. A.; McDonald, T. M.; Bloch, E. D.; Herm, Z. R.; Bae, T.; Long, J. R. *Chem. Rev.* **2012**, *112*, 724-781.

24) Li, G.; Xia, P.; Webley, P.; Zhang, J.; Singh, R. *Energy Procedia* **2009**, *1*, 1123.

25) (a) Liu, K.; Li, B.; Li, Y.; Li, X.; Yang, F.; Zeng, G.; Peng, Y.; Zhang, Z.; Li, G.; Shi, Z.; Feng, S.; Song, D. *Chem. Commun.* **2014**, *50*, 5031. (b) Liu, M. –M.; Bi, Y. –L.; Dang, Q.-Q.; Zhang, X.-M. *Dalton Trans.* **2015**, *44*, 19796. (c) Li, P. –Z.; Wang, X. –J.; Liu, J.; Lim, J. S.; Zou, R.; Zhao, Y. *J. Am. Chem. Soc.* **2016**, *138*, 2142-2145.

26) (a) Lin, Y.; Kong, C.; Chen, L. *RSC Adv.* **2016**, *6*, 32598-32614. (b) Yeon, J. S.; Lee, W. R.; Kim, N. W.; Jo, H.; Lee, H.; Song, J. H.; Lim, K. S.; Kang, D. W.; Seo, J. G.; Moon, D.; Wiers, B.; Hong, C. S. *J. Mater. Chem. A* **2015**, *3*, 19177-19185. (c) Martinez, F.; Sanz, R.; Orcajo, G.; Briones, D.; Yanguez, V. *Chem. Eng. Sci.* **2016**, *142*, 55.

27) Torrisi, A.; Mellot-Draznieks, C.; Bell, R. G. *J. Chem. Phys.* **2010**, *132*, 044705.

28) The Economist. *Novel Sources of Uranium: Rising from the Ashes*, April 8, 2010, http://www.economist.com/node/15865280?story_id=15865280, accessed September 10, 2010.

29) Balonov, M.; et al. *Radiological Conditions in the Dnieper River Basin*; Radiological Assessment Reports Series; International Atomic Energy Agency: Vienna, 2006.

30) Schwochau, K. *Top. Curr. Chem.* **1984**, *124*, 91.

31) Stockmann, T. J.; Ding, Z. *Anal. Chem.* **2011**, *83*, 7542-7549.

32) Sather, A. C.; Berryman, O. B.; Rebek, J. *J. Am. Chem. Soc.* **2010**, *132*, 13572-13574.

33) Pearson, R. G. *J. Am. Chem. Soc.* **1963**, *85*, 3533.

34) (a) Cram, D. J.; Lehn, J. M. *J. Am. Chem. Soc.* **1985**, *107*, 3657. (b) Hay, B. P.; Hancock, R. D. *Coord. Chem. Rev.* **2001**, *212*, 61.

35) (a) Szigethy, G.; Raymond, K. N. *J. Am. Chem. Soc.* **2011**, *133*, 7942-7956. (b) Watson, L. A.; Hay, B. P. *Inorg. Chem.* **2011**, *50*, 2599-2605. (c) Beer, S.; Berryman,

O. B.; Ajami, D.; Rebek, J. *Chem. Sci.* **2010**, *1*, 43-47. (d) Sather, A. C.; Berryman, O. B.; Rebek, J. *J. Am. Chem. Soc.* **2010**, *132*, 13572-13574.

36) Qiu, J.; Burns, P. C. *Chem. Rev.* **2013**, *113*, 1097−1120.

37) Wang, K.; Chen, J. *Acc. Chem. Res.* **2011**, *44*, 531-540.

38) Pasquale, S.; Sattin, S.; Escudero-Adan, E. C.; Martinez-Belmonte, M.; Mendoza, J. *Nat. Commun.* **2012**, *3*, 785.

39) Thuery, P.; Harrowfield, J. *Cryst. Growth Des.* **2017**, *17*, 2881-2892.

Chapter 2: Bipyrrole-Strapped Calix[4]pyrroles: Strong Anion Receptors That Extract the Sulfate Anion

2.1 INTRODUCTION

The selective recognition and extraction of sulfate (SO_4^{2-}) is a particular challenge because this anion has a very high hydration energy (–1080 kJ/mol) and is far down the Hofmeister series.[1,2] From an application point of view, the sulfate anion is a target of interest in connection with disposing of millions of gallons of sulfate-containing high-level liquid waste (HLLW) stored at the Hanford site, involving pretreatment and vitrification prior to long-term storage.[3,4] Sulfate interferes with vitrification, primarily due to the inability to immobilize it in borosilicate glass.[5,6] In addition, SO_4^{2-} decreases the durability of glass logs while increasing the mobility and leach rates of stored actinides.[5,7] Sulfate can engender other problems. For instance, it promotes corrosion of the glass smelter, the constituent electrodes, and the superstructure components. This not only reduces performance, but it can also create a safety hazard (e.g., the explosive release of steam).[4] One potential means of removing sulfate from tank waste is via liquid–liquid extraction (LLE) using anion or ion pair receptors.[4,8,9] In 2008, we demonstrated that β-fluorinated calix[4]pyrrole and calix[5]pyrrole are able to extract the sulfate anion from aqueous solution.[10] More recently, it was found that the use of a methyltrialkylammonium cation allows simple, unfunctionalized calix[4]pyrrole **2.1** to function as a sulfate anion extractant.[11] This success was rationalized in terms of ion pairing effects, specifically, the concurrent binding of the sulfate anion and the methyltrialkylammonium cation to the cone-conformation of the calix[4]pyrrole.[11] More recently, Wu and co-workers reported a tren-based tripodal hexaurea receptor capable of

§ Kim, S. K; Lee, J.; Willams, N. J.; Lynch, V. M.; Hay, B. P.; Moyer, B. A.; Sessler, J. L. Bipyrrole-Strapped Calix[4]pyrroles: Strong Anion Receptors That Extract the Sulfate Anion. *J. Am. Chem. Soc.* **2014**, *136*, 15709-15085. The author is a second author of the publication and was responsible for the synthesis of the precursors, ^{1}H NMR/UV-vis spectroscopic titration studies, and determination of the association constants.

extracting the sulfate anion from an aqueous solution to a chloroform organic phase in the presence of tetrabutylammonium chloride (TBACl).[9] In recent years, considerable efforts have also been devoted for sulfate and hydrogen sulfate recognition with a variety of strategies including multiple hydrogen bonding donors (cyclopeptide, urea, thiourea, and squramide) functionalization[12a-h], crystallization / metal complexation-based sequestration[12i-k], and positively charged moieties-based fluorescent detection.[12l-n]

However, there still remains a challenge for a practical LLE extractant due to the intrinsic difficulties associated with the design and synthesis of receptors that bind the sulfate anion with sufficient affinity to overcome the high hydration energy associated with this particular hydrophilic tetrahedral oxoanion. With such considerations in mind and as a test of the underlying hypothesis, we have now designed and synthesized the two calix[4]pyrrole-based anion receptors **2.2** and **2.3**. These two systems contain rigid or flexible bipyrrole units, respectively, that serve to span the top of what is an overall strapped calix[4]pyrrole core. Compared with the parent calix[4]pyrrole **2.1**,[13] receptors **2.2** and **2.3** possess two additional relatively acidic hydrogen-bonding donors within what are effectively well-defined three-dimensional structures.

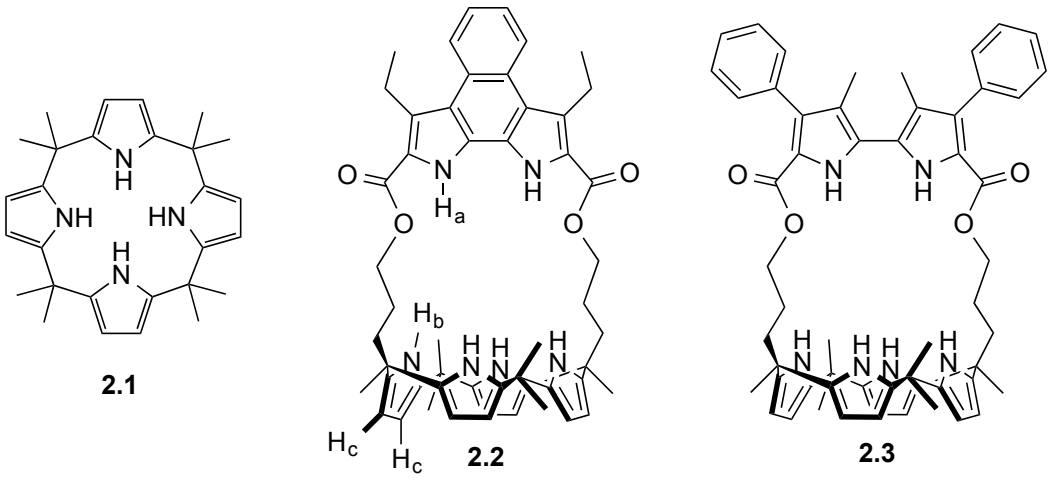

Figure 2.1 Chemical structures of compounds **2.1**, **2.2** and **2.3**.

As detailed below, receptors **2.2** and **2.3** display relatively high affinities for anions, including tetrahedral oxoanions. This increase in affinity is ascribed to the presence of the additional hydrogen bond donors provided by the bipyrrole units, as well as to anion encapsulation. Consistent with their increased anion affinities, the bipyrrole-strapped calix[4]pyrroles **2.2** and **2.3** were found to extract the sulfate anion (as the methyltrialkyl(C_{8-10})-ammonium ($A336^+$) salt) from aqueous solutions into organic media with considerably greater efficiency than the parent system **2.1**. Receptors **2.2** and **2.3**, but not **2.1**, were also found to solubilize into chloroform the otherwise insoluble sulfate salt, $(TMA)_2SO_4$ (tetramethylammonium sulfate).

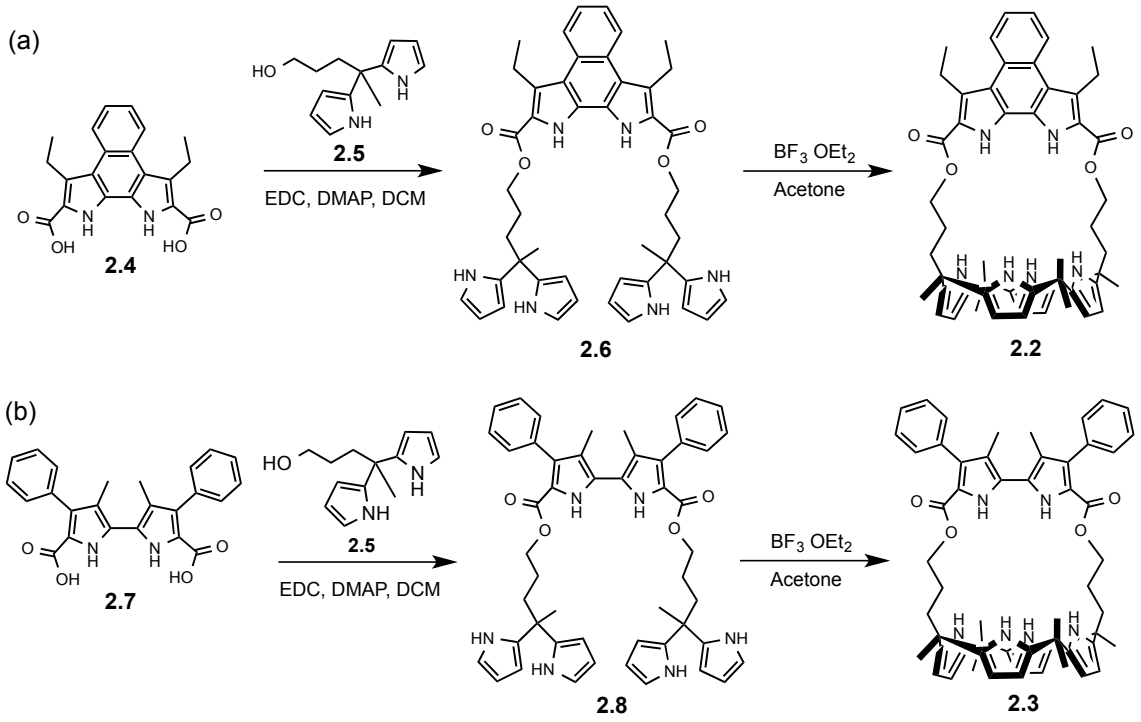

Scheme 2.1 Synthesis of (a) compound **2.2** and (b) compound **2.3**.

2.2 RESULT AND DISCUSSION

The synthesis of receptors **2.2** and **2.3** is summarized in Scheme 1. Briefly, the dicarboxyl functionalized naphthobipyrrole **2.4**[14] and bipyrrole **2.7**[15] were coupled with 5-(3-hydroxypropyl)-5-methyl dipyrromethane (**2.5**) in the presence of EDCI (1-ethyl-3-(3-(dimethylamino)propyl)carbodiimide) and DMAP (4-dimethylaminopyridine) in dichloromethane. This afforded the corresponding esters **2.6** and **2.8** in 52% and 49% yield, respectively. A subsequent condensation with acetone in the presence of $BF_3 \cdot OEt_2$ (~1.0 equiv) produced the desired compounds (**2.2** and **2.3**) in 17% and 18% yield, respectively.

Initial evidence that receptors **2.2** and **2.3** could bind the sulfate anion with significantly enhanced affinity relative to the unsubstituted calix[4]pyrrole (**2.1**) in solution came from ^{1}H NMR spectroscopic analyses carried out in CD_2Cl_2. As shown in Figures **2.2** and **2.3**, when exposed to the sulfate anion (added in excess as the tetrabutylammonium (TBA^+) salt), the NH protons of both the calix[4]pyrrole framework and bipyrrole units of the strap undergo a remarked downfield shift ($\Delta\delta_{Ha}$ = 1.36 and 1.49 ppm; $\Delta\delta_{Hb}$ = 2.00 and 1.43 ppm for **2.2** and **2.3**, respectively) while the peaks for the β-pyrrolic proton resonances shift to higher field. These changes in the chemical shifts are ascribed to hydrogen bonding between the pyrrolic NHs and the sulfate anion. When the naphthobipyrrole–strapped calix[4]pyrrole **2.2** was titrated with increasing quantities of $(TBA)_2SO_4$, two sets of distinguishable resonances for the NH proton signals of both pyrrole and bipyrrole units were seen in the ^{1}H NMR spectra recorded before a full molar equivalent of the sulfate anion had been added (Figure 2.2). The observed signals correspond to the free ligand and sulfate-complexed forms of receptor **2.2**, respectively.

The observation of two sets of peaks in the ^{1}H NMR spectra recorded before saturation is reached is consistent with the binding/release equilibrium between receptor **2.2** and the sulfate anion being slow on the NMR time scale. It is also consistent with the formation of a strong 1:1 complex between the sulfate anion and receptor **2.2**,

presumably reflecting the fact that all six NH protons of this receptor participate in hydrogen bonding with the bound sulfate anion.

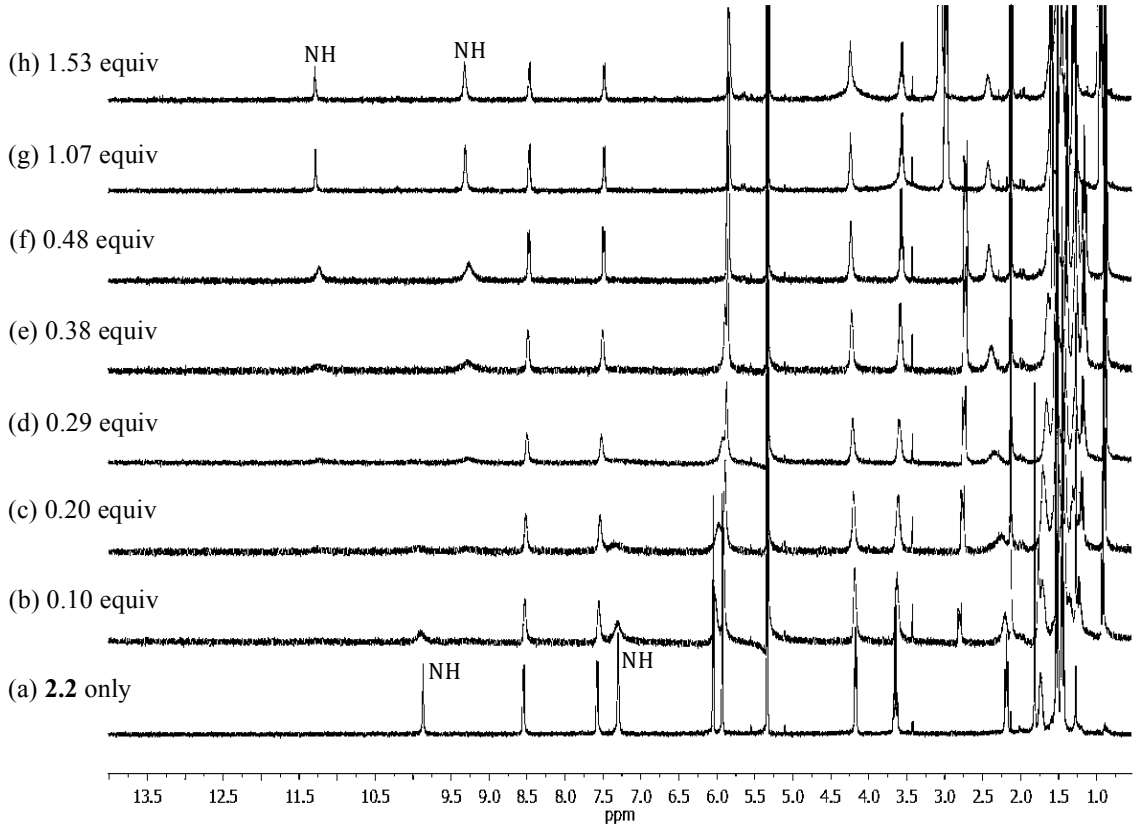

Figure 2.2 ^{1}H NMR spectra recorded during the titration of receptor **2.2** (3 mM) with tetrabutylammonium sulfate ($(TBA)_2SO_4$) in CD_2Cl_2.

In contrast to the above, in the case of receptor **2.3**, the NH proton signals were observed to shift to lower field as the relative and absolute concentration of the sulfate anion increased, with saturation being reached after the addition of 1 mol equiv of $(TBA)_2SO_4$ (Figure 2.3). These changes in the chemical shifts are consistent with the formation of a strong, 1:1 complex, albeit with a fast binding/release equilibrium. This

observation stands in sharp contrast to what was seen with calix[4]pyrrole **2.1**, which displays no appreciable chemical shift change in the presence of excess sulfate anion (Figure 2.4).

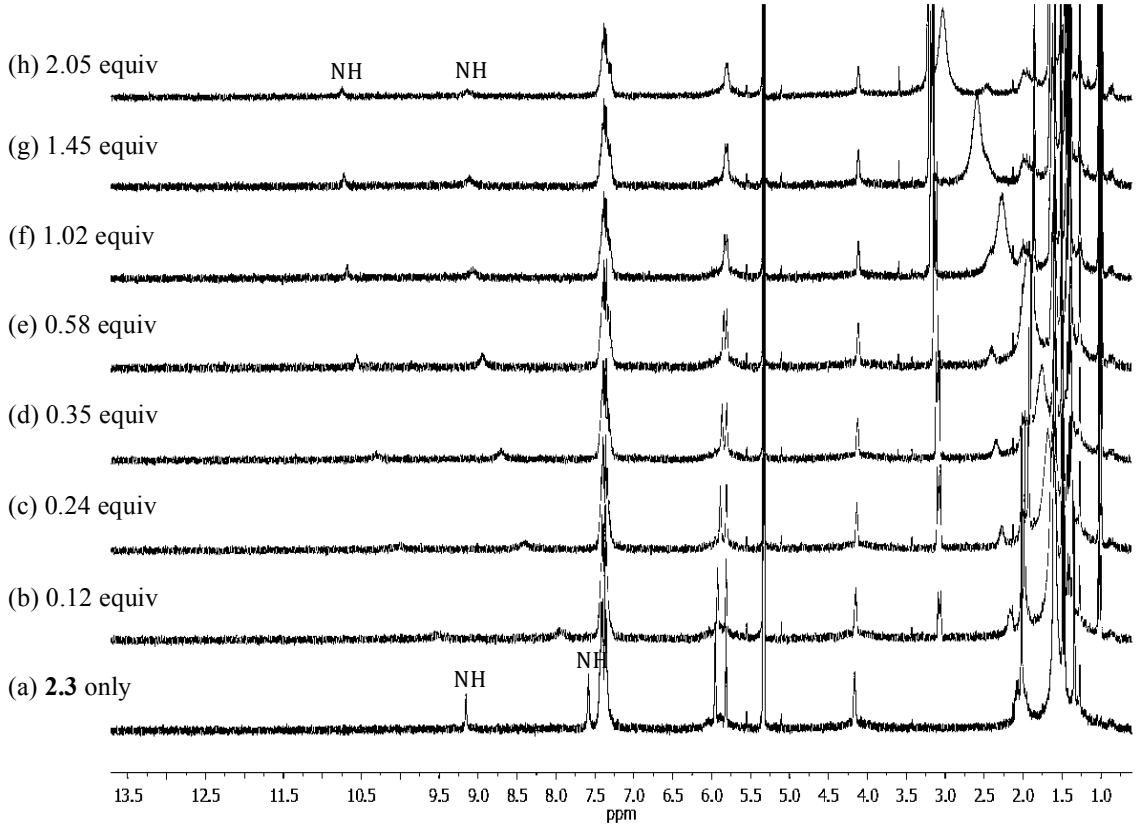

Figure 2.3 ^{1}H NMR spectra recorded during the titration of receptor **2.3** (3 mM) with tetrabutylammonium sulfate ($(TBA)_2SO_4$) in CD_2Cl_2.

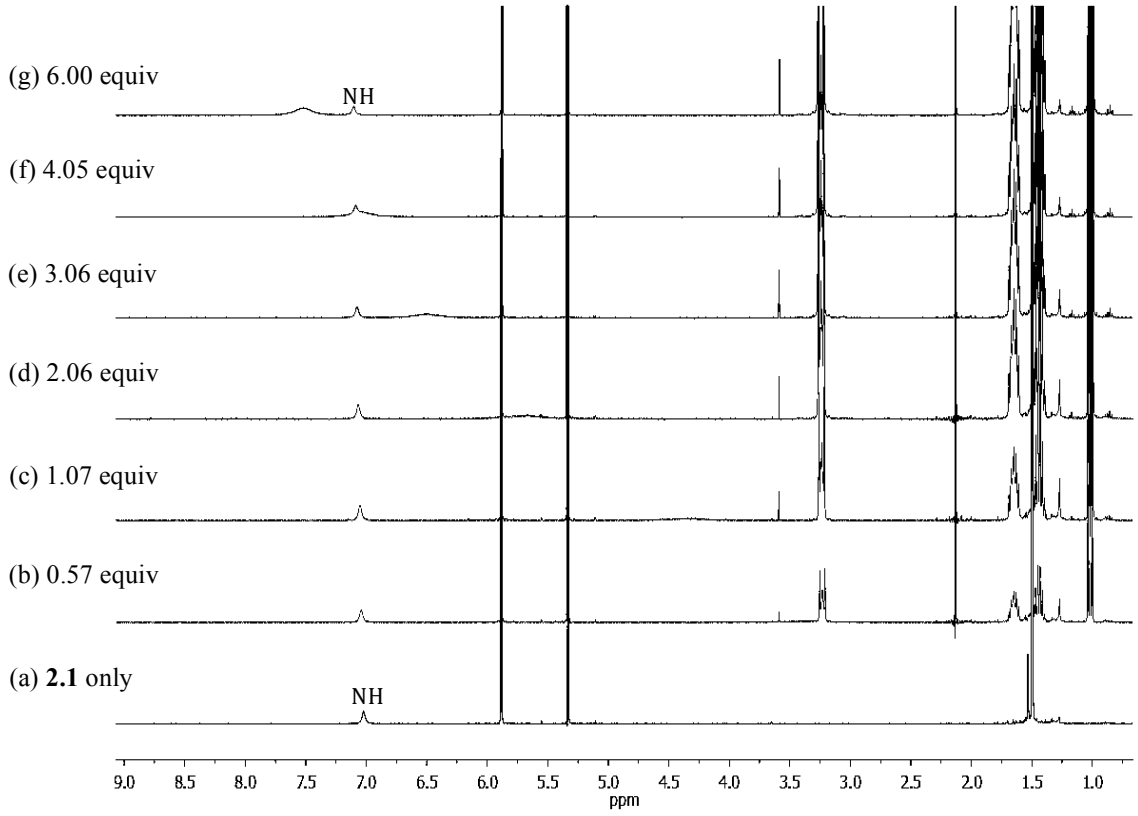

Figure 2.4 ^{1}H NMR spectra recorded during the titration of receptor **2.1** (3 mM) with tetrabutylammonium sulfate ($(TBA)_2SO_4$) in CD_2Cl_2.

On the basis of the above findings, we conclude that receptors **2.2** and **2.3** both bind the sulfate anion with high affinity. An indication of their relative binding affinities for sulfate was gleaned from molecular mechanics calculations carried out using the MMFF94 force field model. The intrinsic binding energy for each receptor (including calix[4]pyrrole **2.1**), defined as $E_{(\text{receptor-sulfate})} - E_{(\text{sulfate})} - E_{(\text{receptor})}$, was computed to be –59.5 kcal/mol, –104.5 kcal/mol, and –99.9 kcal/mol for receptors **2.1**, **2.2**, and **2.3**, respectively. Optimized structures are shown in Figure 2.5. It is noteworthy that the interaction between the bipyrrolic NH protons and the bound sulfate are different in the case of receptors **2.2** and **2.3**. Specifically, in the case of **2.2** a single sulfate oxygen atom

is bound by the bipyrrole subunit, whereas in the case of **2.3** the bipyrrole NH protons interact with two different sulfate oxygen atoms.

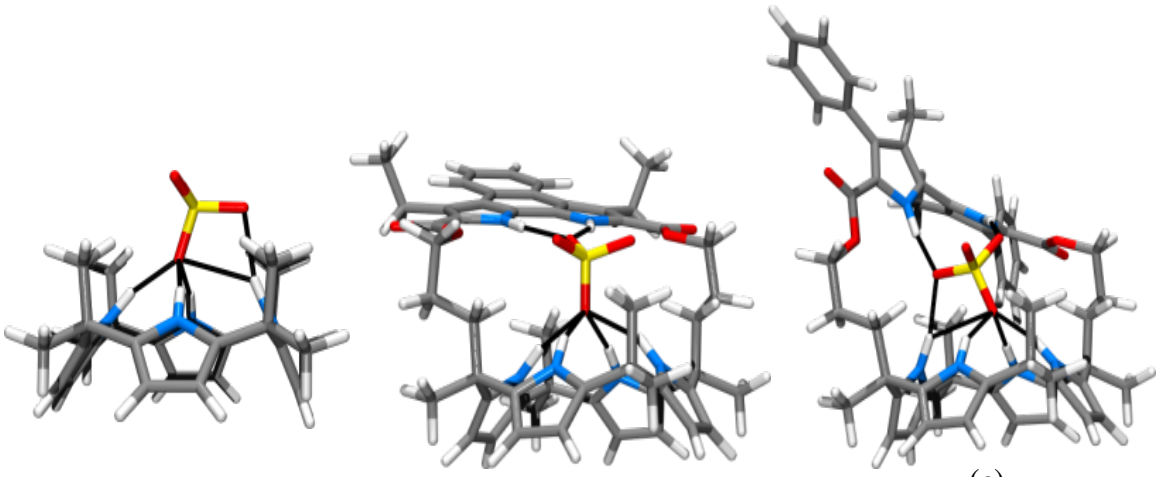

Figure 2.5 Optimized geometry for (a) **2.1**·SO_4^{2-}, (b) **2.2**·SO_4^{2-}, and (c) **2.3**·SO_4^{2-}.

To quantify the binding affinities of receptors **2.2** and **2.3** for sulfate, UV–vis spectroscopic analyses were performed in dichloromethane. When solutions of receptor **2.2** were titrated with $(TBA)_2SO_4$, a hypsochromic shift in the main absorption band was observed. In contrast, a bathochromic shift was observed for receptor **2.3** (cf. Figure 2.6). The absorption band shift of receptor **2.3** to a longer wavelength is rationalized in terms of an enhancement in the planarity of the bipyrrole unit as the result of sulfate binding. Such conformational motions were expected to be less pronounced in the case of **2.2**.

By fitting the UV–vis spectroscopic titration curves to a standard 1:1 binding profile, association constants (K_a) corresponding to the interactions between receptors **2.2** and **2.3** and sulfate could be determined; the values were found to be 1.67×10^5 M^{-1} and 1.37×10^5 M^{-1}, respectively (Figure 2.6). In contrast, no evidence of appreciable sulfate binding was seen in the case of the parent calix[4]pyrrole (**2.1**) under identical experimental conditions (i.e., titration with $(TBA)_2SO_4$, in CH_2Cl_2) (Figure 2.4).

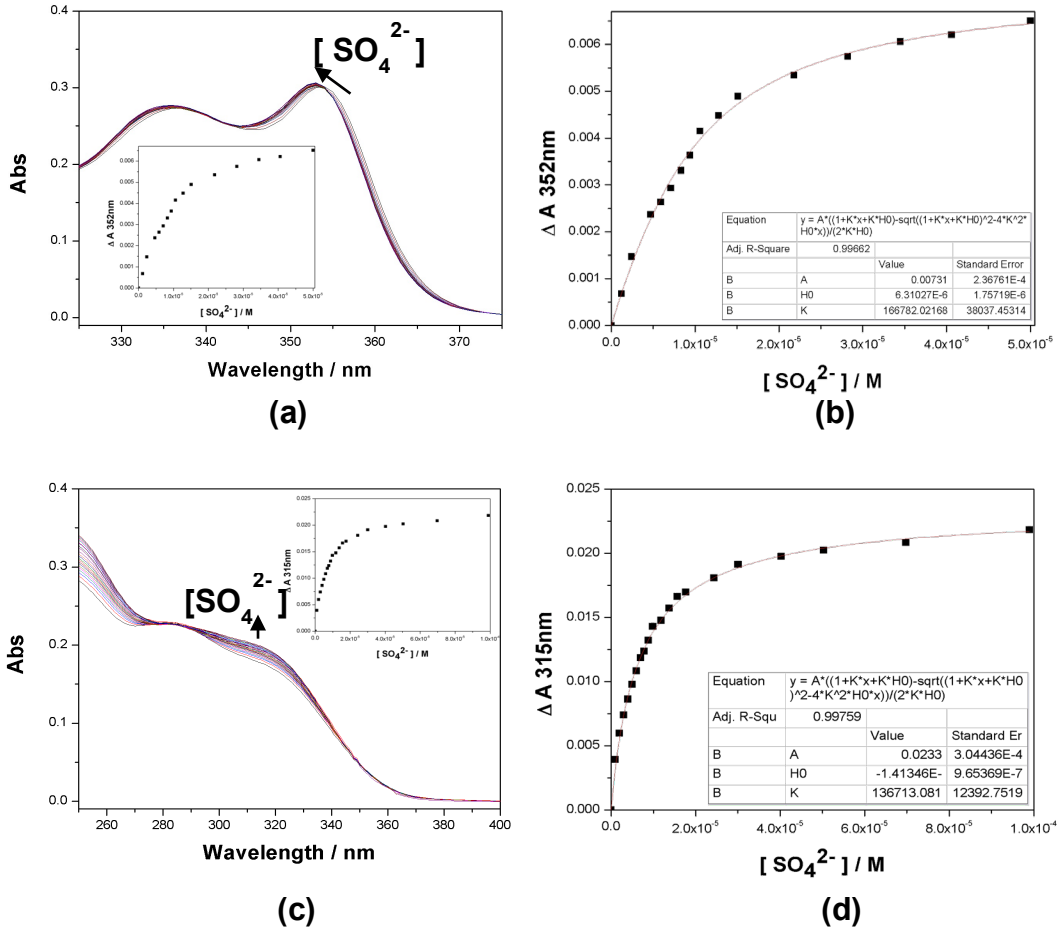

Figure 2.6. UV-vis spectra of (a) **2.2** and (c) **2.3** (1.00×10^{-5} M) recorded in dichloromethane with increasing quantities of $(TBA)_2SO_4$ (tetrabutylammonium sulfate, $0 \sim 5.0 \times 10^{-5}$ M), and the binding isotherm of (b) **2.2** and (d) **2.3** for $(TBA)_2SO_4$ ($K_a = 1.67 \times 10^5$ M^{-1}).

The strong sulfate anion binding inferred in the case of receptor **2.2** was further supported by a solid–liquid extraction experiment using tetramethylammonium sulfate ($(TMA)_2SO_4$).

This latter salt is essentially insoluble in chloroform. The extraction test thus consisted of subjecting a $CDCl_3$ solution of a mixture of **2.2** and tetramethylammonium sulfate (2 molar equiv) to sonication for 10 min, followed by filtration. This produced a clear filtrate that was analyzed by ^{1}H NMR spectroscopy. This analysis revealed that the

NH protons of both the calix[4]pyrrole and the naphthobipyrrole groups were shifted to lower field as compared to a corresponding solution of **2.2** ($\Delta\delta_{Ha}$ = 3.44 ppm and $\Delta\delta_{Hb}$ = 4.58 ppm). Likewise, the β-pyrrolic proton signals were seen to shift to higher field ($\Delta\delta_{Hc}$ = –0.45 ppm) (Figure 2.7). Such findings are consistent with strong complexation between **2.2** and tetramethylammonium sulfate.

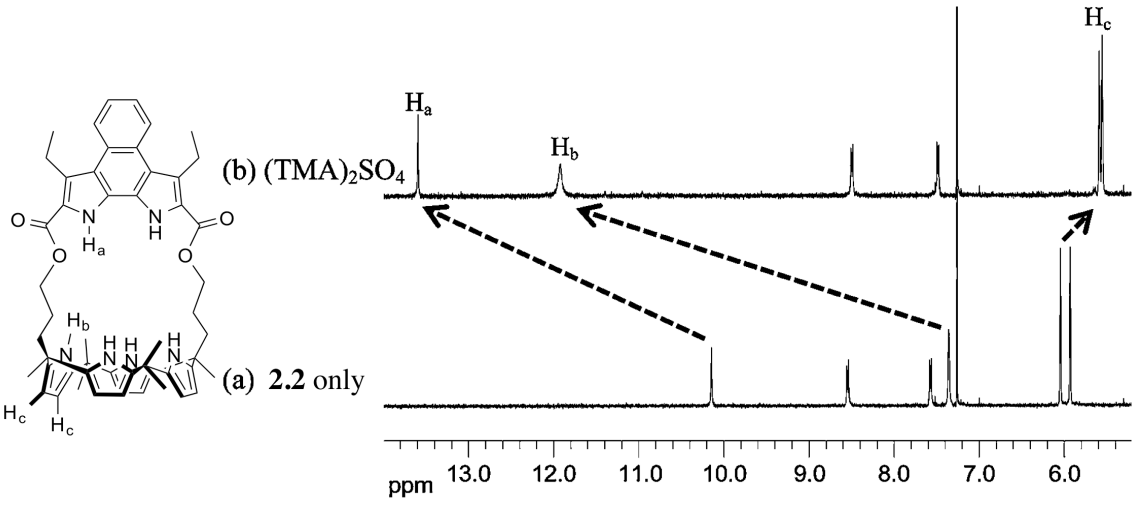

Figure 2.7. Partial ^{1}H NMR spectra of **2.2** recorded at room temperature in $CDCl_3$ (a) before and (b) after the addition of $(TMA)_2SO_4$ (as a solid, 2 equiv), followed by sonication for 10 min and filtration. The spectrum is of the filtrate.

Analogously, when receptor **2.3** was exposed to solid $(TMA)_2SO_4$ in $CDCl_3$, all of its NH protons underwent slight downfield shifts; presumably, these shifts reflect complexation and solubilization of the sulfate anion by **2.3** (Figure 2.8). This presumption was further supported by the observation of a proton signal ascribable to the TMA^+ cation at 3.24 ppm (Figure 2.8).

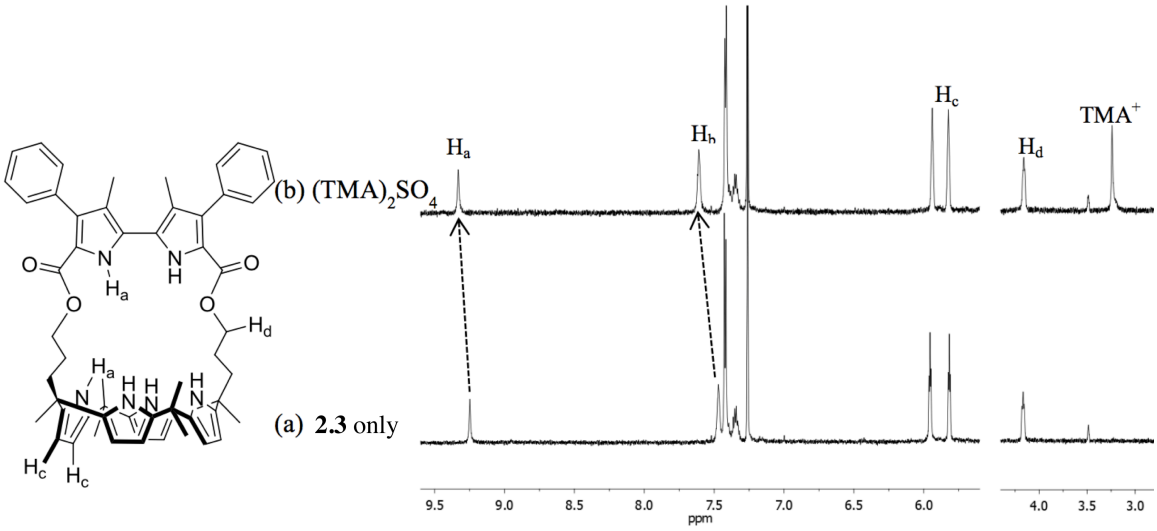

Figure 2.8. Partial ^1H NMR spectra of **2.3** recorded at room temperature in $CDCl_3$ (a) before and (b) after the addition of $(TMA)_2SO_4$ (as a solid, 2 equiv), followed by sonication for 10 min and filtration. The spectrum is of the filtrate.

The chemical shift changes seen for **2.2** and **2.3** stand in contrast to what was seen with compound **2.1**. In the case of the latter receptor, no appreciable chemical shift changes and no signal corresponding to TMA^+ were observed upon exposure to $(TMA)_2SO_4$ in $CDCl_3$ (Figure 2.9).

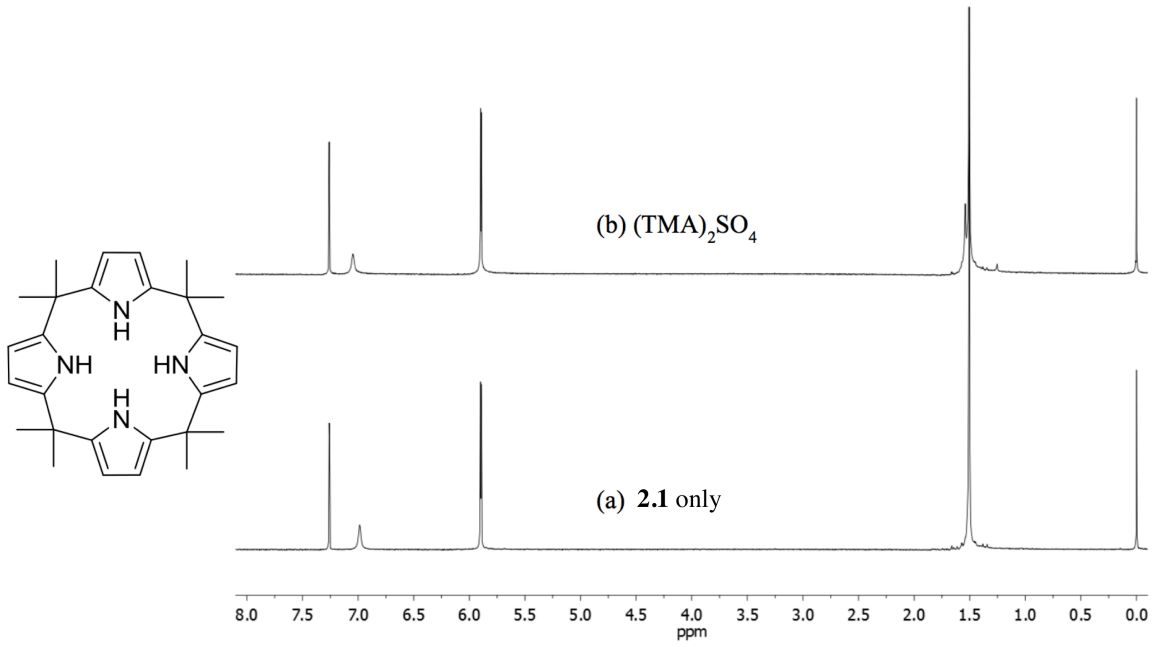

Figure 2.9. Partial ^1H NMR spectra of **2.1** recorded at room temperature in $CDCl_3$ (a) before and (b) after the addition of $(TMA)_2SO_4$ (as a solid, 2 equiv), followed by sonication for 10 min and filtration. The spectrum is of the filtrate.

Further evidence that receptor **2.2** can interact with sulfate came from a single crystal X-ray diffraction analysis. Suitable single crystals of the $(TMA)_2SO_4$ complex were obtained by subjecting a chloroform/methanol mixture of receptor **2.2** to slow evaporation in the presence of $(TMA)_2SO_4$ (5 equiv). The resulting crystal structure revealed that, as predicted by the calculation (see Figure 2.5), receptor **2.2** forms a 1:1 complex with $(TMA)_2SO_4$ in the solid state where two oxygen atoms of the SO_4^{2-} guest are bound to the calix[4]pyrrole and the naphthobipyrrole, respectively, via six hydrogen-bonding interactions with distances of 2.79–2.99 Å for the O···N interactions (Figure 2.10). One of the TMA^+ countercations is bound to the cone-shaped calix[4]pyrrole cavity via CH-π interactions between one of its methyl groups and the π-faces of the pyrroles (Figure 2.10). This TMA^+ cation also interacts directly with another sulfate anion from a different complex to form a contact ion pair. The second TMA^+ cation was found to be coordinated to the outside of the calix[4]pyrrole cavity via apparent CH-π interactions (Figure 2.10). Overall, the structure resembles closely the optimized structure calculated for the sulfate complex of **2.2**

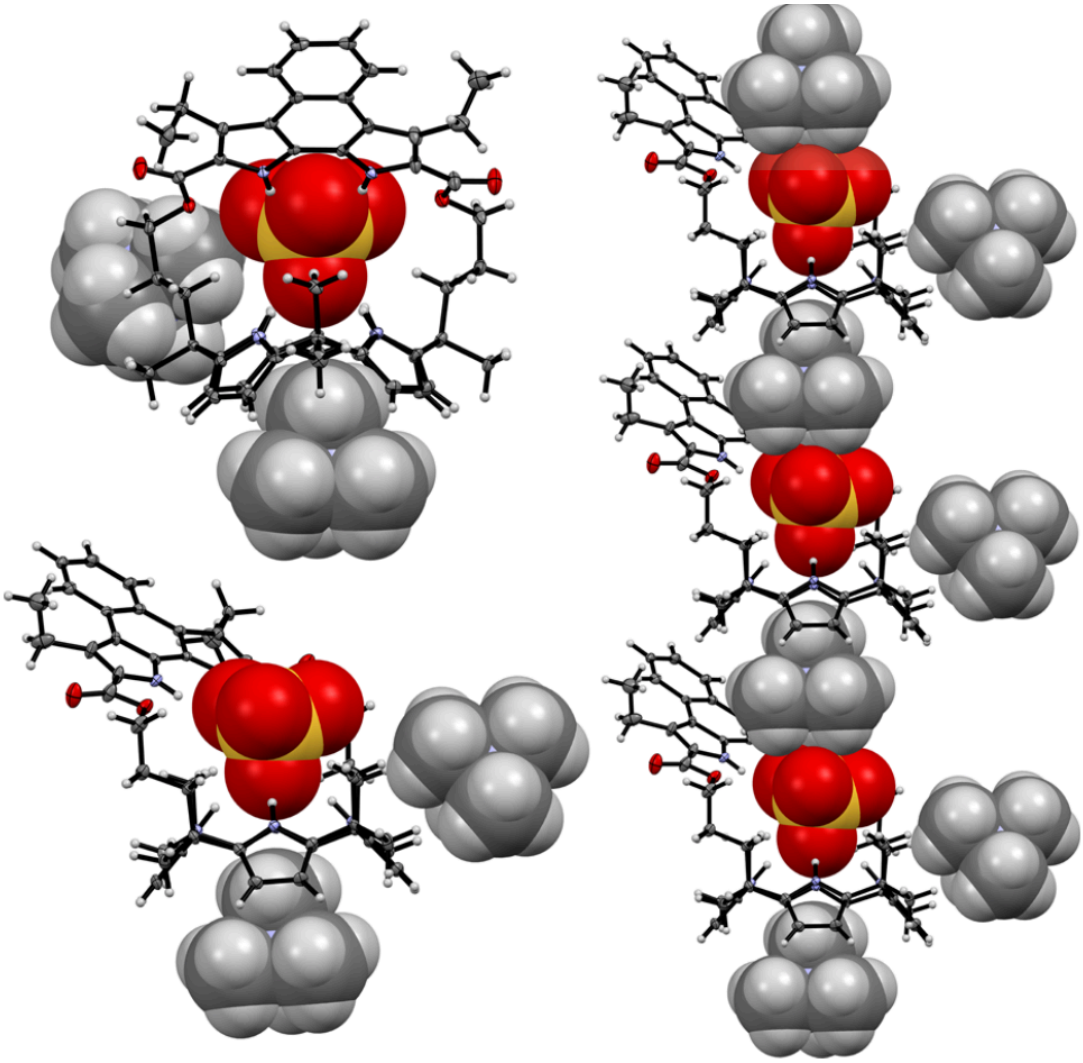

Figure 2.10. Left : Two different views of the single-crystal structure of the $(TMA)_2SO_4$ complex of receptor **2.2**. Right : Partial view of the extended structure seen in the crystal lattice. Solvent molecules have been removed for clarity.

The ability of receptors **2.2** and **2.3** to extract the sulfate in competition with the chloride anion was investigated using ^{35}S-labeled sulfate and beta liquid scintillation to monitor the exchange of sulfate. The exchange was effected from an aqueous solution containing sodium sulfate (0.1 mM) and excess sodium chloride (10 mM) into an organic layer (chloroform) that contained varying concentrations of the receptor in question and Aliquat 336-chloride (methyltrialkyl-(C_{8-10})-ammonium chloride; A336Cl). The use of

A336Cl reflects previous findings that tetraalkylammonium cations having at least one methyl group can synergize sulfate extraction in the case of the parent **2.1** by forming an ion pair complex wherein the methyl group is included in the cone-shaped calix[4]pyrrole cavity.[11]

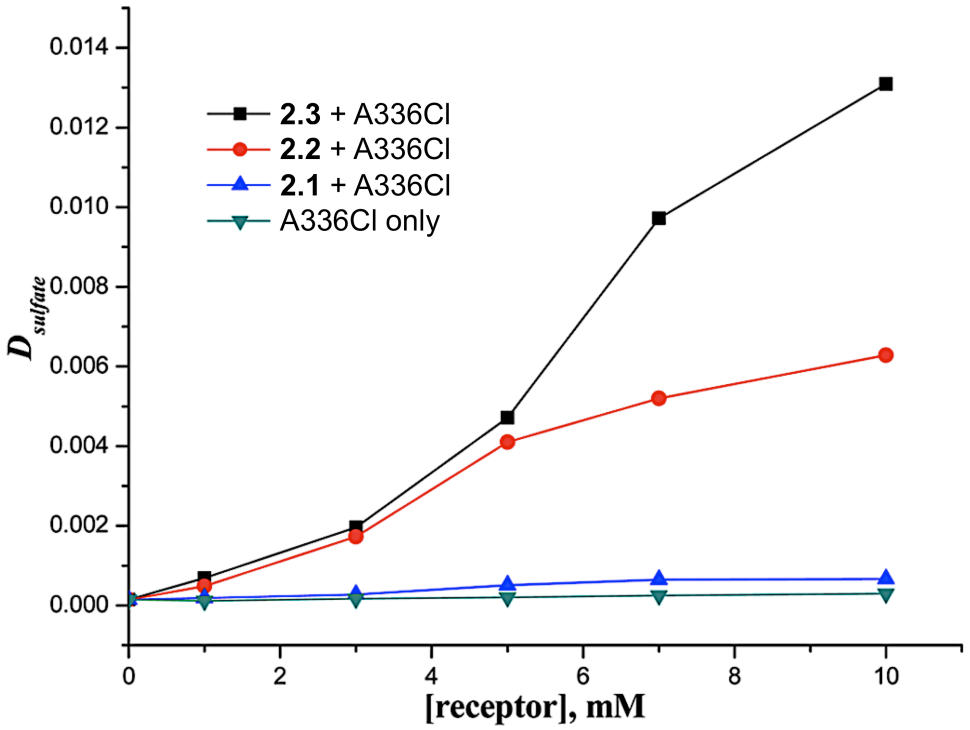

Figure 2.11. The distribution ratio for the extraction of the sulfate ion (as Na_2SO_4 in the aqueous phase) from water using a chloroform solution containing varying concentrations of 1:1 mixtures of receptors **2.1**, **2.2**, and **2.3** with A336Cl. The aqueous phase consisted of 10 mM NaCl and 0.1 mM Na_2SO_4 in Mili-Q water.

Figure 2.11 shows the distribution ratio of the sulfate anion ($D_{sulfate}$ = $[SO_4^{2-}]_{org}/[SO_4^{2-}]_{aq}$) measured for varying concentrations of compounds **2.1**, **2.2**, and **2.3** with A336Cl in the organic phase. Under these conditions, the bipyrrole strapped calix[4]pyrroles **2.2** and **2.3** proved capable of extracting the sulfate anion much more effectively than the parent calix[4]pyrrole (**2.1**) ($D_{sulfate}$ = 0.00055, 0.00614, and 0.013 for compounds **2.1**, **2.2**, and **2.3** at 10 mM concentrations, respectively, in the presence of

equimolar A336Cl) (cf. Figure 2.11 and Table 2.1). The increase of $D_{sulfate}$ by a factor of 11 for **2.2** and a factor of 24 for **2.3** relative to **2.1** under identical experimental conditions is ascribed to the relatively strong interactions between the sulfate anion and receptors **2.2** and **2.3** in competition with chloride ion in the organic phase. While receptor **2.2** binds sulfate more strongly than **2.3** in the absence of chloride, as shown in the titration experiments and molecular mechanics calculations presented above, the extraction results shown in Figure 2.11 and Table 2.1 further reveal that **2.3** is the more selective of the two receptors for sulfate versus chloride in the liquid–liquid exchange system. The sulfate selectivity may arise in part from the divergent NH vectors of the bipyrrole in **2.3**, which can accommodate binding two oxygen atoms of the sulfate guest but would not be expected to be efficient for spherical chloride.

Table 2.1. Distribution ratios of sulfate for experiments where the concentrations of extractants were varied.[a]

[mM]	**2.3** + A336	**2.2** + A336	**2.1** + A336	**2.1**	A336
1	5.65×10^{-4}	3.39×10^{-4}	6.03×10^{-5}	7.40×10^{-5}	5.15×10^{-5}
3	1.85×10^{-3}	1.58×10^{-3}	1.55×10^{-4}	7.21×10^{-5}	5.11×10^{-5}
5	4.60×10^{-3}	3.96×10^{-3}	3.96×10^{-4}	8.49×10^{-5}	8.65×10^{-5}
7	9.59×10^{-3}	5.06×10^{-3}	5.35×10^{-4}	1.06×10^{-4}	1.31×10^{-4}
10	1.30×10^{-2}	6.14×10^{-3}	5.50×10^{-4}	1.18×10^{-4}	1.80×10^{-4}

[a] All synergistic mixtures were 1:1

An analysis of the formal synergistic factors [e.g., $S_{\mathbf{2.3}+A336Cl} = D_{sulfate,\mathbf{2.3}+A336Cl}/(D_{sulfate,\mathbf{2.3}} + D_{sulfate,A336Cl})$] revealed evidence for classical synergism, namely, that performance of the whole exceeds that of the sum of its parts. The values of $S_{\mathbf{2.1}+A336Cl}$ and $S_{\mathbf{2.3}+A336Cl}$ were found to be 2.3 and 12.5 (Table 2.2), respectively, for **2.1** and **2.3** at 5 mM in combination with 5 mM A336Cl in chloroform. It was not possible to obtain the

synergistic factor for **2.2** + A336Cl because of the formation of a precipitate when **2.2** was used alone. The observed synergistic factors exceed unity, indicating a high level of synergism for the strapped calixpyrrole. It was also observed that substitution of the symmetrical long-chain anion exchanger tetraheptylammonium chloride (THACl) for A336Cl greatly reduces the synergistic factor (cf. 12.5 for A336Cl vs 1.6 for THACl, Table 2.2). Such a reduction is consistent with our previously expressed hypothesis that the methyl group of the quaternary ammonium cation A336 resides in the cup of the calix[4]pyrrole.[11]

Table 2.2. Distribution ratios of sulfate for individual components and synergistic mixtures at 5 mM.

Extractant(s)	$D_{sulfate}$
Aliquat 336 (A336)	8.65×10^{-5}
Tetraheptylammonium cation (THA)	2.87×10^{-5}
2.1	8.49×10^{-5}
2.1 + THA	2.01×10^{-4}
2.1 + A336	3.96×10^{-4}
2.3	2.82×10^{-4}
2.2	Third phase[a]
2.3 + THA	5.06×10^{-4}
2.2 + THA	Third phase[a]
2.3 + A336	4.60×10^{-3}
2.2 + A336	3.96×10^{-3}

[a] The ligand formed a crystalline third phase so a $D_{sulfate}$ could not be obtained.

To obtain deeper insights into the extraction process, continuous-variation experiments with receptors **2.2** and **2.3** were carried out. This was accomplished by changing the mole fraction (X) of each of these receptors relative to the A336Cl additive (X = [receptor]/([receptor] + [A336Cl]) under the condition [receptor] + [A336Cl] = 10 mM). On the basis of these studies, it was found that receptors **2.2** and **2.3** extract the sulfate anion with maximum efficiency at X = 0.30 and 0.25, respectively (Figure 2.12). Such findings are consistent with the notion that the extraction process is aided via the

formation of higher order species, wherein more than one A336Cl ion pair interacts with the sulfate–receptor complex in the organic phase. Such aggregation effects are expected to improve the stability of the sulfate anion complex (or complexes) in the organic phase, thus enhancing the extraction process. We suggest a model exchange reaction stoichiometry as follows, where Q is the quaternary ammonium cation and R is the receptor:

$$QRCl_{(org)} + nQCl_{(org)} + SO_4^{2-}{}_{(aq)} \rightleftharpoons Q_2RSO_4 \cdot (n-1)QCl_{(org)} + 2Cl^-_{(aq)} \qquad (1)$$

which is valid for the condition $n \geq 1$. On the basis of our previous equilibrium analysis of sulfate extraction by **2.1** and other receptors in combination with A336 salts,[16,17] we expect that all organic-phase species will be neutral with the receptor initially in the form of a complex with A336Cl when A336Cl is in excess. Binding constants of **2.2** and **2.3** with TBACl in excess of 10^5 M^{-1} (vide infra) imply that more than 99% of the receptor is bound to A336Cl in the form of the QRCl complex over most of the range of the continuous-variation experiments. In the context of eq 1, the sharp continuous-variation maxima (X_{max}) at 0.30 and 0.25 seen in Figure 2.12 are consistent with $n = 0.7$ and $n = 1$ for receptors **2.2** and **2.3**, respectively, when X_{max} is derived as a function of n. It thus appears probable that an A336Cl ion pair plays a role in stabilizing the sulfate complex, even though the resolution of the experiment precludes a definitive assignment of stoichiometry.

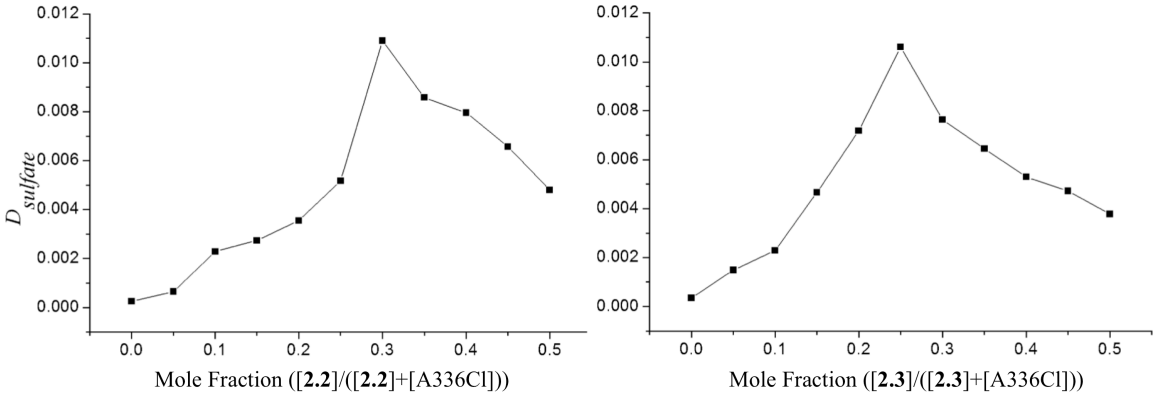

Figure 2.12. Distribution ratios of sulfate resulting from continuous-variation experiments involving Aliquat 336Cl (A336Cl) and receptors **2.2** (left) and **2.3** (right).

The unusual sharpness of the maxima in the continuous-variation experiments provides additional insight into the extraction stoichiometry. Equation 1 is defined only for n ≥ 1, covering only the range $0 < X \leq 0.33$. The condition $X > 0.33$ implies a deficiency of QCl to support the proposed anion exchange. We therefore consider that extraction under these conditions occurs as follows:

$$2QRCl_{(org)} + SO_4^{2-}{}_{(aq)} \rightleftharpoons Q_2RSO_{4(org)} + R_{(org)} + 2Cl^-_{(aq)} \qquad (2)$$

The sharp downturn occurring at $X \geq 0.33$ in Figure 2.12 is consistent with the process of eq 2 being markedly less favorable than that given by eq 1. The unfavorable nature of eq 2 makes sense in that one receptor molecule must be decomplexed from a QRCl species. This represents a large energy penalty given that the binding constants for chloride recorded in organic media were found to be larger than 10^5 M^{-1} (vide infra). In addition, free QCl ion pairs are not available to interact with, and stabilize, the Q_2RSO_4 complex. Thus, Figure 2.12 provides empirical support for the conclusion that the maximum level of synergism occurs in the approximate range $0.25 \leq X \leq 0.33$. We likewise conclude that

above this range, the extraction mechanism abruptly changes, reflecting a process that is much less efficient in terms of receptor utilization.

Table 2.3. Association constants (K_a, M^{-1})[a] of receptors **2.1**, **2.2**, and **2.3** for anions as determined by UV-visible spectroscopic titrations in CH_2Cl_2 at room temperature.

Anion added	Stability constant (M^{-1})		
	2.1[b,c]	**2.2**	**2.3**
F^-	1.72×10^4	3.26×10^5	6.53×10^5
Cl^-	3.50×10^2	6.50×10^5	1.50×10^6
Br^-	10	5.72×10^5	3.00×10^5
I^-	<10	4.45×10^4	1.93×10^4
$H_2PO_4^-$	97	3.18×10^5	2.90×10^5
$HP_2O_7^{3-}$	N.D.	1.41×10^6	1.00×10^6
SO_4^{2-}	N.D.	1.67×10^5	1.37×10^5
NO_3^-	N.D.	1.08×10^6	9.07×10^4

[a]All anions were used in the form of their respective tetrabutylammonium (TBA) salts. [b]Values obtained from ^{1}H NMR titrations in CH_2Cl_2 at room temperature. [c]From ref 18; N.D., not determined.

The ability of receptors **2.2** and **2.3** to interact with other anions, such as the halides, nitrate, phosphate, and pyrophosphate anions (as the TBA^+ salts), was also analyzed via ^{1}H NMR and UV–vis spectroscopy in CD_2Cl_2. As compared with calix[4]-pyrrole **2.1**, the association constants (K_a) of receptors **2.2** and **2.3** are significantly enhanced (by at least 3 orders of magnitude) in the case of all anions tested except for F^- (Table 2.3). As inferred from the ^{1}H NMR and UV/Vis spectral changes induced by anion addition, this enhancement in the K_a values is attributable to two additional hydrogen-bonding interactions provided by the bipyrrole units. Interestingly, in contrast to what was seen with **2.1**, a receptor that is highly selective for fluoride over other anions in CD_2Cl_2 (K_a for F^-/K_a for X^- ($S_{F/X}$) = 49, 1720, and >1720 for Cl^-, Br^-, and I^-, respectively),[18]

the selectivity of **2.2** and **2.3** for other anions is enhanced relative to F^-. For example, the $S_{F/X}$ values of receptor **2** were calculated to be 0.50, 0.56, and 7.32 for Cl^-, Br^-, and I^-, respectively, while those of receptor **2.3** were 0.62, 2.18, and 33.8 for Cl^-, Br^-, and I^-, respectively. The reversed selectivity of both of receptors **2.2** and **2.3**, that is, favoring chloride relative to fluoride, is consistent with the notion that the bipyrrole units, which provide more hydrogen-bonding donors but with constrained geometry, help stabilize complexation of this and other larger anions.

Another selectivity reversal to be noted from Table 2.3 relates to an apparent difference in binding selectivity versus extraction selectivity. The extraction results displayed in Figure 2.11, for example, show that both **2.2** and **2.3** enhance sulfate extraction selectivity versus chloride when these receptors are combined with the anion exchanger A336Cl. Alternately, the data in Table 2.3 reveals that both receptors bind the chloride anion more strongly than sulfate in homogeneous solution (albeit in CH_2Cl_2 vs $CHCl_3$ used in the extraction). Moreover, **2.2** binds sulfate with greater selectively (versus chloride) than does **2.3** (Table 2.3). In contrast, whereas **2.3** extracts sulfate more selectively versus chloride than does **2.2** (Figure 2.11). Notwithstanding the difference in diluents used in the binding and extraction studies, the fundamental chemistry involved in binding and extraction differs in several key ways that bear strongly upon the net selectivity observed in each case. While binding and extraction can be exactly related in special cases,[17] the effects of anion-partitioning and aggregation behavior are often more pronounced under conditions of extraction than in the homogeneous media typically used for binding studies. Unfortunately, in the present case the effects of these nonlinear phenomena cannot be evaluated quantitatively, precluding a more detailed interpretation. It is clear, however, that the aggregation behavior exemplified in eq 1 has an influence on the selectivity obtained to the extent that it can reverse the order of receptors with respect to their sulfate versus chloride selectivity seen under the conditions of the binding studies.

Evidence for hydrogen-bonding interactions involving the bipyrrole and their role in stabilizing complexes with larger anions came from ^{1}H NMR spectroscopic analyses.

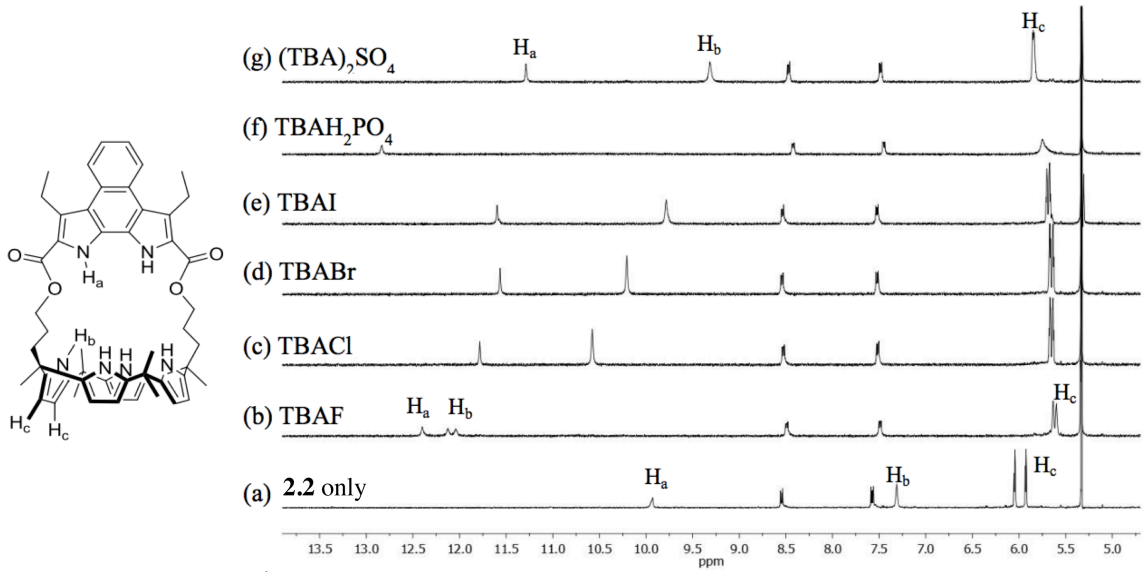

Figure 2.13. Partial ^{1}H NMR spectra of (a) **2.2** (3 mM) only, (b) **2.2** + 1 equiv of TBAF (tetrabutylammonium fluoride), (c) **2.2** + 1 equiv of TBACl (tetrabutylammonium chloride), (d) **2.2** + 1 equiv of TBABr (tetrabutylammonium bromide), (e) **2.2** + 1 equiv of TBAI (tetrabutylammonium iodide) and (f) **2.2** + 1 equiv of $TBAH_2PO_4$ (tetrabutylammonium phosphate), and (g) **2.2** + 1 equiv of $(TBA)_2SO_4$ (tetrabutylammonium sulfate) in CD_2Cl_2.

For instance, upon exposure of receptors **2.2** and **2.3** to the fluoride anion, a relatively small downfield shift in the NH proton signal of the bipyrrole units ($\Delta\delta_{Ha}$ = 2.48 and 2.05 ppm for **2.2** and **2.3**, respectively) relative to that of the calix[4]pyrrole framework ($\Delta\delta_{Hb}$ = 5.00 and 4.50 ppm for **2.2** and **2.3**, respectively) was seen (Figures 2.13 and 2.14). Moreover, the NH proton resonance of the bipyrrole unit remained a singlet while that of the calix[4]pyrrole unit was split into a doublet, an effect ascribed to the coupling between the pyrrolic NH and the fluoride anion (Figures 2.13 and 2.14).[19] Such findings are consistent with the notion that the fluoride anion is more strongly hydrogen-bonded to the calix[4]pyrrole moiety than to the bipyrrole units.

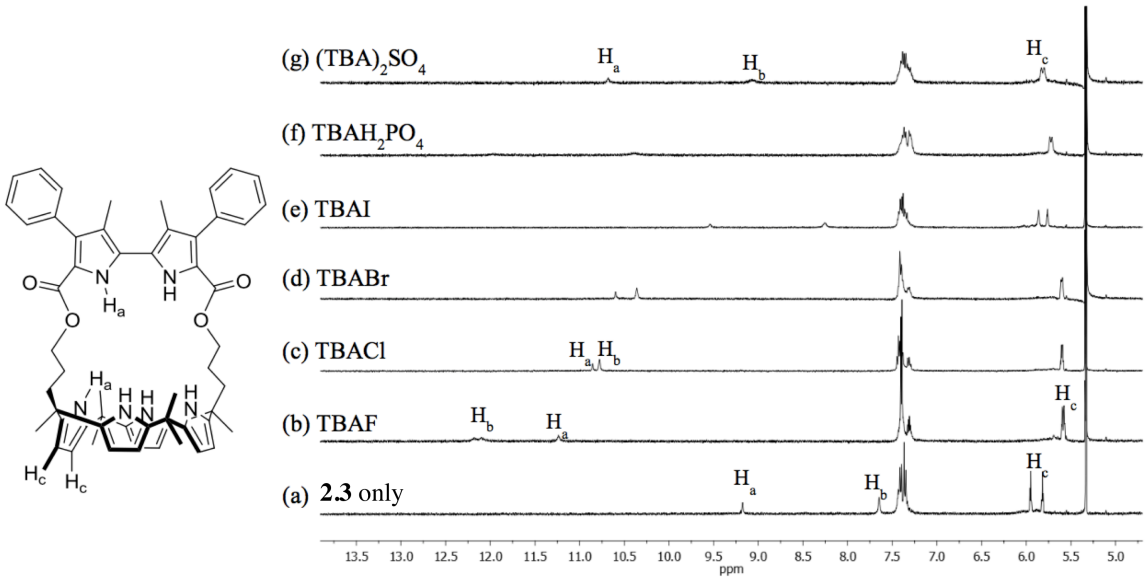

Figure 2.14. Partial ^{1}H NMR spectra of (a) **2.3** (3 mM) only, (b) **2.3** + 1 equiv of TBAF (tetrabutylammonium fluoride), (c) **2.3** + 1 equiv of TBACl (tetrabutylammonium chloride), (d) **2.3** + 1 equiv of TBABr (tetrabutylammonium bromide), (e) **2.3** + 1 equiv of TBAI (tetrabutylammonium iodide) and (f) **2.3** + 1 equiv of $TBAH_2PO_4$ (tetrabutylammonium phosphate), and (g) **2.3** + 1 equiv of $(TBA)_2SO_4$ (tetrabutylammonium sulfate) in CD_2Cl_2.

Presumably, this reflects the fact that cavities of receptors **2.2** and **2.3** are too big for all six NH protons to contribute strongly to fluoride anion binding. In contrast, shifts in NH signals of both the bipyrrole and the calix[4]pyrrole moiety were seen when chloride (TBA^+ salt) was added to CD_2Cl_2 solutions of **2.2** and **2.3** ($\Delta\delta_{Ha}$ = 1.80 and 1.68 ppm and $\Delta\delta_{Hb}$ = 3.26 and 3.12 ppm for **2.2** and **2.3**, respectively).

Single-crystal X-ray diffraction analyses were used to obtain further insights into the binding modes of the fluoride and chloride anions with receptor **2.2**. The resulting crystal structure revealed that only the NH protons of the calix[4]pyrrole moiety are directly hydrogen bonded to the fluoride anion, while those of the naphthobipyrrole units interact with the anion via a solvent (methanol) bridge (Figure 2.15). The relevant $N\cdots F^-$ distances were found to be 2.81–2.86 Å and 4.70–4.77 Å for the calix[4]pyrrole and the naphthobipyrrole, respectively. In contrast, and in analogy to what was seen with the sulfate complex, all six NH protons of receptor **2.2** are in contact with the chloride anion via direct hydrogen bonds. In the solid state, the $N\cdots Cl^-$ distances are 3.34–3.45 Å and 3.33–3.46 Å for the calix[4]pyrrole and the naphthobipyrrole, respectively (Figure 2.15). Taken in concert, the combination of solution phase and solid state data leads us to conclude that the interaction of the bipyrrole NH protons with anions plays a crucial role in determining both the anion binding affinities and selectivities of receptors **2.2** and **2.3**.

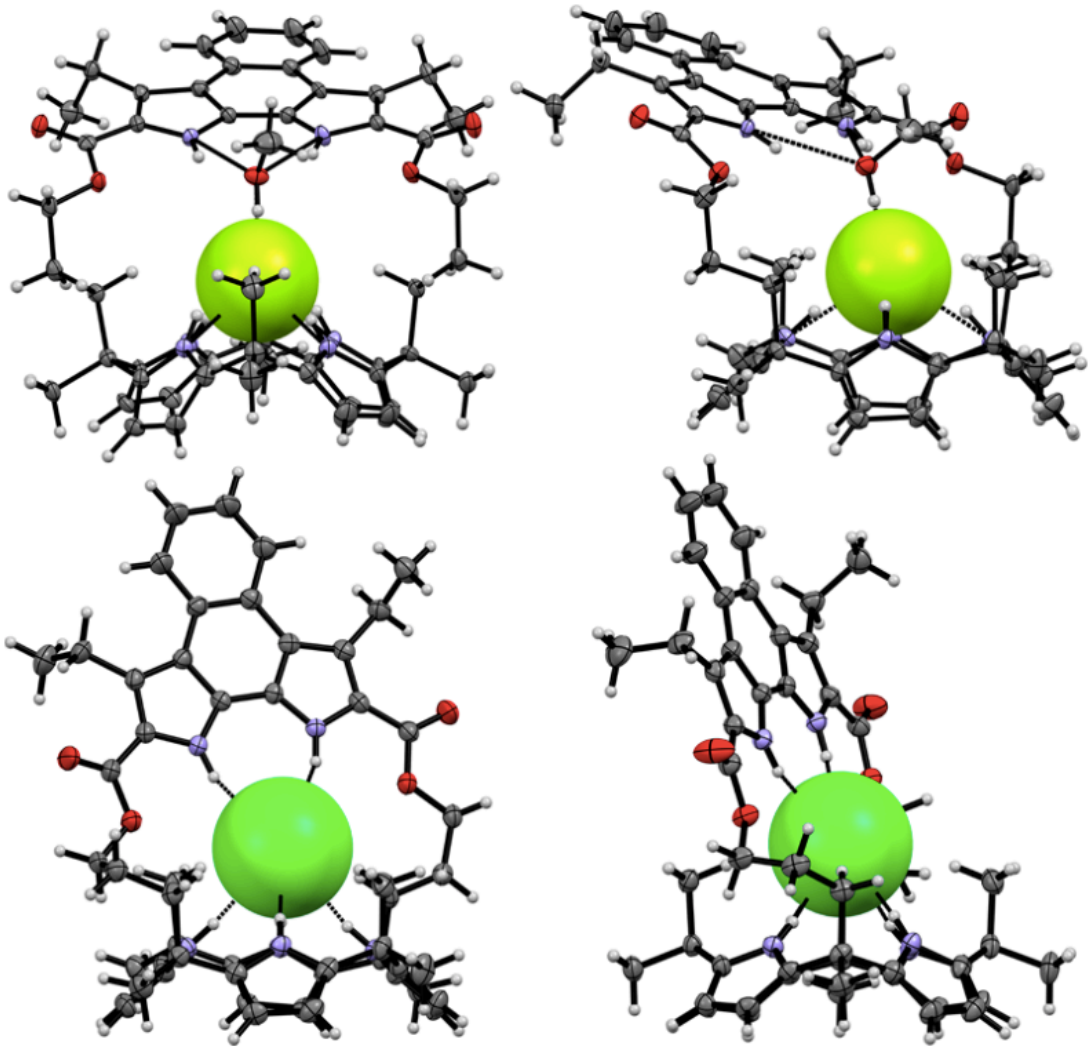

Figure 2.15. Top: Two different views of the single crystal structures of the CsF complex of receptor **2.2** (**2.2**·CsF·CH_3OH). A methanol molecule is bridged between the F^- anion and the NH protons of the naphthobipyrrole group. Bottom: Two different views of the single crystal structures of the TEACl (tetraethylammonium chloride) complex of receptor **2.2** (**2.2**·TEACl). Dashed lines indicate hydrogen bonds. Thermal ellipsoids are scaled to the 50% probability level. The Cs^+ and TEA^+ cations sitting in the bowl-shaped calix[4]pyrrole cavities have been omitted for clarity.

2.3 CONCLUSIONS

In summary, cryptand-like bipyrrole-strapped calix[4]- pyrroles **2.2** and **2.3** have been synthesized. Compared with the parent calix[4]pyrrole (**2.1**), they exhibit significantly enhanced anion binding affinities and improved selectivities for other anions relative to fluoride. The strong binding interactions between receptors **2.2** and **2.3** and sulfate are thought to account for the ability to extract this highly hydrophilic species into an organic solvent from aqueous solutions relative to the simple calix[4]pyrrole **2.1** when A336Cl was used as a coextractant. Strong receptor-sulfate anion interactions are also thought to underline the solid-liquid extractions of $(TMA)_2SO_4$ seen in the case of **2.2** and **2.3**.

2.4 REFERENCES

1) Hofmeister, F. *Arch. Exp. Pathol. Pharmakol.* **1888**, *24*, 247-260.
2) Custelcean, R.; Moyer, B. A. *Eur. J. Inorg. Chem.* **2007**, *10*, 1321-1340.
3) *Report to Congress: Status of Enviornmental Management Initiatives to Accelerate the Reduction of Environmental Risks and Challenges Posed by the Legacy of the Cold War;* Report DOE/EM-0001; U. S. Department of Energy, Office of Environmental management: Washington, DC, Jan. 2009.
4) Moyer, B. A.; Custelcean, R.; Hay, B. O.; Sessler, J. L.; Bowman-James, K.; Day, V. W.; Kang, S. *Inorg. Chem.* **2013**, *52*, 3473-3490.
5) Ojovan, M. I.; Lee, W. E. *An Introduction to Nuclear Waste Immobilisation;* Elsevier: Amsterdam, Netherlands, 2005; Chapter 17.
6) Manara, D.; Grandjean, A.; Pinet, O.; Dussossoy, J. L.; Neuville, D. R. J. *Non-Cryst. Solids* **2007**, *353*, 12-23.
7) Pirlet, V. J. J. *Nucl. Mat.* **2001**, *298*, 47-54.
8) Ravikumar, I.; Ghosh, P. *Chem. Soc. Rev.* **2012**, *41*, 3077-3098.
9) Jia, C.; Wu, B.; Li, S.; Huang, X.; Zhao, Q.; Li, Q. S.; Yang, X. J. *Angew. Chem. Int. Ed.* **2011**, *50*, 486-490.
10) Fowler, C. J.; Haverlock, T. J.; Moyer, B. A.; Shriver, J. A.; Gross, D. E.; Marquez, M.; Sessler, J. L.; Hossain, M. A.; Bowman-James, K. *J. Am. Chem. Soc.* **2008**, *130*, 14386-14387.
11) Borman, C. J.; Custelcean, R.; Hay, B. P.; Bill, N. L.; Sessler, J. L.; Moyer, B. A. *Chem. Comm.* **2011**, 7611-7613.
12) (a) Kubik, S.; Kirchner, R.; Nolting, D.; Seidel, J. *J. Am. Chem. Soc.* **2002**, *124*, 12752–12760. (b) Kim, J.-i.; Juwarker, H.; Liu, X.; Lah, M. S.; Jeong, K.-S. *Chem. Commun.* **2010**, *46*, 764–766. (c) Young, P. G.; Clegg, J. K.; Bhadbhade, M.; Jolliffe, K. A. *Chem. Commun.* **2011**, *47*, 463–465. (d) Busschaert, N.; Karagiannidis, L. E.; Wenzel, M.; Haynes, C. J. E.; Wells, N. J.; Young, P. G.; Makuc, D.; Plavec, J.; Jolliffe, K. A.; Gale, P. A. *Chem. Sci.* **2014**, *5*, 1118–1127. (e) Elmes, R. B. P.; Yuen, K. K. Y.; Jolliffe, K. A. *Chem. Eur. J.* **2014**, *20*, 7373-7380.

(f) Sommer, F.; Kubik, S. *Org. Biomol. Chem.* **2014**, *12*, 8851-8860. (g) Naini, S. R.; Lalancette, R. A.; Gorlova, O.; Ramakrishna, K. V. S.; Yadav, J. S.; Ranganathan, S. *Eur. J. Org. Chem.* **2014**, 7015-7022. (h) Brunetti, E.; Picron, J.; Flidrova, K.; Bruylants, G.; Bartik, K.; Jabin, I. *J. Org. Chem.* **2014**, *79*, 6179-6188. (i) Custelcean, R.; Willams, N. J.; Seipp, C. A. *Angew. Chem. Int. Ed.* **2015**, *54*, 10525-10529. (j) Custelcean, R.; Williams, N. J.; Seipp, C. A.; Ivanov, A. S.; Bryantsev, V. S. *Chem. Eur. J.* **2016**, *22*, 1997-2003. (k) Ahmed, B. M.; Mezei, G. *Chem. Commun.* **2017**, *53*, 1029-1032. (l) Zhou, H.; Zhao, Y.; Gao, G.; Li, S.; Lan, J.; You, J. *J. Am. Chem. Soc.* **2013**, *135*, 14908-14911. 9 (m) Song, N. R.; Moon, J. H.; Choi, J.; Jun, E. J.; Kim, Y.; Kim, S.; Lee, J. Y.; Yoon, J. *Chem. Sci.* **2013**, *4*, 1765-1771. (n) Saini, R.; Kumar, S. *RSC Adv.* **2013**, *3*, 21856-21862.

13) Gale, P. A.; Sessler, J. L.; Král, V. *Chem. Commun.* **1998**, 1-8.

14) Roznyatovskiy, V. V.; Roznyatovskaya, N. V.; Weyrauch, H.; Pinkwart, K.; Tübke, J.; Sessler, J. L. *J. Org. Chem.* **2010**, *75*, 8355-8362.

15) Boev, N. V.; Ustynyuk, Y. A. Russ. *J. Org. Chem.* **2007**, *43*, 297-304.

16) Moyer, B. A.; Sloop, F. V., Jr.; Fowler, C. J.; Haverlock, T. J.; Kang, H.-A.; Delmau, L. H.; Bau, D. M.; Hossain, A.; Bowman-James, K.; Shriver, J. A.; N. Bill; Gross, D. E.; Marquez, M.; Sessler, J. L. *Supramol. Chem.* **2010**, *22*, 653–671.

17) Borman, C. J.; Bonnesen, P. V.; Moyer, B. A. *Anal. Chem.* **2012**, *84*, 8214–8221.

18) Gale, P. A.; Sessler, J. L.; Král, V.; Lynch, V. *J. Am. Chem. Soc.* **1996**, *118*, 5140-5141.

19) Sato, W.; Miyaji, H.; Sessler, J. L. *Tetrahedron Lett.* **2000**, *41*, 6731-6736.

Chapter 3: Ship in a Breakable Bottle: Fluoride-induced Release of an Organic Molecule From a Pr(III)-linked Molecular Cage

3.1 INTRODUCTION

Considerable effort has been devoted to the development of porous materials that allow for the accommodation, detection, and spatially confined reactions of small molecules.[1] In this context, the host-guest chemistry of artificial molecular cages has received particular attention. The liberation of guests and other species, including *inter alia* reaction products, from these systems has typically relied on the use of external stimuli, such as treatment with acid, heating, photoreduction, or simple solvent washing.[2] However, the anion-induced release of entrapped organic species within porous molecular frameworks has not been extensively explored, if at all. Herein, we report a calix[4]pyrrole-based coordination cage system that encapsulates the free supramolecular ligand within the pores of network. Treatment with fluoride anion induces guest release.

Calix[4]pyrroles are non-conjugated tetrapyrrolic synthetic compounds that were first synthesized by Baeyer.[3] They are generally easy to prepare through the acid-catalyzed condensation between pyrrole and a methyl ketone. Due to their anion and neutral substrate binding properties, these systems have attracted attention in recent years as molecular receptors, sensors, and containers.[4] Their ease of preparation and functionalization have made elaborated calix[4]pyrroles attractive for use as receptors for various anion and ion pair receptors, as well as of interest as potential extractants for species present in high-level liquid waste (HLLW)[5] and as transporters for biological important ions in connection with therapeutic aims.[6] Functionalization of the calix[4]pyrrole *meso* position allows the incorporation of additional binding sites for cations. This might permit construction of functional metal-organic frameworks (MOFs) or coordination polymers based on calix[4]pyrroles.

---

§ Lee, J.; Waggoner, N. W.; Polanco, L.; You, G. R.; Lynch, V. M.; Kim, S. K.; Humphrey, S. M.; Sessler, J. L. Ship in a breakable bottle: fluoride-induced release of an organic molecule from a Pr(III)-linked molecular cage. *Chem. Commun.* **2016**, *52,* 8514-8517. The author is a first author of the publication and was responsible for the syntheses of all the compounds, XRD spectroscopic analyses, FT-IR spectroscopy, thermogravimetric analysis, illustrations, ^{1}H NMR spectroscopic studies, and CO_2 supercritical extractions.

Metal-organic frameworks, formed by the coordination of metal clusters or ions with organic linkers, have received considerable attention due to their great potential in various applications, such as gas storage, separation, sensing and catalysis.[1] Within the MOF community, there is a growing interest in macrocycle-based materials, e.g., metal-macrocycle frameworks (MMFs). To date, various macrocycles, including crown ethers, cyclodextrins (CDs), calixarenes, cucurbiturils (CBs), metalloporphyrins, azamacrocycles, and pillararenes, have been exploited as linking elements or so-called secondary building units (SBUs), to create unique MOFs.[7] However, MMFs based on calixpyrrole SBUs have yet to be reported in spite of their expected ease of synthesis and potential utility. This has prompted us to construct a new metal-macrocycle framework, **NMC-1**, that contains a Pr(III) node and an anion responsive flexible calix[4]pyrrole ligand. The choice of Pr(III) reflects an appreciation that there are examples of Ln-acetate clusters (and also MOFs) that form easily with Pr and Nd, presumably because these earlier 4f ions have radii that accommodate well the O-bridged motifs of carboxylate ligands.[8]

3.2 RESULT AND DISCUSSION

Scheme 3.1 shows the synthesis of the benzoic acid-functionalized calix[4]pyrrole (**3.1**) SBU used to construct **NMC-1**. Methyl 4-acetyl benzoate (**3.2**) was reacted with pyrrole as a solvent in the presence of trifluoroacetic anhydride (TFAA) at 60 °C to give compound **3.3** in 72% yield. Compound **3.3** was then reacted with TFAA in a 1:1 (v/v) acetone/methanol mixture. This afforded compound **3.4** in 15% yield. Hydrolysis yielded the dibenzoic acid calix[4]pyrrole (**3.1**) in 95% yield based on **3.4**. Single crystals of **3.1** suitable for X-ray diffraction analysis were obtained by slow evaporation from DMF (Figure 3.1).

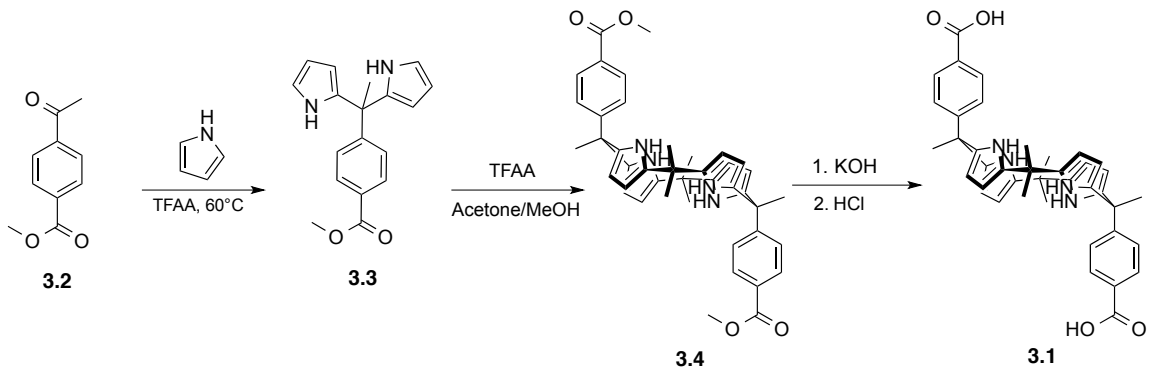

Scheme 3.1 Synthesis of compound **3.1**.

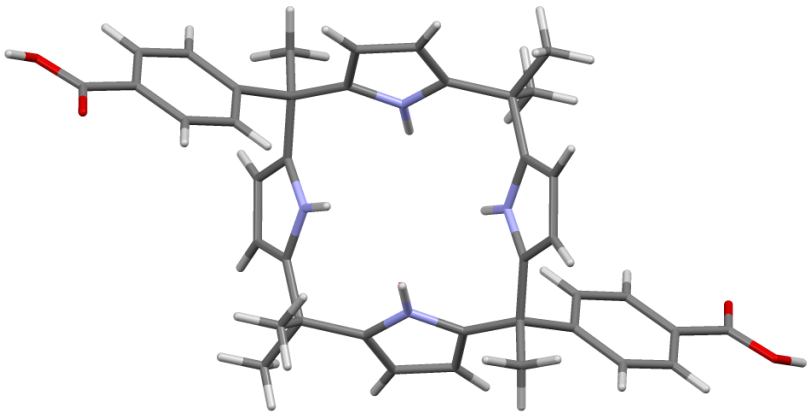

Figure 3.1 X-ray structure of compound **3.1**.

NMC-1 was synthesized via the solvothermal reaction of **3.1** and $Pr(NO_3)_3 \cdot 6H_2O$ with oxalic acid/NaOH in a 2:2:1 (v/v) DMF/DEF (*N*,*N*'-diethylformamide)/H_2O mixture at 100 °C for 3 days. Single crystal X-ray diffraction analysis revealed that **NMC-1** is composed of tetranuclear Pr(III) units, which serve as metal nodes coordinated by a total of ten benzoate anions from the constituent macrocyclic ligands; this results in a 3-D framework having 1D channels that propagate throughout the structure (Scheme 3.2).

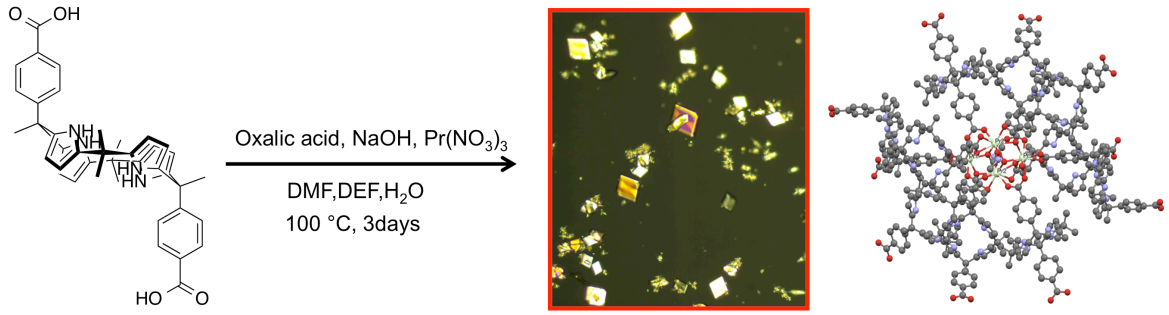

Scheme 3.2 Synthesis and crystal structure of **NMC-1**.

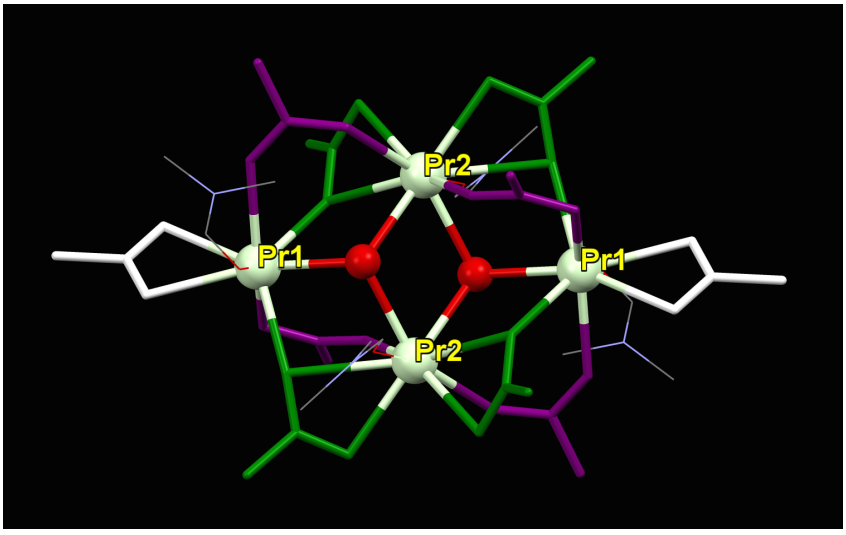

Figure 3.2 Wireframe rendering of the central metal cluster of **NMC-1**.

Each calix[4]pyrrole ligand interacts with two DMF molecules. This results in stabilization of a 1,2-alternate conformation, rather than the 1,3-alternate form typically seen in the absence of a bound guest.[9] The carboxylates display three different types of coordination modes toward the Pr_4 nodes (1,2-chelating, *syn-syn*, and chelate-*syn*). The central metal cluster contains four Pr(III) centers that are bridged by two μ_3-OH ligands giving rise to two edge-sharing $Pr_3(OH)$ triangles (Figure 3.2). The metal ions are 8- and 9-coordinate.

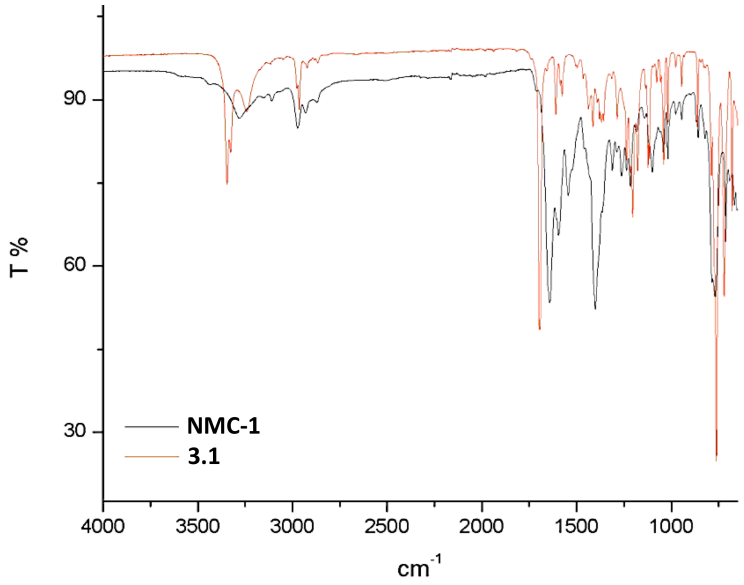

Figure 3.3 Overlaid infrared spectra of **NMC-1** (black) and **3.1** (red).

A comparison of the FT-IR spectra of the starting ligand and **NMC-1** (both measured in the solid state) provided further evidence for the formation of a coordinated species. Notably, a shift in the position of the carbonyl peak (from 1694.1 to 1641.8 cm^{-1}) and a reduction in the intensity due to the carboxylic acid O-H stretching mode were observed (Figure 3.3). Powder X-ray diffraction (PXRD) studies of **NMC-1** after exposure to the air for 2 days confirmed its stability as inferred by the good comparison of the sample to the simulated pattern obtained from the single crystal X-ray experiment discussed above (Figure 3.4a). Thermogravimetric analysis likewise revealed no significant mass loss prior to the onset of framework decomposition ca. 350°C (Figure 3.4b).

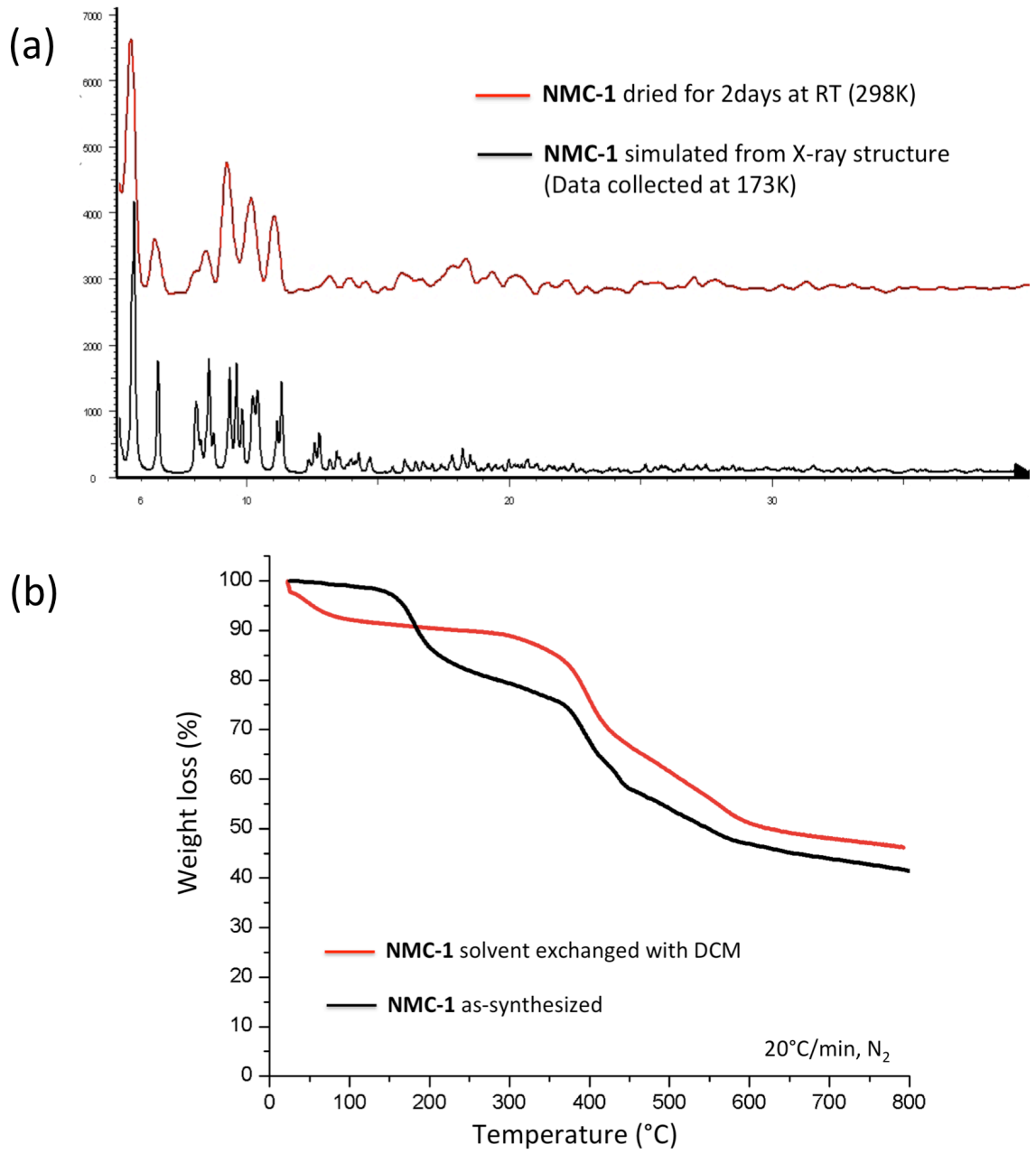

Figure 3.4 (a) Powder X-ray diffraction data of **NMC-1** (red) after being air-dried and the simulated powder pattern deduced from the solved crystal structure of **NMC-1** (black). (b) Thermogravimetric analysis data of as-synthesized **NMC-1** (black) and dichloromethane (DCM)-exchanged **NMC-1** (red).

An analysis of the crystal structure of **NMC-1** revealed an open cage-like tilted-octahedron structure with six metal nodes and ten secondary binding units **3.1** (Figure 3.5a). The distances between the metal nodes at each of the opposing vertices are 29.414, 23.775, and 29.232 Å, respectively (Figure 3.6). The free (i.e., uncomplexed) form of **3.1** is found to reside within the resulting cage and with a site occupancy factor (SOF) of 0.5 (Figure 3.5b and 3.5c). This means that about half of the channels are filled with the calix[4]pyrrole subunits. Based on the metric parameters, the molecules of **3.1** appeared to be physically trapped, rather than being chemically constrained (e.g., via H-bonding interactions; Figure 3.7). Efforts were thus made to see if the bound species, **3.1**, could be removed by chemical means.

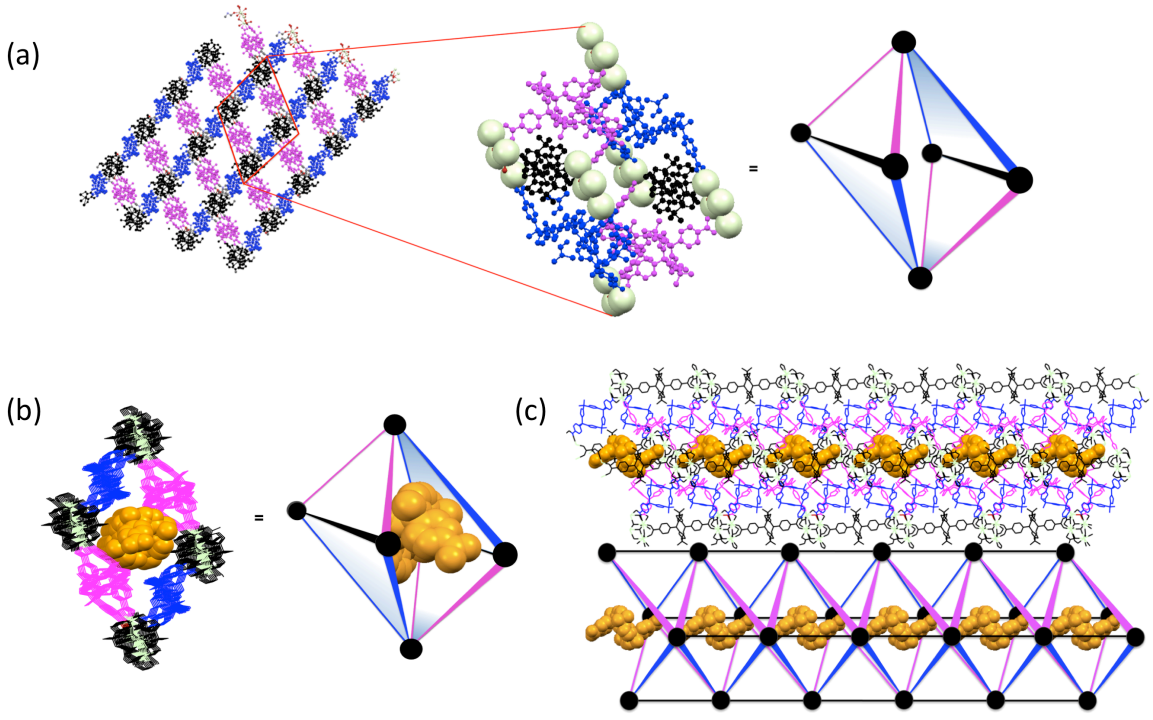

Figure 3.5 (a) Representation of 1-dimensional mesoporous channels made of infinite cage-like pore units. (b) X-ray structure and a simplified cartoon of the free calix[4]pyrrole molecule in the pore. (c) Representation of the free (non-complexed) calix[4]pyrrole within the frameworks in side views of the channel.

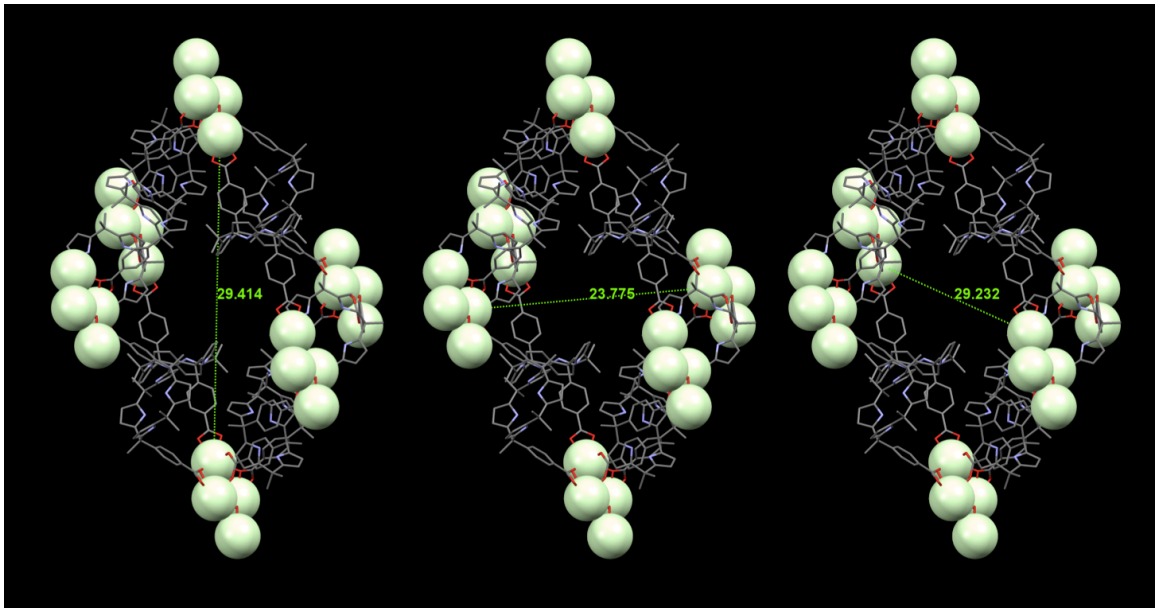

Figure 3.6 Distances between the opposing vertices established by the metal nodes of **NMC-1**.

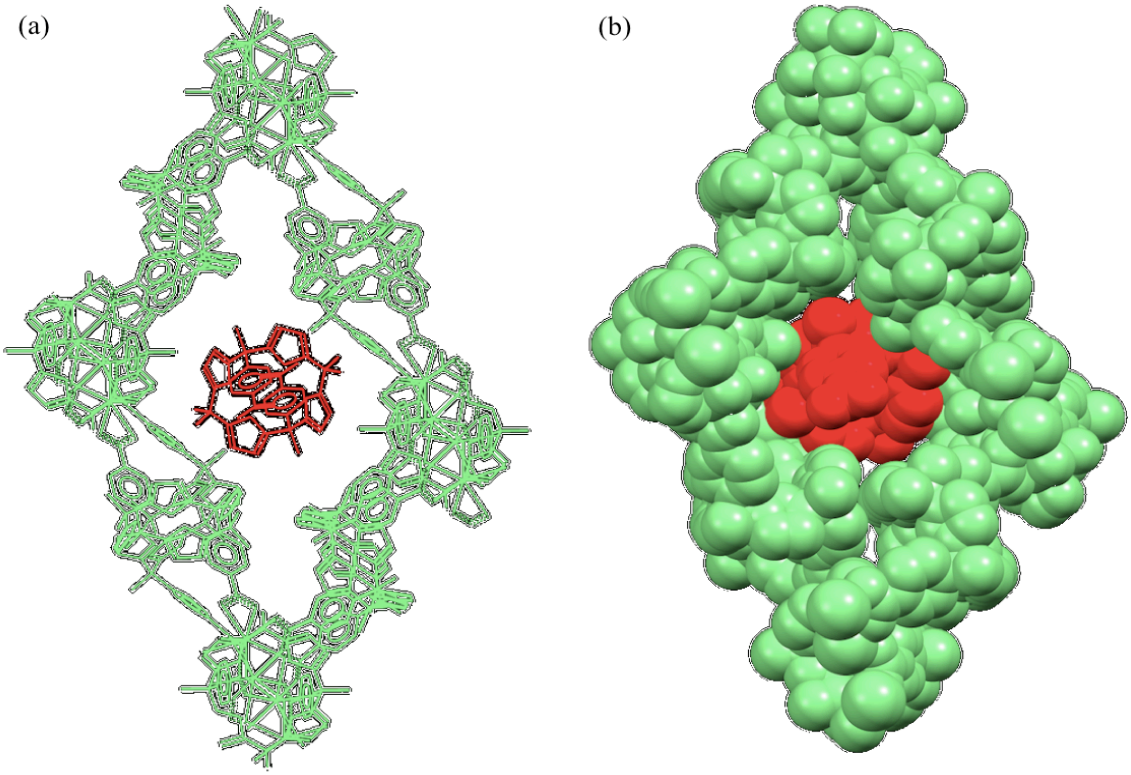

Figure 3.7 (a) Capped stick- and (b) space filling-rendered views of free **3.1** inside the **NMC-1** pore.

In an attempt to remove the uncomplexed calix[4]pyrrole (**3.1**) included within the pore, 10 mg of **NMC-1** crystals were soaked in CD_2Cl_2 or DMSO-d_6 in the presence of 1 μL of ethyl acetate as an internal standard for up to 1 week. Aliquots were obtained daily by decanting off the solvent and refreshing the soaking solution. Analysis by ^{1}H-NMR spectroscopy revealed no peaks ascribable to free calix[4]pyrrole, whereas with time increasing intensity was seen for signals ascribable to DMF and DEF (Figure 3.8).

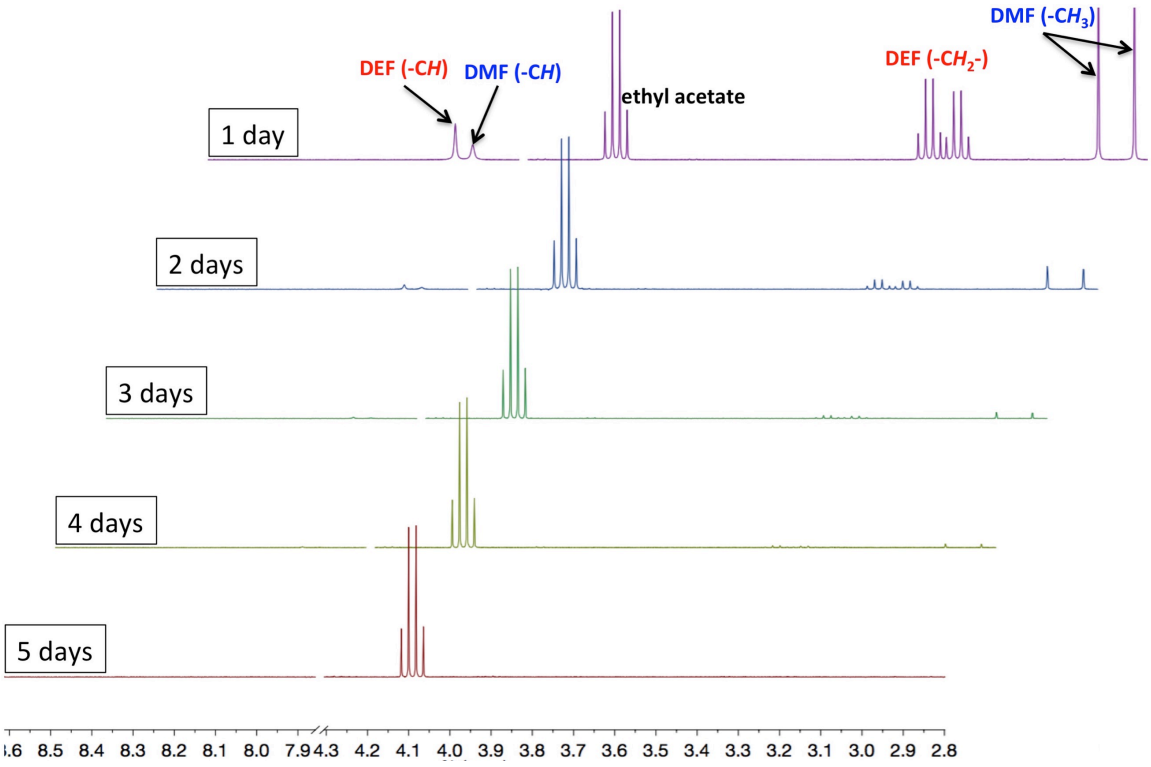

Figure 3.8 Time-dependent views of the upfield region of the ^{1}H-NMR spectra of **NMC-1** soaked in CD_2Cl_2 in the presence of 1 μL of ethyl acetate added as an internal standard.

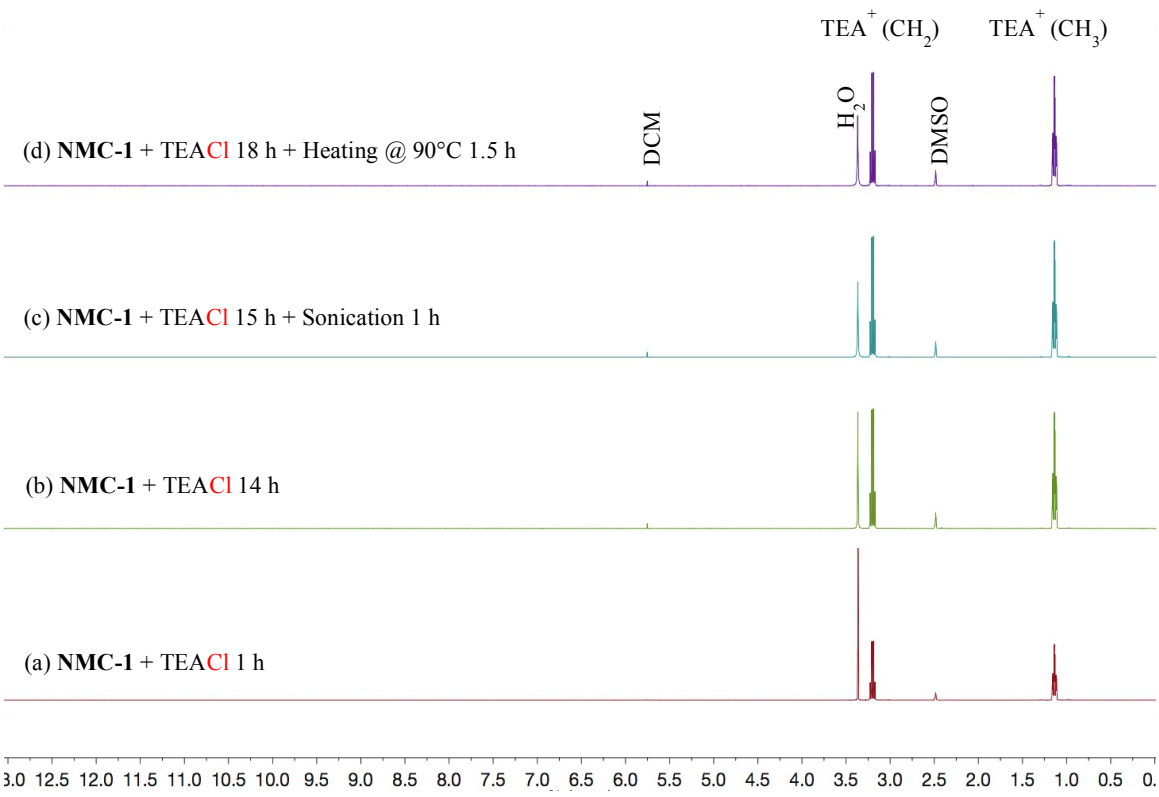

Figure 3.9 ^{1}H-NMR spectra observations of **NMC-1** in the presence of excess of TEACl recorded in DMSO-d_6 under different conditions; (a) soaking for 1 h, (b) soaking for 14 h, (c) sonication for 1 h, following by soaking 15 h, (d) heating at 90 °C for 1 h, following soaking for 18 h.

Heat treatment or sonication proved equally ineffective (Figure 3.9 and 10). Extraction with supercritical CO_2 also failed to remove appreciable quantities of the trapped calix[4]pyrrole, if any, as inferred from an single crystal X-ray diffraction analysis of a sample obtained after subjecting **NMC-1** to this washing process. On this basis, we conclude that the organic fragment contained within the pores of **NMC-1** are not subject to facile removal using standard conventional preservation methods.[2]

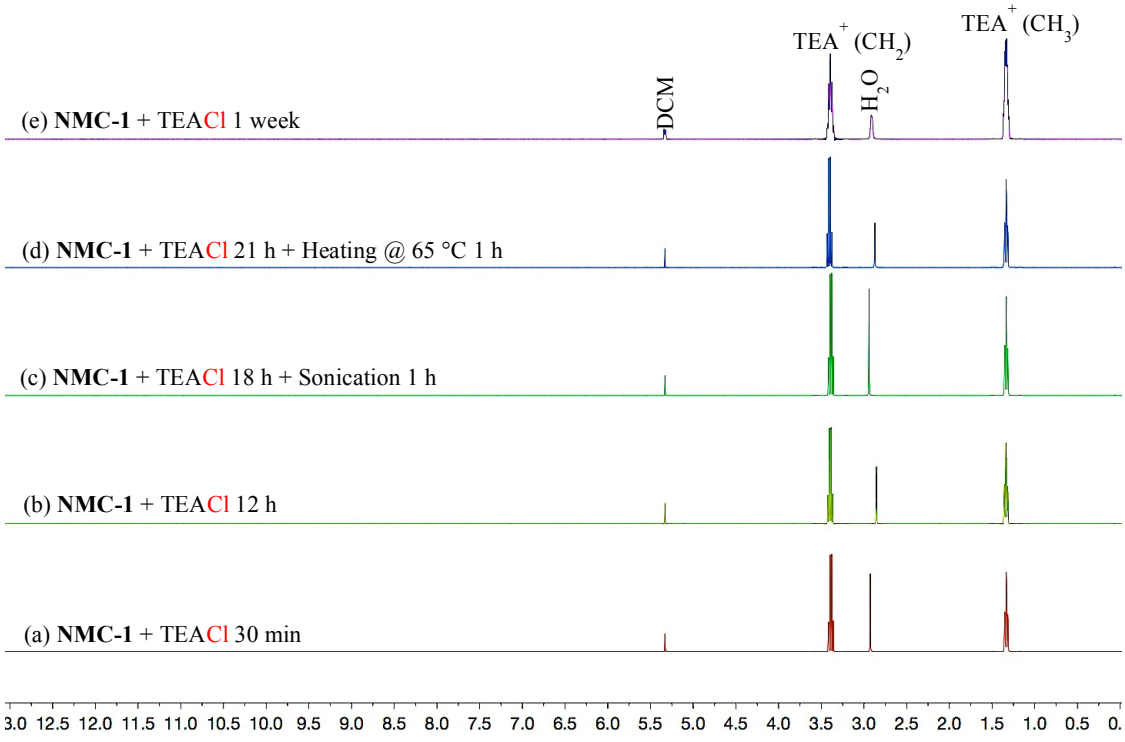

Figure 3.10 ^{1}H NMR spectroscopic observations of **NMC-1** in the presence of excess TEACl recorded in CD_2Cl_2 under different conditions; (a) soaking for 0.5 h, (b) soaking for 12 h, (c) sonication for 1 h, following soaking for 18 h, (d) heating at 65 °C for 1 h, following soaking for 21 h, (e) soaking for 1 week.

The entrapped nature of the guest within **NMC-1** makes the system as a whole reminiscent of a 'ship in a bottle', a classic mechanical puzzle wherein an elaborate species is constrained within a glass vessel with an orifice too small to allow its entry. Only breaking of the bottle permits facile release of the intact construct (the ship in the macroscopic analogy) without requiring its microscopic disassembly. With such a consideration in mind, an effort was made to find a species that would allow for destruction of the networked molecular cage **NMC-1** and release of the embedded ligand, **3.1**. It was found that treatment with fluoride anions induced breakage of the framework

and release of the bound **3.1** 'ship'. Specifically, when the insoluble, crystalline material **NMC-1** was soaked in a DMSO-d_6 solution of tetraethylammonium fluoride (TEAF), appreciable release was engendered within 12 h as inferred from ^{1}H NMR spectral analysis (Figure 3.11). In particular, proton signals corresponding to the fluoride-bound form of **3.1** were seen. It is noteworthy that fluoride treatment is more suitable for use in this framework decomposition and calix[4]pyrrole release process than exposure to acid, since the latter leads to decomposition of the calix[4]pyrrole molecule. In contrast, tetraethylammonium chloride (TEACl) proved ineffective under similar conditions.

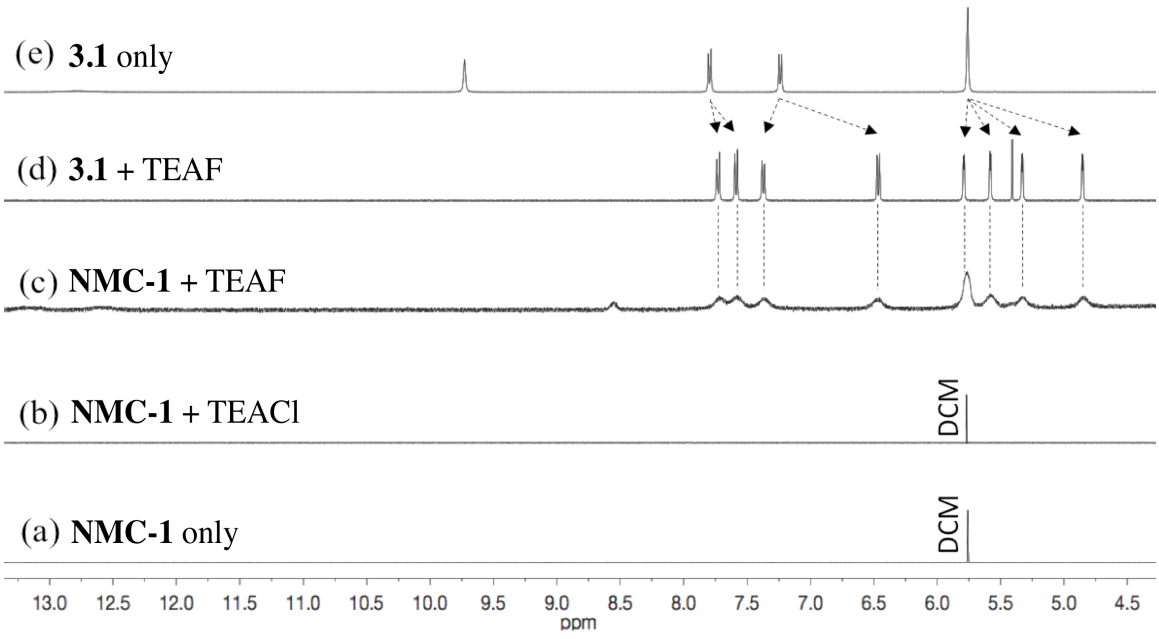

Figure 3.11 Partial ^{1}H NMR spectra of (a) **NMC-1** (10 mg) only, (b) **NMC-1** + TEACl, (c) **NMC-1** + TEAF, (d) **3.1** + TEAF, (e) **3.1** only in DMSO-d_6. TEACl = tetraethylammonium chloride, TEAF = tetraethylammonium fluoride. Anion salts were used in excess. Spectra for (a)-(c) were taken after 12 h.

To understand better the fluoride anion-induced decomposition of **NMC-1**, a control 3D porous framework (**NMC-2**) was constructed via the solvothermal reaction of biphenyl-4,4'-dicarboxylic acid (**3.5**) and $Pr(NO_3)_3 \cdot 6H_2O$ (Scheme 3.3, Figure 3.12).

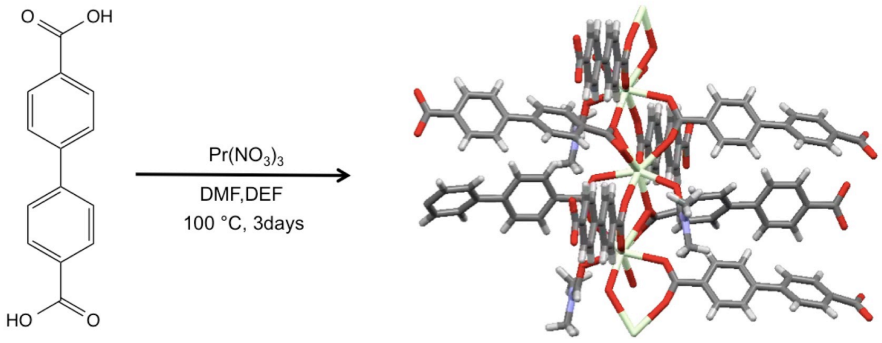

3.5 **NMC-2**

Scheme 3.3 Synthesis and crystal structure of **NMC-2**.

When this control material was soaked in a TEAF-DMSO-d_6 solution for 12 h, ^{1}H NMR spectral analysis revealed the presence of two Ar*H* doublet peaks corresponding to the free biphenyl subunit. This is taken as an indication that the framework was being destroyed. On this basis, we conclude that the 'bottle breakage' reaction leading to release of **3.1** from **NMC-1** is based on the reaction between the fluoride anion and the Pr(III) cluster (Figure 3.13). It is possible, however, that interactions between the calix[4]pyrrole building block and the fluoride anion facilitates this breakup process.

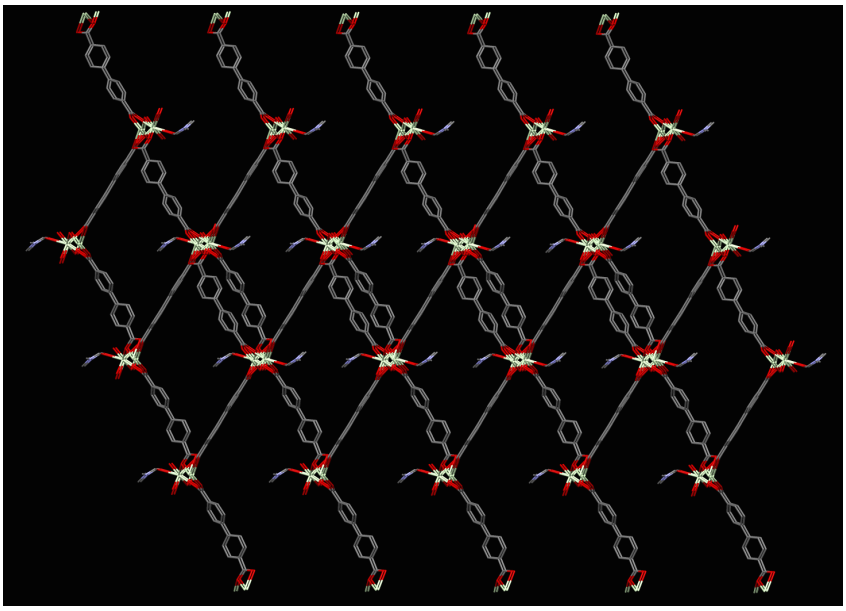

Figure 3.12 Single crystal X-ray diffraction structure of **NMC-2**.

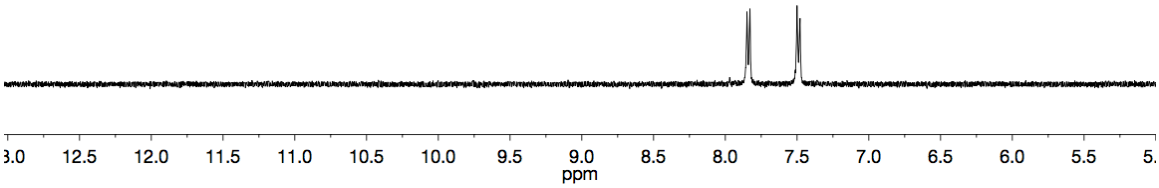

Figure 3.13 Partial ^{1}H NMR spectra of **NMC-2** in DMSO-d_6 recorded 12 h after the addition of an excess of TEAF.

The gas adsorption features of **NMC-1** were also investigated. In 2010, Torrisi and co-workers reported that lone pair donor atoms (N, O) and hydrogen bond donors can enhance the CO_2 binding energies of MOFs by up to 8 kJ mol^{-1} and 3–4 kJ mol^{-1}, respectively.[10] Calix[4]pyrrole provides multiple pre-organized lone pairs and hydrogen bonding donor groups and, in fact, **NMC-1** displayed selective CO_2 adsorption over CH_4, O_2, H_2, and N_2 with a calculated BET surface area of 250 m^2 g^{-1} (Figure 3.14).

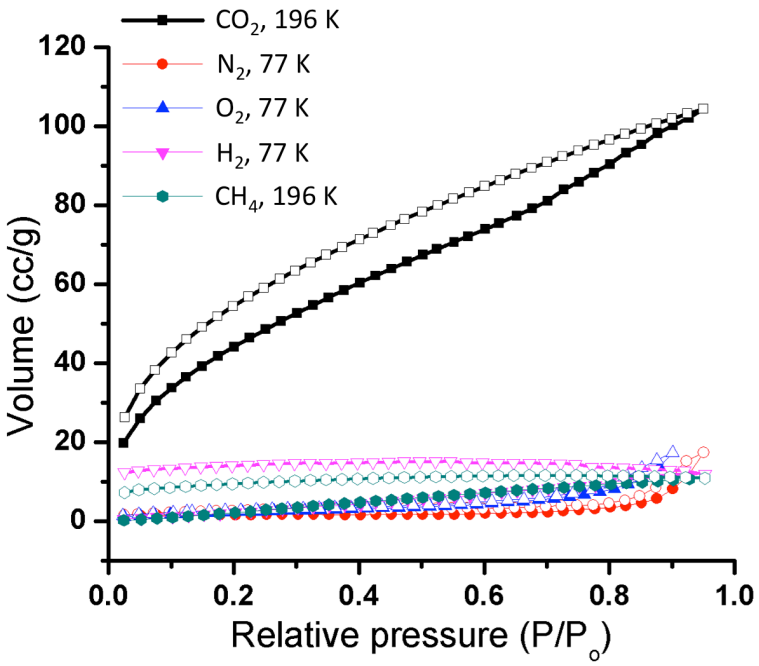

Figure 3.14 Gas adsorption and desorption isotherms of **NMC-1** for CO_2 at 196K, N_2 at 77K, O_2 at 77K, H_2 at 77K, and CH_4 at 196K.

The reversible CO_2 adsorption isotherm at 196K is consistent with a microporous material characterized by pseudo-type-I adsorption behavior. In addition to evidence of a subtle step in the CO_2 adsorption rate at $P/P_o = 0.7$, a moderate hysteresis was evident upon CO_2 removal. Both of these observations are consistent with pore-filling and un-filling dynamics commonly associated with larger pores that contain bottlenecks.[11] The dramatically lower uptake seen for other probe gases at 1.0 atm leads is consistent with pore openings that restrict their adsorption through selective gating.[12]

3.3 CURRENT AND FUTURE WORK

Investigation of the magnetic characteristics of lanthanide-based metal organic frameworks is of interest due to their possible larger spin quantum numbers and the lack of covalent bonding associated with the 4*f* orbitals. This makes it possible to produce clusters with relatively high magnetization.[13] Magnetic susceptibility data for **NMC-1** (**NMC-1$_{Pr}$**) and its isostructure congener, **NMC-1$_{Nd}$** were obtained. The isostructural framework **NMC-1$_{Nd}$** was constructed via the solvothermal reaction of **3.1** and $Nd(NO_3)_3 \cdot 6H_2O$ with oxalic acid/NaOH in a 2:2:1 (v/v) DMF/DEF/H_2O mixture at 100 °C for 3 days.

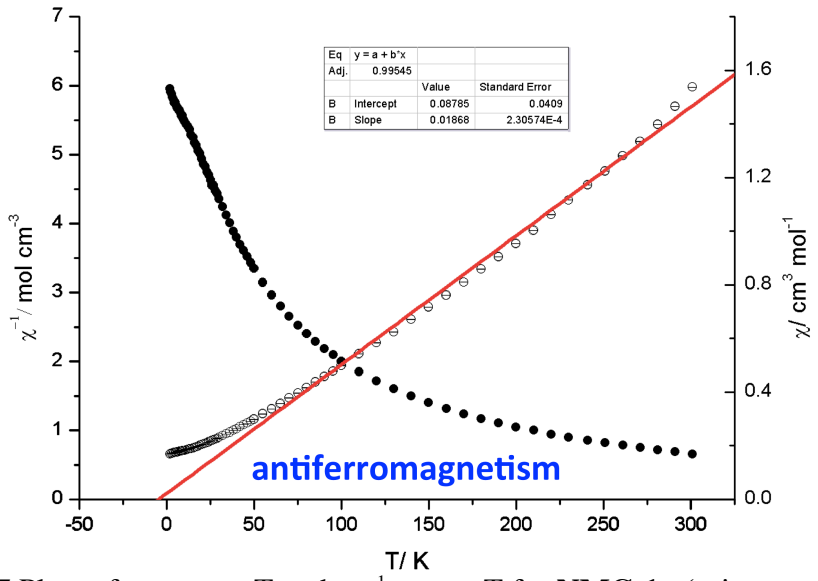

Figure 3.15 Plots of χ_m versus T and χ_m^{-1} versus T for **NMC-1$_{Pr}$** (x-intercept = -4.7 K).

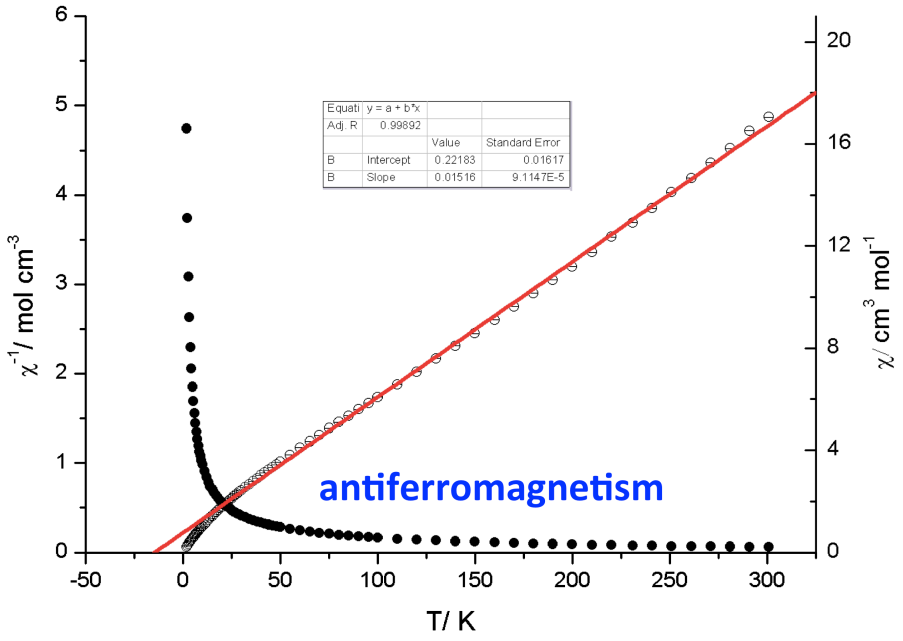

Figure 3.16 Plots of χ_m versus T and χ_m^{-1} versus T for **NMC-1$_{Nd}$** (x-intercept = -14.6 K).

The field-cooled magnetic susceptibilities of **NMC-1$_{Pr}$** and **NMC-1$_{Nd}$** were recorded at an external field of 1000 Oe over the 0.5-300 K range of temperature. Both sets of χ_m versus T data were characterized by continuously increasing susceptibilities with a decrease in temperature occurring without discontinuity. Inverse chi plots revealed that the Pr^{3+} and Nd^{3+} materials have negative Weiss values of -4.7 K and -14.6 K, respectively. This was taken as an indication that both frameworks are antiferromagnetically ordered (Figure 3.15 and 3.16). We are currently collaborating with Dr. Paul Wood of the University of Cambridge to compare theoretical models of magnetic behavior to the experimental magnetic susceptibility data shown above.

3.4 CONCLUSION

In summary, we have developed a novel meso-functionalized calix[4]pyrrole-based 3D network, **NMC-1**, that acts as a molecular cage. This material retains free calix[4]pyrrole molecules within its pores and represents a molecular-scale analogue of a 'ship in a bottle'. Like its macroscopic analogues, **NMC-1** will only allow release of its bound substrate when it is broken. This requisite destruction can be achieved by treating with a fluoride anion source, which serves to release free (uncomplexed) calix[4]pyrrole in the form of its fluoride anion complex. The present system also displays classic MOF-like features and acts as an absorbent for small gases. It shows a particularly high affinity for CO_2 relative to other gaseous guests, an effect ascribed to the lone pair and hydrogen bonding donors provided by the calix[4]pyrrole-based building block used to link the Pr(III) clusters present in **NMC-1**. Given its unusual properties, we predict that **NMC-1** and its analogues based on **3.1** or other calix[4]pyrrole SBUs will have a role to play in the stabilization of new, interesting MOF structures.

3.5 REFERENCES

1) Special issue of *Chem. Rev.* **2012**, *112*, 673-1268. (b) Special issue of *Chem. Soc. Rev.* **2014**, *43*, 5415-6172.

2) Garcia-Simon, C.; Carcia-Borras, M.; Gomez, L.; Parella, T.; Osuna, S.; Juanhuix, J.; Imaz, I.; Maspoch, D.; Costas, M.; Ribas, X. *Nat. Commun.* **2014**, *5*, 5557.

3) Baeyer, A.; *Ber. Dtsch. Chem. Ges.* **1886**, *19*, 2184–2185.

4) (a) Kim, D. S.; Sessler, J. L. *Chem. Soc. Rev.* **2015**, *44*, 532-546. (b) Saha, I.; Lee, J. T.; Lee, C. *Eur. J. Org. Chem.* **2015**, 3859-3885. (c) Adriaenssens, L.; Ballester, P. *Chem. Soc. Rev.* **2013**, *42*, 3261. (d) Osorio-Planes, L.; Espelt, M.; Pericas, M. A.; Ballester, P. *Chem. Sci.* **2014**, *5*, 4260. (e) Valderrey, V.; Escudero-Adan, E. C.; Ballester, P. *Angew. Chem. Int. Ed.* **2013**, *52*, 6898-6902.

5) (a) Kim, S. K.; Lee, J.; Williams, N. J.; Lynch, V. M.; Hay, B. P.; Moyer, B. A.; Sessler, J. L. *J. Am. Chem. Soc.* **2014**, *136*, 15079-15085. (b) Borman, C. J.; Custelcean, R.; Hay, B. P.; Bill, N. L.; Sessler, J. L.; Moyer, B. A. *Chem. Commun.* **2011**, 7611-7613.

6) Ko, S.; Kim, S. K.; Share, A.; Lynch, V. M.; Park, J.; Namkung, W.; Rossom, W. V.; Busschaert, N.; Gale, P. A.; Sessler, J. L.; Shin, I. *Nat. Chem.* **2014**, *6*, 885-892. (b) Cafeo, G.; Carbotti, G.; Cuzzola, A.; Fabbi, M.; Ferrini, S.; Kohnke, F. H.; Papanikolaou, G.; Plutino, M. R.; Rosano, C.; White, A. J. *J. Am. Chem. Soc.* **2013**, *135*, 2544-2551.

7) (a) Zhang, H.; Zou, R.; Zhao, Y. *Coord. Chem. Rev.* **2015**, *292*, 74-90. (b) Li, Q.; Zhang, W.; Miljanic, O.S.; Sue, C.H.; Zhao, Y.L.; Liu, L.; Knobler, C.B.; Stoddart, J. F.; Yaghi, O. M. *Science* **2009**, *325*, 855. (c) Vukotic, V. N.; Harris, K. J.; Zhu, K.; Schurko, R. W.; Loeb, S. J. *Nat. Chem.* **2012**, *4*, 456. (d) Hartlieb, K. J.; Holcroft, J.

M.; Moghadam, P. Z.; Vermeulen, N. A.; Algaradah, M. M.; Nassar, M. S.; Botros, Y. Y.; Snurr, R. Q.; Stoddart, J. F. *J. Am. Chem. Soc.* **2016**, *138*, 2292-2301. (e) Ni, X.; Xiao, X.; Cong, H.; Liang, L.; Cheng, K.; Cheng, X.; Ji, N.; Zhu, Q.; Xue, S.; Tao, Z. *Chem. Soc. Rev.* **2013**, *42*, 9480-9508. (f) Wang, K.; Feng, D.; Liu, T.; Su, J.; Yuan, S.; Chen, Y.; Bosch, M.; Zou, X.; Zhou, H. *J. Am. Chem. Soc.* **2014**, *136*, 13983-13986. (g) Kubota, R.; Tashiro, S.; Shiro, M.; Shionoya, M. *Nat. Chem.* **2014**, *6*, 913. (h) Strutt, N. L.; Fairen-Jimenez, D.; Iehl, J.; Lalonde, M. B.; Snurr, R. Q.; Farha, O. K.; Hupp, J. T.; Stoddart, J. F. *J. Am. Chem. Soc.* **2012**, *134*, 17436-17439. (i) Chen, T.; Schneemann, A.; Fischer, R. A.; Cohen, S. M. *Dalton Trans.* **2016**, *45*, 3063.

8) (a) Mikhalyova, E. A.; Kolotilov, S. V.; Zeller, M.; Thompson, L. K.; Addison, A. W.; Pavlishchuk, V. V.; Hunter, A. D. *Dalton Trans.* **2011**, *40*, 10989. (b) Zhang, X.; Fan, L.; Sun, Z.; Zhang, W.; Fan, W.; Sun, L.; Zhao, X. *Cryst. Eng. Comm.* **2013**, *15*, 4910.

9) Allen, W. E.; Gale, P. A.; Brown, C. T.; Lynch, V. M.; Sessler, J. L. *J. Am. Chem. Soc.* **1996**, *118*, 12471-12472.

10) Torrisi, A.; Mellot-Draznieks, C.; Bell, R. G. *J. Chem. Phys.* **2010**, *132*, 044705.

11) Fernandez, C. A.; Liu, J.; Thallapally, P. K.; Strachan, D. M. *J. Am. Chem. Soc.* **2012**, *134*, 9046.

12) (a) Chen, Q.; Chang, Z.; Song, W. –C.; Song, H.; Song, H. -B.; Hu, T. -L.; Bu, X. -H. *Angew. Chem., Int. Ed.* **2013**, *52*, 11550. (b) Fairen-Jimenez, D.; Moggach, S. A.; Wharmby, M. T.; Wright, P. A.; Parsons, S.; Duren, T. *J. Am. Chem. Soc.* **2011**, *133*, 8900. (c) Nijem, N.; Wu, H.; Canepa, P.; Marti, A.; Balkus, K. J.; Thonhauser, T.; Li, J.; Chabal, Y. J. *J. Am. Chem. Soc.* **2012**, *134*, 15201.

13) Waggoner, N. W.; Saccoccia, B.; Ibarra, I. A.; Lynch, V. M.; Wood, P. T.; Humphrey, S. M. *Inorg. Chem.* **2014**, *53*, 12674-12676.

Chapter 4: Uranyl Bearing Extended Calix[4]pyrrole Framework

4.1 INTRODUCTION

Uranium can be found in a variety of sources and is present in both terrestrial and aqueous environments. The principal form of uranium on Earth is the uranyl dication (UO_2^{2+}), as the most stable form in oxidizing environment. Typical uranium ores and coal ash contain uranium at the ~1000 and 300 ppm levels, respectively.[1] The Dnieper River in Kiev is contaminated with uranium at the 11.5 ppm level and the concentration of uranium in of Bavarian drinking water has reached 10 ppb.[2] More than 99% of all global uranium resides in the Earth's oceans, where uranium is presented in the form of the uranyl cation (UO_2^{2+}) at a concentration of ~ 3 ppb.[3] The use of uranium as a fuel for nuclear energy is providing an incentive to develop effective methods for recognition of actinide and dealing with nuclear waste. The linear geometry and short uranium-oxygen bonds of the uranyl ion create an unusual challenge for the rational design of selective complexing ligands.[4]

Ligand design strategies for uranyl complexation are largely based on two traditional coordination chemistry concepts, namely the "Hard and soft, acids and bases" (HSAB) principle[5] and matching the spatial array of donor group to the coordination sites on the metal ion.[6] Since the uranyl ion is classified as a hard ion, it has an enhanced affinity for oxygen atoms; accordingly, many uranyl ion receptors containing carboxylate, catechol, and hydroxypyridinone-amide moieties have been reported.[7] The linearity of the uranyl dioxo atoms limits the approach of donor atoms to the so-called equatorial positions. Typically, 5 or 6 donor atoms are found in the equatorial positions. In natural aqueous environments, three carbonate ligands are typically positioned around the uranyl center in an equatorial coplanar arrangement.[8]

One newer approach to sequestering the uranyl cation involves the creation of uranyl-based nanostructural cages. Burns and co-workers have reported C_{60} fullerene-type, polyhedral cages incorporating uranyl peroxide components with various sized anions, including nitrate, oxalate, and phosphate.[9] In these nanoclusters, the peroxide anions act as bridges between two uranyl clusters to create overall pentagonal or hexagonal bipyramidal structures. However, as a general rule, the lack of axial coordination (other than oxo ligands) favors formation of either one-dimensional chains or two-dimensional sheets. Formation of well-organized three-dimensional structures is particularly challenging when planar aromatic ligands are involved.[10] In 2012, giant regular polyhedral made up from calixarene carboxylates and the uranyl cation were described by Mendoza and co-workers.[11] These researchers showed that the use of bowl-shaped calix-[4]- and -[5]-arenes carboxylic acids in conjunction with a uranyl cation source promotes self-assembly into hexameric cages and icosahedral structures, respectively. In a very recent report, Thuery and Harrowfield showed that racemic or enantiopure (1*R*, 2*R*) forms of *trans*-1,2-cyclohexanedicarboxylic acid could be used to form pseudotetrahedral cluster cages.[12] The clusters in question were obtained under solvohydrothermal conditions from the corresponding diacids in the presence of uranyl nitrate and guanidinium nitrate in a ratio of 4 : 3 (uranyl : diacid). These anionic clusters can incorporate alkali or alkaline-earth metal cations, such as Na^+, K^+, Ba^{2+}, Rb^+, and Cs^+, to form either higher dimensionality assemblies or heterometallic cuboidal clusters depending on the conditions.

In this chapter the chemistry of new uranyl-based cage complexes constructed from dibenzoic acid functionalized *cis*-calix[4]pyrrole is reported. As detailed below, the reaction of *cis*-calix[4]pyrrole dibenzoic acid **4.1** with the uranyl cation in the presence of organic bases (triethylamine and pyridine) under aerobic condition allows the formations

of tri- (**cage-1**) and tetrapodal (**cage-2**) cage structures. The product obtained depends on the existence and nature of the actual uranyl peroxide species (Figure 4.1).

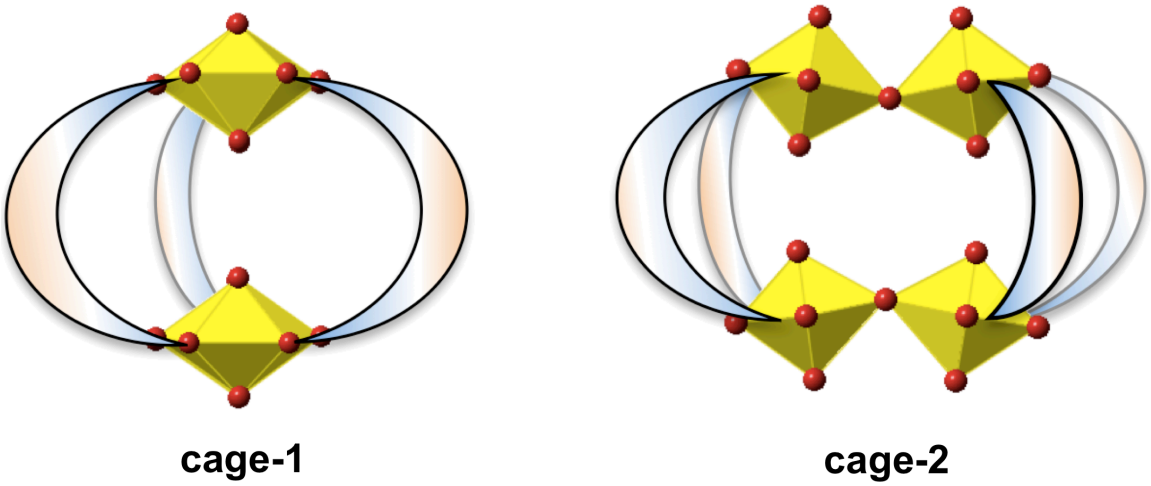

Figure 4.1 Simplified cartoon representations of the tri- and tetrapodal cages, **cage-1** and **cage-2**.

4.2 RESULT AND DISCUSSION

The synthesis of *cis*-calix[4]pyrrole dibenzoic acid **4.1** is shown in Scheme 4.1. The *cis* form of disubstituted methyl benzoate calix[4]pyrrole **4.2** was obtained by condensing of **3.3** with acetone in the presence of TFAA in 9% yield. A subsequent hydrolysis produced the desired compound **4.1** in 95% yield based on **4.2**. Single crystals of **4.1** suitable for X-ray diffraction analysis were obtained by slow evaporation from acetonitrile (Figure 4.2).

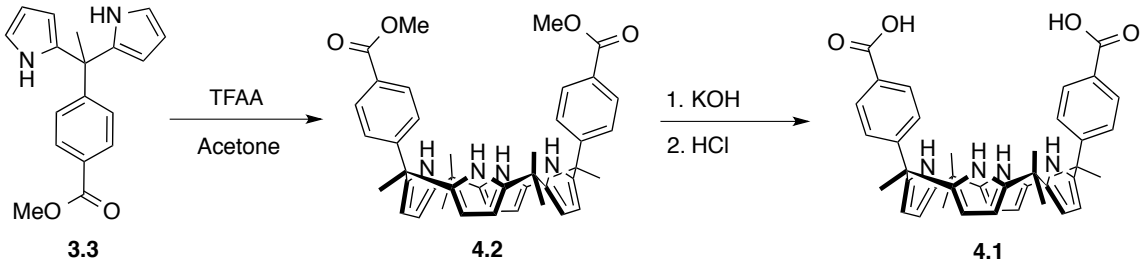

Scheme 4.1 Synthesis of compound **4.1**.

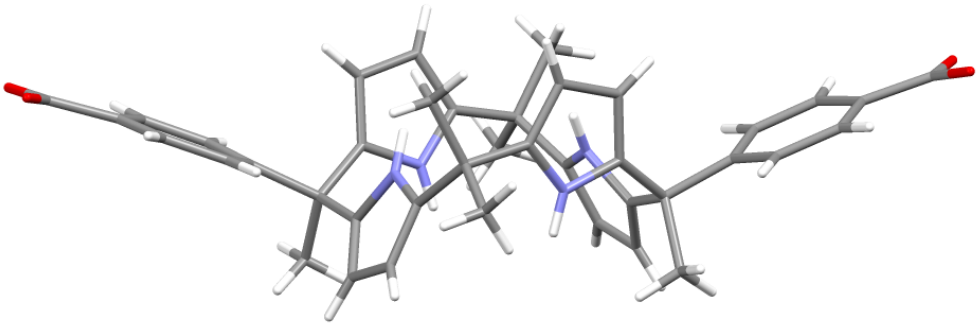

Figure 4.2 X-ray structure of compound **4.1**.

Formation of cages was achieved in the presence of organic bases, such as either triethylamine or pyridine, which allows deprotonation of the carboxylic acids moieties present in the ligands.

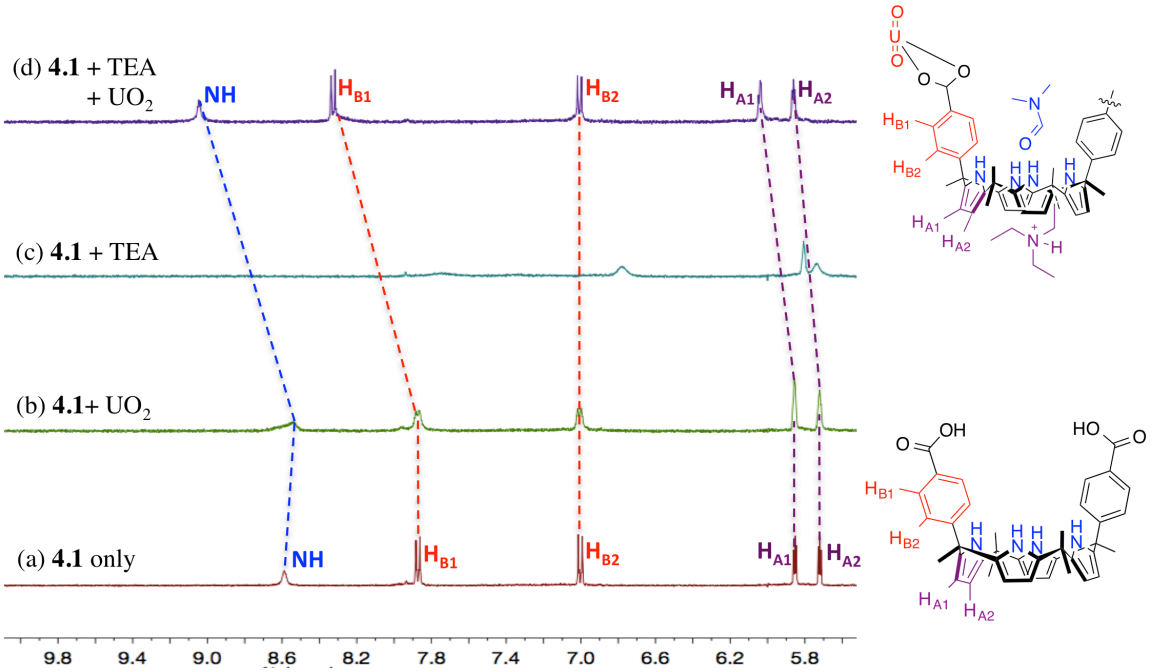

Figure 4.3 Partial ^{1}H NMR spectra of (a) **4.1** only (3.75 mM), (b) **4.1** + 0.66 equiv of $UO_2(NO_3)_2{\cdot}6H_2O$, (c) **4.1** + 38.22 equiv of TEA (triethylamine), and (d) **4.1** + 0.66 equiv of $UO_2(NO_3)_2{\cdot}6H_2O$ + 38.22 equiv of TEA, recorded at room temperature in CD_3CN (1.5% DMF-d_7)

Initial evidence that **4.1** supports formation of a uranyl complex in solution came from ^{1}H NMR spectroscopic analyses carried out in CD_3CN (1.5% DMF-d_7). As shown in Figure 4.3, when exposed to both uranyl nitrate and triethylamine, a proton signal corresponding to the ortho-position (H_{B1}) on the benzoate unit undergoes a downfield shift ($\Delta\delta_{HB1}$ = 0.44 ppm), whereas no substantial chemical shift is observed under conditions of exposure to the uranyl ion or triethylamine individually. The change in the chemical shift of the H_{B1} signal is ascribed in to the proton adjacent to the carboxylate moiety becoming deshielded as the result of uranyl complexation. In addition, downfield shifts for the NH proton and β-pyrrolic proton resonances are seen. These changes are ascribed to hydrogen bonding between the pyrrolic NHs and the carbonyl group of DMF-d_7 (*N,N'*-dimethylformamide-d_7) and cation-π interactions between the pyrrole rings and a protonated triethylamine moiety. These changes are taken as evidence that the calix[4]pyrrole unit adopts a cone-like conformation with a pair of parallel benzoates due to interactions with DMF and protonated triethylamine cation. This stands in contrast to the 1,3-conformation seen for the free calix[4]pyrrole, where the two benzoic acids are oriented in opposite directions from one another, as seen in the X-ray structure of **4.1** (Figure 4.2). The conformational locking seen upon uranyl complexation imparts rigidity to the normally flexible ligand **4.1** and facilitates the formation of tripodal **cage-1**. In the cage structure each benzoate anion is bound to two separate uranyl cations. As typical for uranyl, these ligands occupy equatorial position and are present in a 3 : 2 (ligand : uranyl) ratio (Figure 4.1).

DOSY spectral analysis of the uranyl complex solution revealed one set of signals for the complex, which indicates only a single complex species dominates at equilibrium (Figure 4.4). This finding was supported by ESI-MS data that proved consistent with what would be expected for **cage-1** (peak at 2456.36 amu).

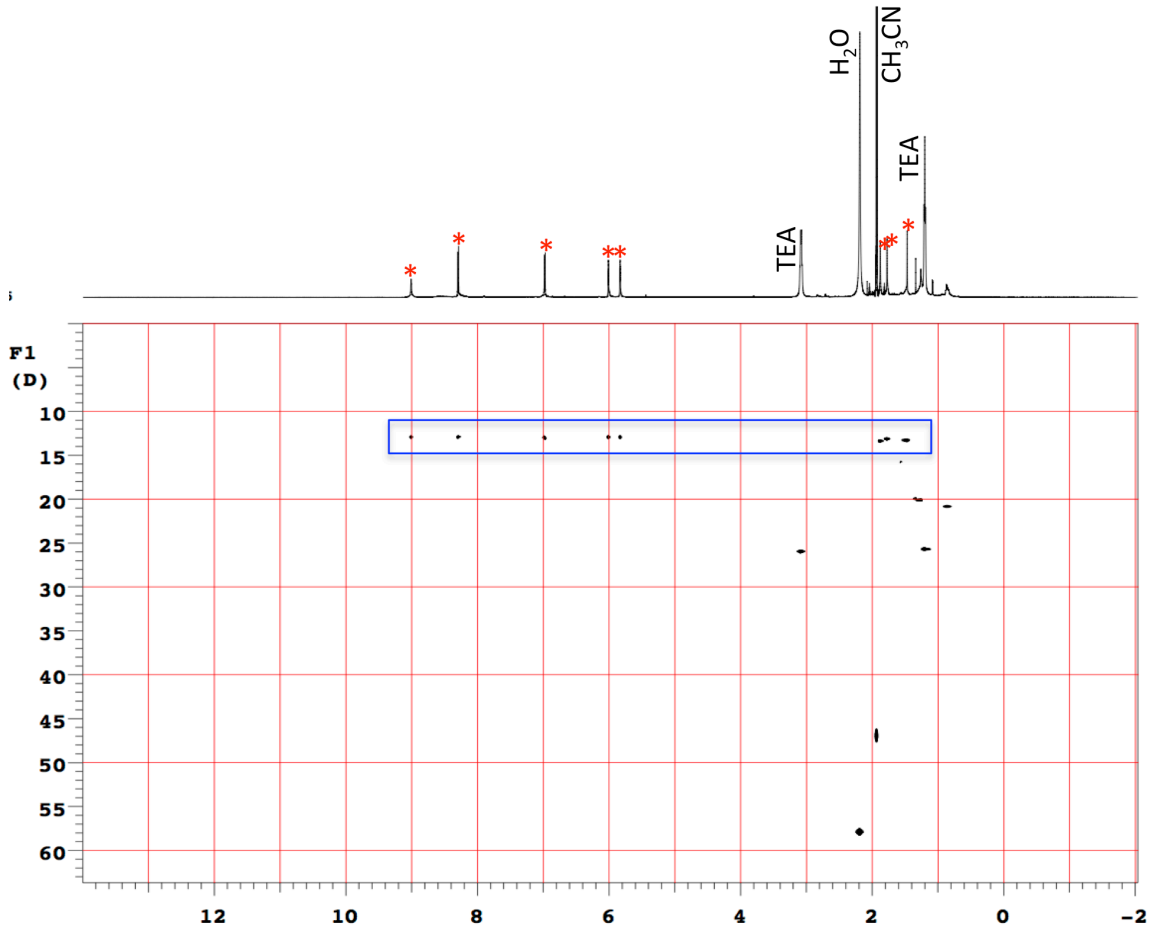

Figure 4.4 DOSY spectrum of **4.1** (3.75 mM) + 0.66 equiv of $UO_2(NO_3)_2 \cdot 6H_2O$ + 38.22 equiv of TEA, recorded at room temperature in CD_3CN (1.5% DMF-d_7).

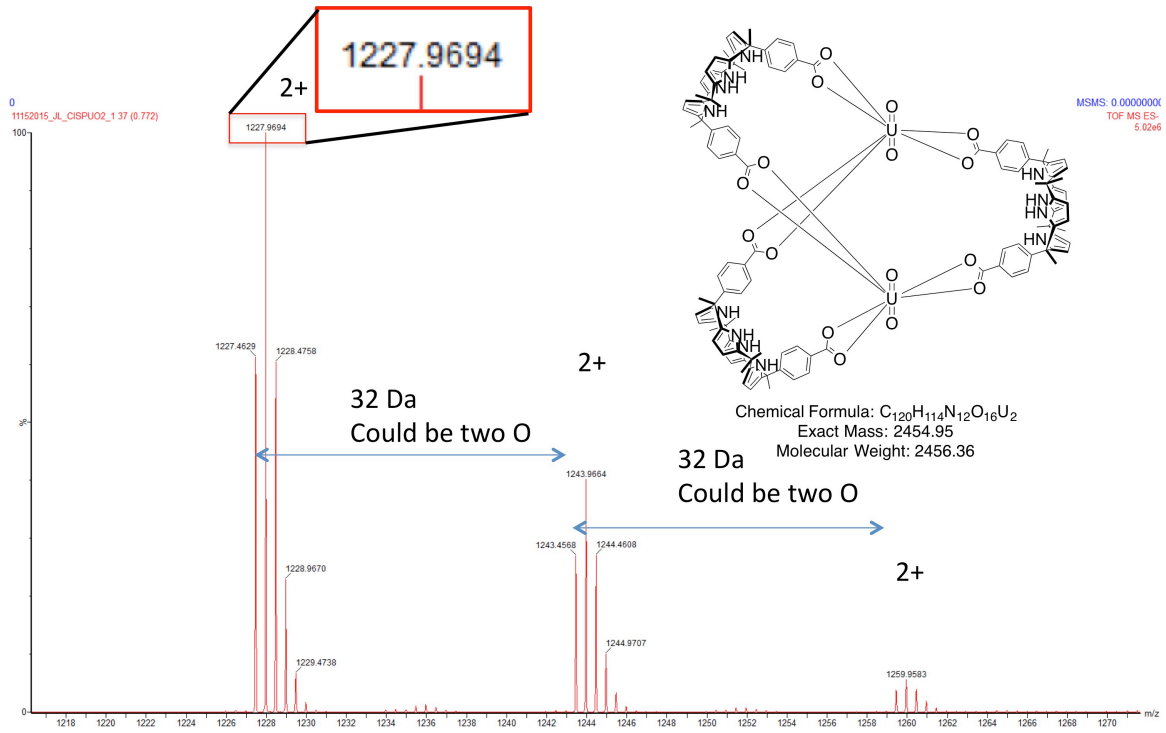

Figure 4.5 ESI-MS data for a mixture of **4.1** + 0.66 equiv of $UO_2(NO_3)_2 \cdot 6H_2O$ + 38.22 equiv of TEA in acetonitrile (1.5% DMF).

A single crystal X-ray diffraction analysis of the **cage-1** was attempted. Block-shape crystals suitable for X-ray diffraction analysis were obtained from the slow evaporation of an acetonitrile (1.5% DMF) mixture of **4.1** and uranyl nitrate (3 : 2 = L : M), where L = ligand and M = metal salt, in the presence of excess (82.74 equiv) of pyridine. The resulting crystal structure revealed that four **4.1** ligands are bound to a uranyl peroxide species to form the tetrapodal **cage-2** structure, instead of the expected tripodal **cage-1** (Figure 4.7). **Cage-2** crystallizes in the primitive monoclinic space group $P2_1/n$ and shows centrosymmetry. The cage is comprised of four calix[4]pyrrole and two uranyl peroxide $[(UO_2)(O_2)]^{2+}$ subunits. In the solid state the pyrrolic NHs of each calix[4]pyrrole unit hydrogen bond to a DMF molecule and are found in their cone

conformations. This is consistent with what was inferred from the ^{1}H NMR spectral analysis.

The formation of the peroxide ions that are bound to the uranyl ions is ascribed to either the sunlight-induced photochemical oxidation of water or oxidation of a hydoxo-bridged diuranyl complex that is produced in a basic solution.[13] Uranyl complex contains peroxo ligands also can be synthesized straightforwardly by reacting H_2O_2 with uranyl.[14] Indeed, an ESI-MS analysis of a solution of **cage-1** mixed with additional H_2O_2 revealed peaks consistent with the formation of **cage-2** (Figure 4.6). These findings provide support for the notion that the transformation from **cage-1** to **cage-2** can be achieved by applying sunlight or via the simple addition of hydrogen peroxide.

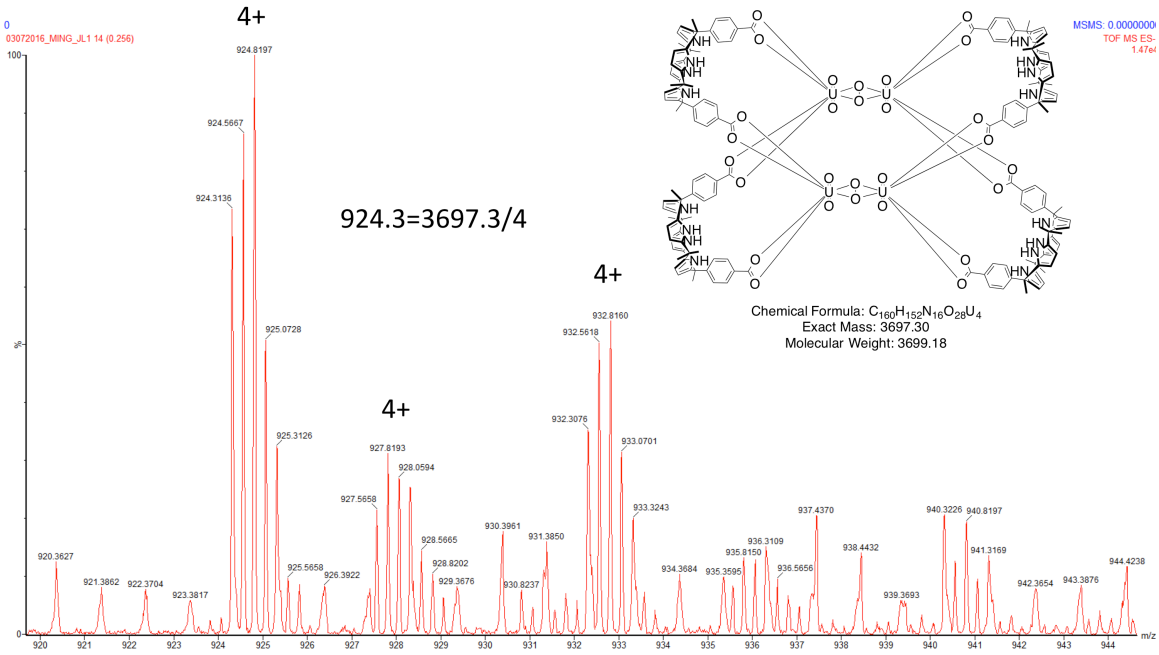

Figure 4.6 ESI-MS analysis of a mixture of **4.1** + 0.66 equiv of $UO_2(NO_3)_2{\cdot}6H_2O$ + 38.22 equiv of TEA + H_2O_2 (excess) in acetonitrile (1.5% DMF).

In separate ongoing work efforts are being made to obtain crystals of **cage-1** grown in a dark environment. To the extent the resulting structure matched our expectations, it would provide additional proof of our findings.

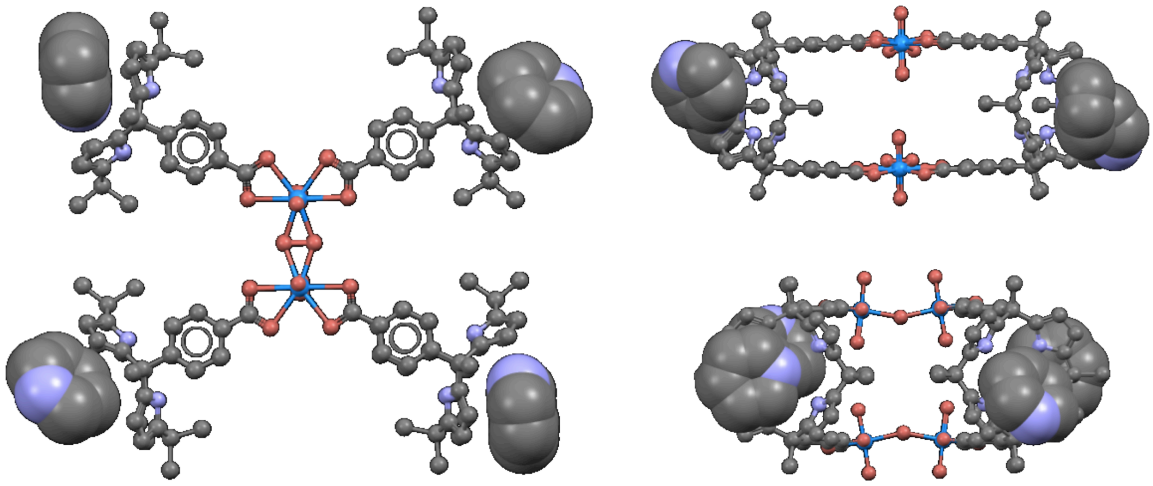

Figure 4.7 Top view (left) and side views (right) of the single-crystal structure of **cage-2**. Solvent molecules have been omitted for clarity.

It is worth noting that the anionic **cage-2,** $[(UO_2)_2(O_2)_2(\mathbf{4.1})_4]^{4-}$ requires four countercations to balance the overall negative charge. As can be seen in the X-ray structure shown in Figure 4.7, a pyridinium cation is incorporated within the "cup" of each calix[4]pyrrole.

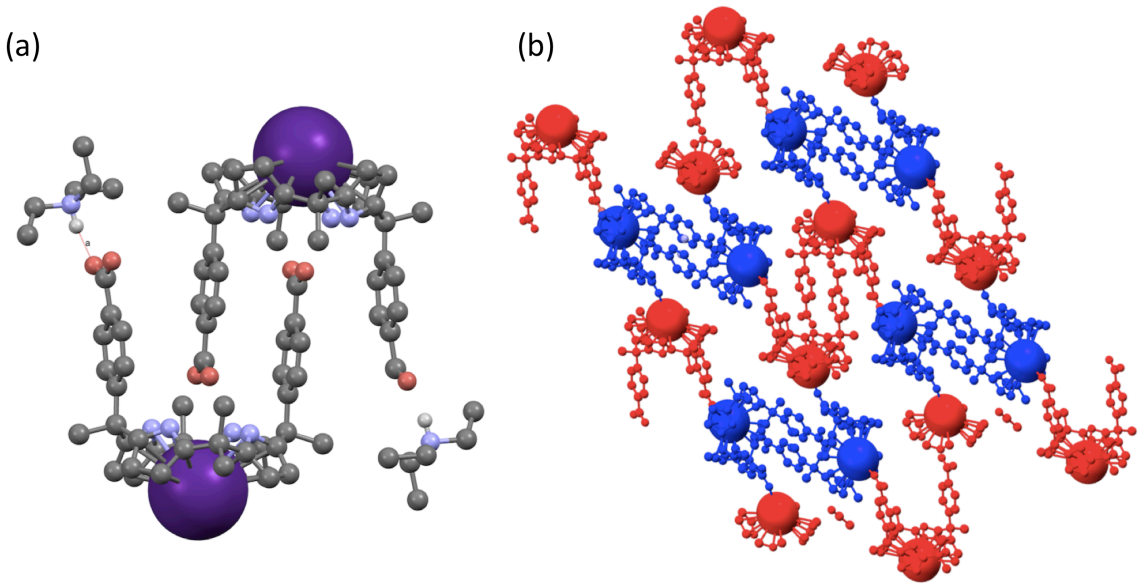

Figure 4.8 Left : Single-crystal structure of Cs^+ complex of dimerized **4.1**. Right : Partial view of the extended 2-dimensional structure seen in the crystal lattice.

Calix[4]pyrroles are known to accommodate appropritately sized charge balancing cations, such as Cs^+ and methyltrialkylammonium, within the "cup" formed by the pyrrole rings. When an acetonitrile (1.5% DMF) solution **4.1** is exposed to $CsNO_3$ in the presence of triethylamine, colorless block shape crystals suitable for X-ray diffraction analysis were obtained within 2 hours (Figure 4.8). The resulting structure revealed that two separate calix[4]pyrrole ligands are dimerized in the cone conformation through hydrogen bonding between the pyrrolic NHs and one of the deprotonated carboxylic acid groups. Being likewise cesium cations are found in the "cup" of each calix[4]pyrrole, where they appear stabilized through cation-π interactions while bound to the other free carboxylate. As a consequence, dimers structures of **4.1** are linked by cesium ions to form a 2-dimensional sheet structure. This finding leads us to suggest that **cage-1** and **cage-2**, if functionalized with appropriately chosen ditopic cations could be used to produce more heavily cross-linked extended structures. To the extent this proven true, it could allow a

new crystallization-based separation of uranyl and $^{137}Cs^{+}$ from radioactive nuclear wastes. The further ability to stabilize uranyl peroxide species (generated via α-radiolysis of water during dissolution of spent nuclear fuel[14]) would be an additional attractive feature of such a carboxylate functionalized calix[4]pyrrole **4.1**–based remediation strategy.

4.3 CONCLUSIONS

In summary, a *meso*-substituted *cis*-dibenzoic acid calix[4]pyrrole **4.1** has been synthesized. In the presence of organic bases, it forms tripodal cage (**cage-1**) structure with the uranyl ion. A presumed sunlight induced photochemical oxidation allows this tripodal cage to transform to tetrapodal structure (**cage-2**), wherein diuranyl peroxide species are located in the middle and on the top and bottom portions of the cage. This transformation also occurs upon addition of hydrogen peroxide to **cage-1**. Both cages accommodate counter cations within the "cup" of the calix[4]pyrrole. The polytopic nature of the structures leads to the suggestion that calix[4]pyrrole **4.1** could support the formation of more extended frameworks in rough use of, e.g., bis-cations. Separately, it is proposed that **4.1** could be used to effect the crystallization-based separation of the uranyl and $^{137}Cs^{+}$ cations.

4.4 REFERENCES

1) The Economist. *Novel Sources of Uranium: Rising from the Ashes*, April 8, 2010, http://www.economist.com/node/15865280?story_id=15865280, accessed September 10, 2010.
2) Balonov, M.; et al. *Radiological Conditions in the Dnieper River Basin*; Radiological Assessment Reports Series; International Atomic Energy Agency: Vienna, 2006.
3) Schwochau, K. *Top. Curr. Chem.* **1984**, *124*, 91.
4) Gorden, A. E. V.; Xu, J.; Raymond, K. N. *Chem. Rev.* **2003**, *103*, 4207-4282.
5) Pearson, R. G. *J. Am. Chem. Soc.* **1963**, *85*, 3533.
6) (a) Cram, D. J.; Lehn, J. M. *J. Am. Chem. Soc.* **1985**, *107*, 3657. (b) Hay, B. P.; Hancock, R. D. *Coord. Chem. Rev.* **2001**, *212*, 61.
7) (a) Szigethy, G.; Raymond, K. N. *J. Am. Chem. Soc.* **2011**, *133*, 7942-7956. (b) Watson, L. A.; Hay, B. P. *Inorg. Chem.* **2011**, *50*, 2599-2605. (c) Beer, S.; Berryman, O. B.; Ajami, D.; Rebek, J. *Chem. Sci.* **2010**, *1*, 43-47. (d) Sather, A. C.; Berryman, O. B.; Rebek, J. *J. Am. Chem. Soc.* **2010**, *132*, 13572-13574. (e) Sather, A. C.; Berryman, O. B.; Moore, C. E.; Rebek, J. *Chem. Commun.* **2013**, *49*, 6379-6381.
8) Cinneide, S. O.; Scanlan, J. P.; Hynes, M. J. *Inorg. Nucl. Chem.* **1975**, *37*, 1013.
9) (a) Qiu, J.; Burns, P. C. *Chem. Rev.* **2013**, *113*, 1097–1120. (b) Burns, P. C.; Kubatko, K.-A.; Sigmon, G.; Fryer, B. J.; Gagnon, J. E.; Antonio, M. R.; Soderholm, L. *Angew. Chem., Int. Ed.* **2005**, *44*, 2135–2139. (c) Qiu, J.; Ling, J.; Jouffret, L.; Thomas, R.; Szymanowski, J. E. S.; Burns, P. C. *Chem. Sci.* **2014**, *5*, 303–310.
10) Wang, K.; Chen, J. *Acc. Chem. Res.* **2011**, *44*, 531-540.

11) Pasquale, S.; Sattin, S.; Escudero-Adan, E. C.; Martinez-Belmonte, M.; Mendoza, J. *Nat. Commun.* **2012**, *3*, 785.

12) Thuery, P.; Harrowfield, J. *Cryst. Growth Des.* **2017**, *17*, 2881-2892.

13) McGrail, B. T.; Pianowski, L. S.; Burns, P. C. *J. Am. Chem. Soc.* **2014**, *136*, 4749-4800.

14) Thangavelu, S. G.; Cahill, C. L. *Inorg. Chem.* **2015**, *54*, 4208-4221.

Chapter 5: Experimental Section

All reagents and solvents were purchased from Aldrich, TCI, and Acros and used without purification. Compounds **2.4**[1] and **2.7**[2] were prepared as previously reported. NMR spectra were recorded on a Varian Direct Drive 400 MHz and Varian MR 400 MHz instruments. The NMR spectra were referenced to solvent and the spectroscopic solvents were purchased from Cambridge Isotope Laboratories. Chemical ionization (CI) and electrospray ionization (ESI) mass spectra were recorded on a VG ZAB-2E instrument and a VG AutoSpec apparatus, respectively. TLC analyses were carried out using Sorbent Technologies silica gel (200 mm) sheets. Column chromatography was performed on Sorbent silica gel 60 O (40–63 mm) or neutral alumina (50–200 mm, Brockmann grade II). For microcalorimetric titrations a MicroCal VP-ITC instrument was used.

Compound 2.6 A mixture of naphthobipyyrole dicarboxylic acid (**2.4**) (2.00 g, 5.71 mmol), 5-(3-hydroxypropyl)-5-methyl dipyrromethane (**2.5**) (2.86 g, 13.1 mmol), EDCI (1-ethyl-3-(3- dimethylaminopropyl)-carbodiimide, 3.28 g, 17.1 mmol) and DMAP (4-dimethylaminopyridine, 1.39 g, 11.4 mmol) in dry dichloromethane (100 ml) was stirred overnight at room temperature and concentrated under reduced pressure to give a yellowish oil. To this crude product, dichloromethane (200 ml) and water (200 ml) were added. The organic phase was separated off and washed twice with water (200 ml). The resulting organic layer was dried over anhydrous $MgSO_4$ and evaporated in vacuo to give a yellowish solid. Recrystallization from dichloromethane/hexanes (1/9), following column chromatography over silica gel (ethyl acetate/hexane = 1/3, eluent), gave **2.6** (2.24 g, 52% yield) as a yellowish solid. ^{1}H NMR (400 MHz, $CDCl_3$): δ 11.32 (br s, 2H,

naphthobipyrrole-N*H*), 8.44-8.41 (dd, 2H, Ar*H* (naphthobipyrrole)), 8.29 (br s, 4H, pyrrole-N*H*), 7.48-7.46 (dd, 2H, Ar*H* (naphthobipyrrole)), 6.60-6.58 (m, 4H, Ar*H* (pyrrole)), 6.07-6.06 (m, 8H, Ar*H* (pyrrole)), 4.31 (t, 4H, OCH_2CH$_2$, J = 6.40), 3.33 (q, 4H, ArCH_2CH$_3$, J = 7.61), 2.23-2.19 (p, 4H, CH$_2$CH_2CH$_2$), 2.01 (s, 6H, CH_3), 1.73-1.66 (m, 4H, CH$_2$CH$_2$CH_2), 1.38 (t, 4H, ArCH$_2$CH_3, J = 7.61). ^{13}C NMR (100 MHz, DMSO-d_6): δ 162.0, 138.7, 129.9, 127.6, 124.1, 120.9, 119.1, 117.3, 107.3, 104.5, 65.2, 39.0, 37.6, 25.8, 25.0, 15.4. HRMS (ESI) m/z 751.39663 $[M + H]^+$ calcd for $C_{46}H_{51}N_6O_4$, found 751.39649.

Compound 2.8 A mixture of bipyyrole dicarboxylic acid (**2.7**) (2.00 g, 5.00 mmol), 5-(3-hydroxypropyl)-5-methyl dipyrromethane (**2.5**) (2.30 g, 10.5 mmol), EDCI (1-ethyl-3-(3-dimethylaminopropyl)-carbodiimide, 2.30 g, 12.0 mmol) and DMAP (4-dimethylaminopyridine, 1.22 g, 10.0 mmol) in dry dichloromethane (100 ml) was stirred overnight at room temperature and concentrated under reduced pressure to give a brownish oil. To this crude product, dichloromethane (200 ml) and water (200 ml) were added and the organic phase was separated and washed twice with water (200 ml). The organic layer was dried over anhydrous $MgSO_4$ and evaporated in vacuo to give a brownish solid. Column chromatography over silica gel (ethyl acetate/hexanes = 1/4), followed by recrystallization from dichloromethane/methanol (1/20), afforded compound **2.8** (1.94 g, 49% yield) as a yellowish solid. ^{1}H NMR (400 MHz, DMSO-d_6): δ 11.67 (br s, 2H, bipyrrole-N*H*), 10.19 (br s, 4H, pyrrole-N*H*), 7.33-7.24 (m, 10H, Ar*H* (phenyl)), 6.54 (br s, 4H, Ar*H* (pyrrole)), 5.83 (br s, 4H, Ar*H* (pyrrole)), 5.68 (br s, 4H, Ar*H* (pyrrole)), 3.93 (t, 4H, OCH_2CH$_2$, J = 6.40), 1.83 (m, 4H, CH$_2$CH_2CH$_2$; 6H, ArCH_3), 1.45 (s, 6H, CH_3), 1.29 (m, 4H, CH$_2$CH$_2$CH_2). ^{13}C NMR (100 MHz, DMSO-d_6): δ 160.9, 139.2, 138.8, 135.6, 131.5, 130.9, 128.1, 125.7, 119.5, 118.9, 117.2, 117.0, 106.9, 104.5,

104.3, 62.1, 38.9, 37.9, 37.4, 28.8, 25.6, 11.3. HRMS (ESI) *m/z* 823.39420 $(M + Na)^+$ calcd for $C_{50}H_{52}N_6O_4Na$, found 823.39400.

Compound 2.2 To compound **2.6** (2.10 g, 2.80 mmol) in acetone (500 ml) was added BF_3•OEt_2 (0.34 ml, 2.80 mmol) in one portion. The resulting solution was stirred for 2 hours at room temperature and then quenched with triethylamine (3 ml). Evaporation of the volatile components in vacuo afforded a reddish solid. To this crude product, dichloromethane (150 ml), water (100 ml), and aqueous NaOH solution (sat., 10 ml) were added and the organic phase was separated off and washed three times with water (100 ml). The organic layer was dried over anhydrous $MgSO_4$ and evaporated in vacuo to give a reddish solid. Recrystallization from a mixture of dichloromethane and methanol (9/1), following column chromatography over silica gel (eluent: dichloromethane), gave 0.40 g (17% yield) of **2.2** as a white solid. ^{1}H NMR (400 MHz, $CDCl_3$): δ 10.10 (br s, 2H, naphthobipyrrole-N*H*), 8.56-8.53 (dd, 2H, Ar*H* (naphthobipyrrole)), 7.59-7.56 (dd, 2H, Ar*H* (naphthobipyrrole)), 7.44 (br s, 4H, pyrrole-N*H*), 6.05 (t, 4H, Ar*H* (pyrrole), *J* = 3.20), 5.93 (t, 8H, Ar*H* (pyrrole), *J* = 3.20), 4.15 (br t, 4H, OCH_2CH_2, *J* = 6.40), 3.66 (q, 4H, $ArCH_2CH_3$, *J* = 7.61), 2.20 (t, 4H, $CH_2CH_2CH_2$, J = 6.80), 1.83 (s, 6H, CH_3), 1.65 (m, 4H, $CH_2CH_2CH_2$), 1.50-1.45 (m, 4H, $ArCH_2CH_3$; 12H, CH_3). ^{13}C NMR (100 MHz, $CDCl_3$): δ 162.6, 139.4, 136.9, 132.7, 127.3, 124.4, 124.1, 123.5, 120.3, 120.1, 104.0, 103.3, 62.9, 38.8, 36.6, 35.5, 30.6, 28.5, 27.6, 25.2, 19.5, 14.3. HRMS (ESI) *m/z* 853.44120 $[M + Na]^+$ calcd for $C_{52}H_{58}N_6O_4Na$, found 853.44050.

Compound 2.3 To compound **2.8** (1.00 g, 1.25 mmol) in acetone (500 ml) was added BF_3•OEt_2 (0.15 ml, 1.25 mmol) in one portion. The resulting solution was stirred

for 1 hour at room temperature and then quenched with triethylamine (3 ml). Evaporation of the volatile components in vacuo afforded a reddish solid. To this crude product, dichloromethane (150 ml), water (100 ml), and aqueous NaOH solution (sat., 10 ml) were added and the organic phase was separated off and washed three times with water (100 ml). The organic layer was dried over anhydrous $MgSO_4$ and evaporated in vacuo to give a reddish solid. Column chromatography over silica gel (eluent: ethyl acetate/hexanes (1/4)) followed by recrystallization from methanol/dichloromethane (9/1), gave 0.20 g (18% yield) of **2.3** as a white solid. ^{1}H NMR (400 MHz, $CDCl_3$): δ 9.27 (br s, 2H, bipyrrole-N*H*), 7.50 (br s, 4H, pyrrole-N*H*), 7.43-7.33 (m, 10H, Ar*H* (phenyl)), 5.95 (t, 4H, Ar*H* (pyrrole), *J* = 2.80), 5.82 (t, 4H, Ar*H* (pyrrole), *J* = 2.80), 4.17 (t, 4H, OC*H*$_2$CH$_2$, *J* = 4.80), 2.05 (t, 4H, CH$_2$CH$_2$C*H*$_2$, *J* = 8.41), 2.05 (s, 6H, ArC*H*$_3$), 1.58 (m, 4H, CH$_2$C*H*$_2$CH$_2$), 1.49 (s, 6H, C*H*$_3$), 1.46 (s, 6H, C*H*$_3$), 1.38 (s, 6H, C*H*$_3$). ^{13}C NMR (100 MHz, DMSO-d_6): δ 160.5, 138.8, 137.5, 134.0, 133.0, 130.2, 127.7, 127.1, 124.3, 121.0, 118.8, 103.6, 102.8, 64.1, 38.6, 37.4, 35.3, 30.3, 28.5, 27.3, 24.8, 10.6. HRMS (ESI) *m/z* 903.45680 $[M + Na]^+$ calcd for $C_{56}H_{60}N_6O_4Na$, found 903.45670.

Compound 3.3 To methyl 4-acetylbenzoate (**3.2**) (5.00 g, 28.06 mmol) in pyrrole (100 mL) was added TFAA (trifluoroacetic anhydride, 2.1 mL, 14.80 mmol). The mixture was stirred for 10 hours at 60 °C. The resulting solution was evaporated in vacuo to remove pyrrole and other volatiles. The material obtained in this way was purified by column chromatography over silica gel (eluent: dicholoromethane) to afford a pale yellow oil. Crystallization from a mixture of dichloromethane and hexanes gave 5.91 g (72% yield) of **3.3** as a white solid. ^{1}H NMR (400 MHz, $CDCl_3$): δ 7.95-7.92 (d, 2H, Ar*H*), 7.80 (br s, 2H, pyrrole-N*H*), 7.20-7.18 (d, 2H, Ar*H*), 6.71-6.69 (m, 2H, Ar*H* (pyrrole)), 6.19-6.17 (m, 2H, Ar*H* (pyrrole)), 5.97-5.95 (m, 2H, Ar*H* (pyrrole)), 3.90 (s,

3H, C*H*$_3$), 2.06 (s, 3H, C*H*$_3$). ^{13}C NMR (100 MHz, $CDCl_3$): δ 167.1, 152.7, 136.7, 129.6, 128.7, 127.6, 117.4, 108.5, 106.7, 52.3, 45.1, 28.7. HRMS (ESI) *m/z* 295.14450 $[M + H]^+$ calcd for $C_{18}H_{18}N_2O_2$ found 295.14410.

Compound 3.4 and 4.2 To a mixture of compound **3.3** (5.91 g, 20.09 mmol) and methanlol/acetone (1:1, 300 mL), TFAA (trifluoroacetic anhydride, 1.42 mL, 10.00 mmol) was added at 0 °C and stirred for 1 hour. The solution was then stirred for 10 hours at room temperature and quenched with triethylamine. The resulting solution was evaporated in vacuo and re-dissolved in dichloromethane, washed with brine, and dried over Na_2SO_4. Column chromatography over silica gel (ethyl acetate/hexanes = 1/9) gave compound **3.4** (964 mg, 15% yield) and **4.2** (578 mg, 9% yield) as white solids. Compound **3.4** ^{1}H NMR (400 MHz, $CDCl_3$): δ 7.94-7.91 (d, 4H, Ar*H*), 7.21-7.19 (d, 4H, Ar*H*), 7.18 (br s, 4H, pyrrole N*H*), 5.94-5.92 (t, 4H, Ar*H* (pyrrole)), 5.76-5.74 (t, 4H, Ar*H* (pyrrole)), 3.90 (s, 6H, C*H*$_3$), 1.91 (s, 6H, C*H*$_3$), 1.53 (s, 12H, C*H*$_3$). ^{13}C-NMR (100 MHz, $CDCl_3$): δ 166.9, 152.0, 138.7, 135.7, 129.2, 128.4, 127.4, 105.9, 103.3, 52.1, 44.9, 35.3, 29.2. HRMS (ESI) *m/z* 669.34370 $(M + H)^+$ calcd for $C_{42}H_{44}N_4O_4$, found 669.34350. Compound **4.2** ^{1}H NMR (400 MHz, $CDCl_3$): δ 7.90-7.88 (d, 4H, Ar*H*), 7.24 (br s, 4H, pyrrole N*H*), 7.05-7.03 (d, 4H, Ar*H*), 5.94-5.92 (t, 4H, Ar*H* (pyrrole)), 5.61-5.59 (t, 4H, Ar*H* (pyrrole)), 3.89 (s, 6H, C*H*$_3$), 1.90 (s, 6H, C*H*$_3$), 1.63 (s, 6H, C*H*$_3$) , 1.53 (s, 6H, C*H*$_3$).

Compound 3.1 A mixture of compound **3.4** (964 mg, 1.44 mmol) and KOH (2.4 g, 43.20 mmol) in H_2O/2-propanol (1:1, 100 mL) was heated at reflux for 10 hours. The reaction was cooled to room temperature and then further cooled to 0 °C. The solution was acidified with hydrochloric acid until it reached pH = 2. The white precipitate

obtained in this way was filtered and washed with water until the washings were neutral. The resulting solid was dried in the air to give compound **3.1** (877 mg, 95% yield). ^{1}H NMR (400 MHz, DMSO-d_6): δ 12.75 (br s, 2H, COO*H*), 9.69 (s, 4H, pyrrole N*H*), 7.77-7.75 (d, 4H, Ar*H*), 7.22-7.20 (d, 4H, Ar*H*), 5.73-5.72 (d, 8H, Ar*H* (pyrrole)), 1.75 (s, 6H, CH_3), 1.47 (s, 12H, CH_3). ^{13}C NMR (100 MHz, DMSO-d_6): δ 167.2, 154.3, 139.4, 135.7, 128.9, 128.4, 127.3, 104.9, 102.1, 44.5, 35.1, 30.8, 30.4. HRMS (ESI) *m/z* 641.31250 (M + H)$^+$ calcd for $C_{40}H_{40}N_4O_4$, found 641.31220.

Compound 4.1 A mixture of compound **4.2** (578 mg, 0.90 mmol) and KOH (1.5 g, 27.00 mmol) in H_2O/2-propanol (1:1, 100 mL) was heated at reflux for 1 hour. The reaction was cooled to room temperature and then further cooled to 0 °C. The solution was acidified with hydrochloric acid until it reached pH = 2. The white precipitate obtained in this way was filtered and washed with water until the washings were neutral. The resulting solid was dried in the air to give compound **4.1** (547 mg, 95% yield). ^{1}H NMR (400 MHz, DMSO-d_6): δ 12.79 (br s, 2H, COO*H*), 9.64 (s, 4H, pyrrole N*H*), 7.84-7.82 (d, 4H, Ar*H*), 7.00-6.98 (d, 4H, Ar*H*), 5.76-5.61 (d, 8H, Ar*H* (pyrrole)), 1.83 (s, 6H, CH_3), 1.63 (s, 6H, CH_3), 1.50 (s, 6H, CH_3). ^{13}C NMR (100 MHz, DMSO-d_6): δ 167.9, 155.6, 140.0, 136.4, 129.5, 129.1, 127.5, 105.6, 102.6, 44.9, 35.1, 31.2, 29.6, 28.1. HRMS (ESI) *m/z* 641.31210 (M + H)$^+$ calcd for $C_{40}H_{40}N_4O_4$, found 641.31220.

^{1}H-NMR titration study: Stock solutions of the host molecules **2.1**, **2.2** and **2.3** being studied were made up in CD_2Cl_2 with the final concentrations being 3×10^{-3} M. Stock solutions of the guest in question were prepared by dissolving 10 equivalents of the tetrabutyl ammonium salts of the anions (F^-, Cl^-, Br^-, I^-, $H_2PO_4^-$, $HP_2O_7^{3-}$, and SO_4^{2-}) under study in 2 mL stock solutions of the host. Making up the anion source solutions in this

way allowed the binding studies to be carried out without having to make mathematical corrections to account for changes in host concentrations as the result of dilution effects. The general procedure for the ^{1}H-NMR titration studies involved making sequential additions of titrant (anionic quest) using Hamilton syringes to a 0.5 mL aliquot of the host stock solution in a NMR tube. The data was then collated and combined to produce plots that showed the changes in host spectral features as a function of guest concentration.

UV-Vis titration study: Stock solutions of the host molecules **2.1**, **2.2** and **2.3** being studied were made up in dichloromethane with the final concentrations being 1×10^{-5} M. Stock solutions of the guest in question were prepared by dissolving 10 equivalents of the tetrabutyl ammonium salts of the anions (F^-, Cl^-, Br^-, I^-, $H_2PO_4^-$, $HP_2O_7^{3-}$, NO_3^-, and SO_4^{2-}) under study in 2 mL stock solutions of the host. Making up the anion source solutions in this way allowed the binding studies to be carried out without having to make mathematical corrections to account for changes in host concentrations as the result of dilution effects. The general procedure for the UV-Vis titration studies involved making sequential additions of titrant (anionic quest) using Hamilton syringes to a 3 mL aliquot of the host stock solution in a spectrometric cell. The data was then collated and combined to produce plots that showed the changes in host spectral features as a function of guest concentration.

Calculations of association constants, K_a: Upon addition of tetrabutylammonium salts, the UV-vis spectra changed gradually. These changes were ascribed to anion binding, with the corresponding association constants K_a being determined by nonlinear curve fitting of the curves obtained by plotting the absorbance changes at a λ value where

the spectral change was maximal (ΔA) against the concentration of the tetrabutylammonium anion salt added, [X-]. The data was fitted to the,

$$\Delta A = A\cdot\{(1 + K_a\cdot[X^-] + K_a\cdot[\text{Host}]) - \text{sqrt}\{(1 + K_a\cdot[X^-] + K_a\cdot[\text{Host}])^2 - 4\cdot K_a^2\cdot[\text{Host}][X^-]\}\} / (2K_a\cdot[\text{Host}])$$

these values were obtained by the fit to the data with good fits ($R^2 \geq 0.99$).

REFERENCES

1) Roznyatovskiy, V. V.; Roznyatovskaya, N. V.; Weyrauch, H.; Pinkwart, K.; Tübke, J.; Sessler, J. L. *J. Org. Chem.* **2010**, *75*, 8355-8362.
2) Boev, N. V.; Ustynyuk, Y. A. Russ. *J. Org. Chem.* **2007**, *43*, 297-304.

Appendix: X-ray experimental and crystallographic data

X-ray Experiment for 3.1: Crystals grew as long, colorless needles by slow evaporation from DMF. The data crystal was cut from a larger crystal and had approximate dimensions; 0.34 x 0.04 x 0.02 mm. The data were collected on an Agilent Technologies SuperNova Dual Source diffractometer using a μ-focus Cu Kα radiation source (λ = 1.5418Å) with collimating mirror monochromators. A total of 1127 frames of data were collected using w-scans with a scan range of 1° and a counting time of 30 seconds per frame with a detector offset of +/- 40.3° and 90 seconds per frame with a detector offset of +/- 108.9°. The data were collected at 100 K using an Oxford Cryostream low temperature device. Details of crystal data, data collection and structure refinement are listed in Table A.1. Data collection, unit cell refinement and data reduction were performed using Agilent Technologies CrysAlisPro V 1.171.37.31. The structure was solved by direct methods using SHELXT and refined by full-matrix least-squares on F^2 with anisotropic displacement parameters for the non-H atoms using SHELXL-2014/7. Structure analysis was aided by use of the programs PLATON98 and WinGX. The hydrogen atoms were calculated in ideal positions with isotropic displacement parameters set to 1.2xUeq of the attached atom (1.5xUeq for methyl hydrogen atoms).

A small peak in the difference electron density map was found near C24. It was twice as large as the next peak and was probably due to a small amount of disorder in the DMF molecule. The disorder was due to a 180 degree rotation about the N4-C24 bond. A disorder model was applied which only involved the oxygen atom, O4, of the affected DMF molecule. The variable x was assigned to the site occupancy for O4, while (1-x) was assigned to the site occupancy for O4a. A common isotropic displacement parameter

was refined for the two atoms while refining x. The geometry of the two atoms was restrained to be equivalent throughout the refinement process. In this way, the site occupancy for O4 refined to 93(1)%.

The function, $\Sigma w(|Fo|^2 - |Fc|^2)^2$, was minimized, where $w = 1/[(\sigma(Fo))2 + (0.0707*P)^2 + (0.6968*P)]$ and $P = (|Fo|^2 + 2|Fc|^2)/3$. $Rw(F^2)$ refined to 0.138, with R(F) equal to 0.0483 and a goodness of fit, S, = 1.02. Definitions used for calculating R(F), $Rw(F^2)$ and the goodness of fit, S, are given below. The data were checked for secondary extinction effects but no correction was necessary. Neutral atom scattering factors and values used to calculate the linear absorption coefficient are from the International Tables for X-ray Crystallography (1992). All figures were generated using SHELXTL/PC.

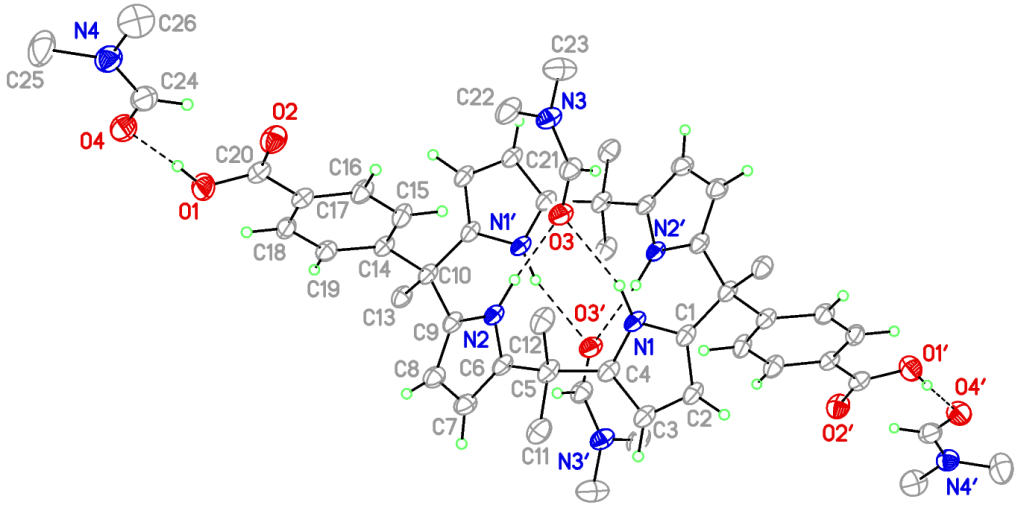

Figure A.1 View of 3.1 showing the atom labeling scheme. Displacement ellipsoids are scaled to the 50% probability level. The complex resides around a crystallographic inversion center at ½, 1, 1. Atoms with labels appended by a ‘ are related by 1-x, 2-y, 2-z. The methyl group H atoms were omitted for clarity.

Table A.1 Crystal data and structure refinement for **3.1**.

Empirical formula	C52 H68 N8 O8	
Formula weight	933.14	
Temperature	100(2) K	
Wavelength	1.54184 Å	
Crystal system	monoclinic	
Space group	P 21/n	
Unit cell dimensions	a = 17.4535(4) Å	a= 90°.
	b = 8.0246(2) Å	b= 97.847(2)°.
	c = 17.7712(4) Å	g = 90°.
Volume	2465.68(10) $Å^3$	
Z	2	
Density (calculated)	1.257 Mg/m^3	
Absorption coefficient	0.692 mm^{-1}	
F(000)	1000	
Crystal size	0.02 x 0.04 x 0.34 mm^3	
Theta range for data collection	3.329 to 74.139°.	
Index ranges	-21<=h<=20, -9<=k<=6, -21<=l<=21	
Reflections collected	13957	
Independent reflections	4904 [R(int) = 0.0407]	
Completeness to theta = 67.684°	100.0 %	
Absorption correction	Semi-empirical from equivalents	
Max. and min. transmission	1.00 and 0.684	
Refinement method	Full-matrix least-squares on F^2	
Data / restraints / parameters	4904 / 3 / 331	
Goodness-of-fit on F^2	1.012	
Final R indices [I>2sigma(I)]	R1 = 0.0483, wR2 = 0.1235	
R indices (all data)	R1 = 0.0668, wR2 = 0.1383	
Extinction coefficient	n/a	
Largest diff. peak and hole	0.333 and -0.260 $e.Å^{-3}$	

X-ray Experimental for NMC-1: Crystals grew as colorless prisms by slow evaporation from a mixture of DMF and DEF. The data crystal had approximate dimensions; 0.17 x 0.11 x 0.06 mm. The data were collected on an Agilent Technologies SuperNova Dual Source diffractometer using a μ-focus Cu Kα radiation source (λ = 1.5418Å) with collimating mirror monochromators. A total of 1056 frames of data were collected using w-scans with a scan range of 0.5° and a counting time of 15 seconds per frame using a detector offset of +/- 40.5° and a counting time of 43 seconds per frame using a detector offset of +/- 111.0°. The data were collected at 100 K using an Oxford Cryostream low temperature device. Details of crystal data, data collection and structure refinement are listed in Table A.2. Data collection, unit cell refinement and data reduction were performed using Agilent Technologies CrysAlisPro V 1.171.37.31. The structure was solved by direct methods using SIR2004 and refined by full-matrix least-squares on F^2 with anisotropic displacement parameters for the non-H atoms using SHELXL-2014/7. Structure analysis was aided by use of the programs PLATON98 and WinGX. The hydrogen atoms were calculated in ideal positions with isotropic displacement parameters set to 1.2xUeq of the attached atom (1.5xUeq for methyl hydrogen atoms.

A molecule of the calixpyrrole dibenzoic acid was located around a crystallographic inversion center at 1,1, ½. This molecule was not coordinated to the Pr ions. It occupied a cavity in the 3D structure of the Pr complex. The electron density of the atoms of this calixpyrrole was lower than what is expected for a fully occupied molecule. The site occupancy for this calixpyrrole was estimated to be 1/2. The complex contained several solvent molecules, both dimethyl formamide and diethyl formamide. Several of these molecules were disordered. Some were badly disordered and could not be modeled effectively. The contributions to the scattering factors due to this solvent

molecule were removed by use of the utility SQUEEZE in PLATON98. PLATON98 was used as incorporated in WinGX.

The function, $\Sigma w(|Fo|^2 - |Fc|^2)^2$, was minimized, where $w = 1/[(\sigma(Fo))^2 + (0.0978*P)2 + (9.1139*P)]$ and $P = (|Fo|^2 + 2|Fc|^2)/3$. $Rw(F^2)$ refined to 0.170, with R(F) equal to 0.0555 and a goodness of fit, S, = 1.08. Definitions used for calculating R(F), $Rw(F^2)$ and the goodness of fit, S, are given below. The data were checked for secondary extinction effects but no correction was necessary. Neutral atom scattering factors and values used to calculate the linear absorption coefficient are from the International Tables for X-ray Crystallography (1992). All figures were generated using SHELXTL/PC.

Table A.2 Crystal data and structure refinement for **NMC-1**.

Empirical formula	C286 H338 N38 O40 Pr4	
Formula weight	5511.56	
Temperature	173(2) K	
Wavelength	1.54184 Å	
Crystal system	triclinic	
Space group	P -1	
Unit cell dimensions	a = 20.6712(4) Å	a= 62.477(2)°.
	b = 21.0386(5) Å	b= 79.558(2)°.
	c = 21.6281(5) Å	g = 67.086(2)°.
Volume	7683.2(3) $Å^3$	
Z	1	
Density (calculated)	1.191 Mg/m^3	
Absorption coefficient	5.329 mm^{-1}	
F(000)	2876	
Crystal size	0.17 x 0.11 x 0.06 mm^3	
Theta range for data collection	2.304 to 76.398°.	
Index ranges	-25<=h<=25, -26<=k<=24, -25<=l<=26	
Reflections collected	51735	
Independent reflections	30831 [R(int) = 0.0320]	
Completeness to theta = 67.684°	99.2 %	
Absorption correction	Semi-empirical from equivalents	
Max. and min. transmission	1.00 and 0.881	
Refinement method	Full-matrix least-squares on F^2	
Data / restraints / parameters	30831 / 2699 / 1746	
Goodness-of-fit on F^2	1.045	
Final R indices [I>2sigma(I)]	R1 = 0.0555, wR2 = 0.1507	
R indices (all data)	R1 = 0.0733, wR2 = 0.1704	
Extinction coefficient	n/a	
Largest diff. peak and hole	1.150 and -1.332 e.$Å^{-3}$	

X-ray Experimental for NMC-2: Crystals grew pale green prisms by vapor diffusion of hexane into a solution of DMF and DEF. The data crystal was cut from a larger crystal and had approximate dimensions; 0.2 x 0.1 x 0.05 mm. The data were collected at -173 °C on a Nonius Kappa CCD diffractometer using a Bruker AXS Apex II detector and a graphite monochromator with MoKa radiation (l = 0.71075Å). Reduced temperatures were maintained by use of an Oxford Cryosystems 600 low-temperature device. A total of 868 frames of data were collected using w-scans with a scan range of 0.5° and a counting time of 76 seconds per frame. Details of crystal data, data collection and structure refinement are listed in Table A.3. Data reduction were performed using SAINT V8.27B. The structure was solved by direct methods using SIR97 and refined by full-matrix least-squares on F^2 with anisotropic displacement parameters for the non-H atoms using SHELXL-2014/7. Structure analysis was aided by use of the programs PLATON98 and WinGX.

A cylindrical region parallel to the c-axis contained some disordered solvent. The solvent appeared to be a mixture of n-hexane and DMF. Attempts to model the disorder were unsatisfactory. The contributions to the scattering factors due to these solvent molecules were removed by use of the utility SQUEEZE in PLATON98.

The function, $\Sigma w(|Fo|^2 - |Fc|^2)^2$, was minimized, where $w = 1/[(\sigma(Fo))^2 + (0.0401*P)2]$ and $P = (|Fo|^2 + 2|Fc|^2)/3$. $Rw(F^2)$ refined to 0.0828, with R(F) equal to 0.0322 and a goodness of fit, S, = 1.04. Definitions used for calculating R(F), $Rw(F^2)$ and the goodness of fit, S, are given below. The data were checked for secondary extinction but no correction was necessary. Neutral atom scattering factors and values used to calculate the linear absorption coefficient are from the International Tables for X-ray Crystallography (1992). All figures were generated using SHELXTL/PC.

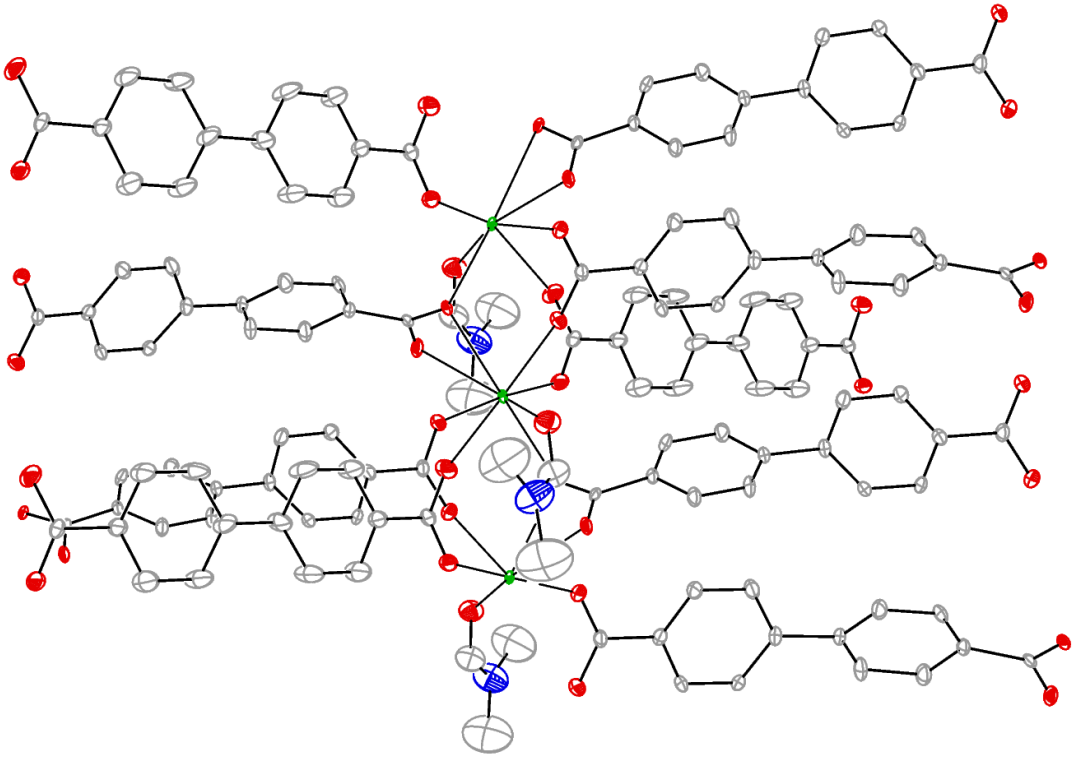

Figure A.2 View of 1 showing the portion of the 3-dimensional array. Displacement ellipsoids are scaled to the 50% probability level.

Table A.3 Crystal data and structure refinement for **NMC-2**.

Empirical formula	C60 H68 N16 O4 Pr2	
Formula weight	1359.12	
Temperature	100(2) K	
Wavelength	0.71073 Å	
Crystal system	monoclinic	
Space group	C 2	
Unit cell dimensions	a = 28.8960(9) Å	a= 90°.
	b = 8.6749(3) Å	b= 116.0560(10)°.
	c = 14.2513(4) Å	g = 90°.
Volume	3209.29(18) $Å^3$	
Z	2	
Density (calculated)	1.406 Mg/m^3	
Absorption coefficient	1.556 mm^{-1}	
F(000)	1380	
Crystal size	0.2 x 0.1 x 0.05 mm^3	
Theta range for data collection	2.475 to 33.678°.	
Index ranges	-44<=h<=28, -12<=k<=10, -17<=l<=21	
Reflections collected	10221	
Independent reflections	7556 [R(int) = 0.0255]	
Completeness to theta = 25.242°	99.6 %	
Absorption correction	Semi-empirical from equivalents	
Max. and min. transmission	1.00 and 0.761	
Refinement method	Full-matrix least-squares on F^2	
Data / restraints / parameters	7556 / 413 / 392	
Goodness-of-fit on F^2	1.033	
Final R indices [I>2sigma(I)]	R1 = 0.0322, wR2 = 0.0805	
R indices (all data)	R1 = 0.0391, wR2 = 0.0828	
Absolute structure parameter	0.110(19)	
Extinction coefficient	n/a	
Largest diff. peak and hole	1.785 and -0.589 $e.Å^{-3}$	

References

Baeyer, A.; *Ber. Dtsch. Chem. Ges.* **1886**, *19*, 2184–2185.

Chelintzev, V. V.; Tronov, B. V. *J. Russ. Phys. Chem. Soc.* **1916**, *48*, 105, 127.

Floriani, C. *Pure Appl. Chem.* **1996**, *68*, 1.

Jubb, J.; Floriani, C.; Chiesi-Villa, A.; Rizzoli, C. *J. Am. Chem. Soc.* **1992**, *114*, 6571.

Piarulli, U.; Floriani, C.; Chiesi-Villa, A.; Rizzoli, C. *J. Chem. Soc. Chem. Commun.* **1994**, 895.

De Angelis, S.; Solari, E.; Floriani, C.; Chiesi-Villa, A.; Rizzoli, C. *J. Am. Chem. Soc.* **1994**, *116*, 5691.

Gale, P. A.; Sessler, J. L.; Kral, V.; Lynch, V. *J. Am. Chem. Soc.* **1996**, *118*, 5140-5141.

Gale, P. A.; Sessler, J. L.; Kral, V. *Chem. Commun.* **1998**, 1-8.

Gale, P. A.; Anzenbacher, P.; Sessler, J. L. *Coord. Chem. Rev.* **2001**, *222*, 57-102.

Gale, P. A.; Lee, C. -H. *Top. Heterocycl. Chem.* **2010**, *24*, 39-73.

Lee, C. –H.; Miyaji, H.; Yoon, D. –W.; Sessler, J. L. *Chem. Commun.* **2008**, 24-34. (e) Kim, D. S.; Sessler, J. L. *Chem. Soc. Rev.* **2015**, *44*, 532-546.

Adriaenssens, L.; Ballester, P. *Chem. Soc. Rev.* **2013**, *42*, 3261-3277.

Custelcean, R.; Delmau, L. H.; Moyer, B. A.; Sessler, J. L.; Cho, W. –S.; Gross, D.; Bates, G. W.; Brooks, S. J.; Light, M. E.; Gale, P. A. *Angew. Chem. Int. Ed.* **2005**, *44*, 2537-2542.

Aydogan, A.; Lee, G.; Lee, C. –H.; Sessler, J. L. *Chem. Eur. J.* **2015**, *21*, 2368-2376.

Sessler, J. L.; Gross, D. E.; Cho, W. –S.; Lynch, V. M.; Schmidtchen, F. P.; Bates, G. W.; Light, M. E.; Gale, P. A. *J. Am. Chem. Soc.* **2006**, *128*, 12281-12288.

Kim, S. K.; Sessler, J. L. *Chem. Soc. Rev.* **2010**, *39*, 3784-3809.

Allen, W. E.; Gale, P. A.; Brown, C. T.; Lynch, V. M.; Sessler, J. L. *J. Am. Chem. Soc.* **1996**, *118*, 12471-12472.

Saha, I.; Lee, J. T.; Lee, C.-H. *Eur. J. Org. Chem.* **2015**, 3859-3885.

Ravikumar, I.; Ghosh, P. *Chem. Soc. Rev.* **2012**, *41*, 3077-3098.

Ojovan, M. I.; Lee, W. E. An Introduction to Nuclear Waste Immobilization; Elsevier: Amsterdam, Netherlands, 2005; Chapter 17.

Das, D.; Bharadwaj, S. R. Thoria-based nuclear fuels: thermophysical and thermodynamic properties, fabrication, reprocessing, and waste management; Springer: London, 2013; Chapter 8.

Moyer, B. A.; Custelcean, R.; Hay, B. O.; Sessler, J. L.; Bowman-James, K.; Day, V. W.; Kang, S. *Inorg. Chem.* **2013**, *52*, 3473-3490.

Raposo, C.; Almaraz, M.; Martin, M.; Weinrich, V.; Mussons, M. L.; Alcazar, V.; Caballero, M. C.; Moran, J. R. *Chem. Lett.* **1995**, 759-760.

Jia, C.; Wu, B.; Li, S.; Huang, X.; Zhao, Q.; Li, Q. S.; Yang, X. J. *Angew. Chem. Int. Ed.* **2011**, *50*, 486-490.

Jin, C.; Zhang, M.; Wu, L.; Guan, Y.; Pan, Y.; Jiang, J.; Lin, C.; Wang, L. *Chem. Commun.* **2013**, *49*, 2025.

Liu, Y.; Qin, Y.; Jiang, D. Analyst **2015**, *140*, 5317-5323.

Schaly, A.; Belda, R.; Garcia-Espana, E.; Kubik, S. *Org. Lett.* **2013**, *15*, 6238-6241.

Busschaert, N.; Karagiannidis, L. E.; Wenzel, M.; Haynes, C. J. E.; Wells, N. J.; Young, P. G.; Makuc, D.; Plavec, J.; Jolliffe, K. A.; Gale, P. A. *Chem. Sci.* **2014**, *5*, 1118−1127.

Custelcean, R.; Williams, N. J.; Seipp, C. A.; Ivanov, A. S.; Bryantsev, V. S. *Chem. Eur. J.* **2016**, *22*, 1997-2003.

Ahmed, B. M.; Hartman, C. K.; Mezei, G. *Inorg. Chem.* **2016**, *55*, 10666-10679.

Zhou, H.; Zhao, Y.; Gao, G.; Li, S.; Lan, J.; You, J. *J. Am. Chem. Soc.* **2013**, *135*, 14908-14911. 9

Song, N. R.; Moon, J. H.; Choi, J.; Jun, E. J.; Kim, Y.; Kim, S.; Lee, J. Y.; Yoon, J. *Chem. Sci.* **2013**, *4*, 1765-1771.

Saini, R.; Kumar, S. *RSC Adv.* **2013**, *3*, 21856-21862.

Pachauri, R. K.; Reisinger, A. *IPCC Fourth Assessment Report*, Intergovernmental Panel on Climate Change, 2007.

Earth System Research Laboratory: http://www.esrl.noaa.gov/gmd/ccgg/trends/, 2017

Rochelle, G. T. *Science* **2009**, *325*, 1652.

Sumida, K.; Rogow, D. L.; Mason, J. A.; McDonald, T. M.; Bloch, E. D.; Herm, Z. R.; Bae, T.; Long, J. R. *Chem. Rev.* **2012**, *112*, 724-781.

Li, G.; Xia, P.; Webley, P.; Zhang, J.; Singh, R. *Energy Procedia* **2009**, *1*, 1123.

Liu, K.; Li, B.; Li, Y.; Li, X.; Yang, F.; Zeng, G.; Peng, Y.; Zhang, Z.; Li, G.; Shi, Z.; Feng, S.; Song, D. *Chem. Commun.* **2014**, *50*, 5031.

Liu, M. –M.; Bi, Y. –L.; Dang, Q.-Q.; Zhang, X.-M. *Dalton Trans.* **2015**, *44*, 19796.

Li, P. –Z.; Wang, X. –J.; Liu, J.; Lim, J. S.; Zou, R.; Zhao, Y. *J. Am. Chem. Soc.* **2016**, *138*, 2142-2145.

Lin, Y.; Kong, C.; Chen, L. *RSC Adv.* **2016**, *6*, 32598-32614.

Yeon, J. S.; Lee, W. R.; Kim, N. W.; Jo, H.; Lee, H.; Song, J. H.; Lim, K. S.; Kang, D. W.; Seo, J. G.; Moon, D.; Wiers, B.; Hong, C. S. *J. Mater. Chem. A* **2015**, *3*, 19177-19185.

Martinez, F.; Sanz, R.; Orcajo, G.; Briones, D.; Yanguez, V. *Chem. Eng. Sci.* **2016**, *142*, 55.

Torrisi, A.; Mellot-Draznieks, C.; Bell, R. G. *J. Chem. Phys.* **2010**, *132*, 044705.

The Economist. *Novel Sources of Uranium: Rising from the Ashes*, April 8, 2010, http://www.economist.com/node/15865280?story_id=15865280, accessed September 10, 2010.

Balonov, M.; et al. *Radiological Conditions in the Dnieper River Basin*; Radiological Assessment Reports Series; International Atomic Energy Agency: Vienna, 2006.

Schwochau, K. *Top. Curr. Chem.* **1984**, *124*, 91.

Stockmann, T. J.; Ding, Z. *Anal. Chem.* **2011**, *83*, 7542-7549.

Sather, A. C.; Berryman, O. B.; Rebek, J. *J. Am. Chem. Soc.* **2010**, *132*, 13572-13574.

Pearson, R. G. *J. Am. Chem. Soc.* **1963**, *85*, 3533.

Cram, D. J.; Lehn, J. M. *J. Am. Chem. Soc.* **1985**, *107*, 3657.

Hay, B. P.; Hancock, R. D. *Coord. Chem. Rev.* **2001**, *212*, 61.

Szigethy, G.; Raymond, K. N. *J. Am. Chem. Soc.* **2011**, *133*, 7942-7956.

Watson, L. A.; Hay, B. P. *Inorg. Chem.* **2011**, *50*, 2599-2605.

Beer, S.; Berryman, O. B.; Ajami, D.; Rebek, J. *Chem. Sci.* **2010**, *1*, 43-47.

Sather, A. C.; Berryman, O. B.; Rebek, J. *J. Am. Chem. Soc.* **2010**, *132*, 13572-13574.

Qiu, J.; Burns, P. C. *Chem. Rev.* **2013**, *113*, 1097–1120.

Wang, K.; Chen, J. *Acc. Chem. Res.* **2011**, *44*, 531-540.

Pasquale, S.; Sattin, S.; Escudero-Adan, E. C.; Martinez-Belmonte, M.; Mendoza, J. *Nat. Commun.* **2012**, *3*, 785.

Thuery, P.; Harrowfield, J. *Cryst. Growth Des.* **2017**, *17*, 2881-2892.

Hofmeister, F. *Arch. Exp. Pathol. Pharmakol.* **1888**, *24*, 247-260.

Custelcean, R.; Moyer, B. A. *Eur. J. Inorg. Chem.* **2007**, *10*, 1321-1340.

Report to Congress: Status of Enviornmental Management Initiatives to Accelerate the Reduction of Environmental Risks and Challenges Posed by the Legacy of the Cold War;

Report DOE/EM-0001; U. S. Department of Energy, Office of Environmental management: Washington, DC, Jan. 2009.

Moyer, B. A.; Custelcean, R.; Hay, B. O.; Sessler, J. L.; Bowman-James, K.; Day, V. W.; Kang, S. *Inorg. Chem.* **2013**, *52*, 3473-3490.

Ojovan, M. I.; Lee, W. E. *An Introduction to Nuclear Waste Immobilisation;* Elsevier: Amsterdam, Netherlands, 2005; Chapter 17.

Manara, D.; Grandjean, A.; Pinet, O.; Dussossoy, J. L.; Neuville, D. R. J. *Non-Cryst. Solids* **2007**, *353*, 12-23.

Pirlet, V. J. J. *Nucl. Mat.* **2001**, *298*, 47-54.

Ravikumar, I.; Ghosh, P. *Chem. Soc. Rev.* **2012**, *41*, 3077-3098.

Jia, C.; Wu, B.; Li, S.; Huang, X.; Zhao, Q.; Li, Q. S.; Yang, X. J. *Angew. Chem. Int. Ed.* **2011**, *50*, 486-490.

Fowler, C. J.; Haverlock, T. J.; Moyer, B. A.; Shriver, J. A.; Gross, D. E.; Marquez, M.; Sessler, J. L.; Hossain, M. A.; Bowman-James, K. *J. Am. Chem. Soc.* **2008**, *130*, 14386-14387.

Borman, C. J.; Custelcean, R.; Hay, B. P.; Bill, N. L.; Sessler, J. L.; Moyer, B. A. *Chem. Comm.* **2011**, 7611-7613.

Kubik, S.; Kirchner, R.; Nolting, D.; Seidel, J. *J. Am. Chem. Soc.* **2002**, *124*, 12752–12760.

Kim, J.-i.; Juwarker, H.; Liu, X.; Lah, M. S.; Jeong, K.-S. *Chem. Commun.* **2010**, *46*, 764–766.

Young, P. G.; Clegg, J. K.; Bhadbhade, M.; Jolliffe, K. A. *Chem. Commun.* **2011**, *47*, 463–465.

Busschaert, N.; Karagiannidis, L. E.; Wenzel, M.; Haynes, C. J. E.; Wells, N. J.; Young, P. G.; Makuc, D.; Plavec, J.; Jolliffe, K. A.; Gale, P. A. *Chem. Sci.* **2014**, *5*, 1118–1127.

Elmes, R. B. P.; Yuen, K. K. Y.; Jolliffe, K. A. *Chem. Eur. J.* **2014**, *20*, 7373-7380. Sommer, F.; Kubik, S. *Org. Biomol. Chem.* **2014**, *12*, 8851-8860.

Naini, S. R.; Lalancette, R. A.; Gorlova, O.; Ramakrishna, K. V. S.; Yadav, J. S.; Ranganathan, S. *Eur. J. Org. Chem.* **2014**, 7015-7022.

Brunetti, E.; Picron, J.; Flidrova, K.; Bruylants, G.; Bartik, K.; Jabin, I. *J. Org. Chem.* **2014**, *79*, 6179-6188.

Custelcean, R.; Willams, N. J.; Seipp, C. A. *Angew. Chem. Int. Ed.* **2015**, *54*, 10525-10529.

Custelcean, R.; Williams, N. J.; Seipp, C. A.; Ivanov, A. S.; Bryantsev, V. S. *Chem. Eur. J.* **2016**, *22*, 1997-2003.

(k) Ahmed, B. M.; Mezei, G. *Chem. Commun.* **2017**, *53*, 1029-1032.

Zhou, H.; Zhao, Y.; Gao, G.; Li, S.; Lan, J.; You, J. *J. Am. Chem. Soc.* **2013**, *135*, 14908-14911. 9

Song, N. R.; Moon, J. H.; Choi, J.; Jun, E. J.; Kim, Y.; Kim, S.; Lee, J. Y.; Yoon, J. *Chem. Sci.* **2013**, *4*, 1765-1771.

Saini, R.; Kumar, S. *RSC Adv.* **2013**, *3*, 21856-21862.

Gale, P. A.; Sessler, J. L.; Král, V. *Chem. Commun.* **1998**, 1-8.

Roznyatovskiy, V. V.; Roznyatovskaya, N. V.; Weyrauch, H.; Pinkwart, K.; Tübke, J.; Sessler, J. L. *J. Org. Chem.* **2010**, *75*, 8355-8362.

Boev, N. V.; Ustynyuk, Y. A. Russ. *J. Org. Chem.* **2007**, *43*, 297-304.

Moyer, B. A.; Sloop, F. V., Jr.; Fowler, C. J.; Haverlock, T. J.; Kang, H.-A.; Delmau, L. H.; Bau, D. M.; Hossain, A.; Bowman-James, K.; Shriver, J. A.; N. Bill; Gross, D. E.; Marquez, M.; Sessler, J. L. *Supramol. Chem.* **2010**, *22*, 653–671.

Borman, C. J.; Bonnesen, P. V.; Moyer, B. A. *Anal. Chem.* **2012**, *84*, 8214–8221.

Gale, P. A.; Sessler, J. L.; Král, V.; Lynch, V. *J. Am. Chem. Soc.* **1996**, *118*, 5140-5141.

Sato, W.; Miyaji, H.; Sessler, J. L. *Tetrahedron Lett.* **2000**, *41*, 6731-6736.

Special issue of *Chem. Rev.* **2012**, *112*, 673-1268. (b) Special issue of *Chem. Soc. Rev.* **2014**, *43*, 5415-6172.

Garcia-Simon, C.; Carcia-Borras, M.; Gomez, L.; Parella, T.; Osuna, S.; Juanhuix, J.; Imaz, I.; Maspoch, D.; Costas, M.; Ribas, X. *Nat. Commun.* **2014**, *5*, 5557.

Kim, D. S.; Sessler, J. L. *Chem. Soc. Rev.* **2015**, *44*, 532-546.

Saha, I.; Lee, J. T.; Lee, C. *Eur. J. Org. Chem.* **2015**, 3859-3885.

Adriaenssens, L.; Ballester, P. *Chem. Soc. Rev.* **2013**, *42*, 3261.

Osorio-Planes, L.; Espelt, M.; Pericas, M. A.; Ballester, P. *Chem. Sci.* **2014**, *5*, 4260.

Valderrey, V.; Escudero-Adan, E. C.; Ballester, P. *Angew. Chem. Int. Ed.* **2013**, *52*, 6898-6902.

Kim, S. K.; Lee, J.; Williams, N. J.; Lynch, V. M.; Hay, B. P.; Moyer, B. A.; Sessler, J. L. *J. Am. Chem. Soc.* **2014**, *136*, 15079-15085.

Borman, C. J.; Custelcean, R.; Hay, B. P.; Bill, N. L.; Sessler, J. L.; Moyer, B. A. *Chem. Commun.* **2011**, 7611-7613.

Ko, S.; Kim, S. K.; Share, A.; Lynch, V. M.; Park, J.; Namkung, W.; Rossom, W. V.; Busschaert, N.; Gale, P. A.; Sessler, J. L.; Shin, I. *Nat. Chem.* **2014**, *6*, 885-892.

Cafeo, G.; Carbotti, G.; Cuzzola, A.; Fabbi, M.; Ferrini, S.; Kohnke, F. H.; Papanikolaou, G.; Plutino, M. R.; Rosano, C.; White, A. J. *J. Am. Chem. Soc.* **2013**, *135*, 2544-2551.

Zhang, H.; Zou, R.; Zhao, Y. *Coord. Chem. Rev.* **2015**, *292*, 74-90.

Li, Q.; Zhang, W.; Miljanic, O.S.; Sue, C.H.; Zhao, Y.L.; Liu, L.; Knobler, C.B.; Stoddart, J. F.; Yaghi, O. M. *Science* **2009**, *325*, 855.

Vukotic, V. N.; Harris, K. J.; Zhu, K.; Schurko, R. W.; Loeb, S. J. *Nat. Chem.* **2012**, *4*, 456.

Hartlieb, K. J.; Holcroft, J. M.; Moghadam, P. Z.; Vermeulen, N. A.; Algaradah, M. M.; Nassar, M. S.; Botros, Y. Y.; Snurr, R. Q.; Stoddart, J. F. *J. Am. Chem. Soc.* **2016**, *138*, 2292-2301.

Ni, X.; Xiao, X.; Cong, H.; Liang, L.; Cheng, K.; Cheng, X.; Ji, N.; Zhu, Q.; Xue, S.; Tao, Z. *Chem. Soc. Rev.* **2013**, *42*, 9480-9508.

Wang, K.; Feng, D.; Liu, T.; Su, J.; Yuan, S.; Chen, Y.; Bosch, M.; Zou, X.; Zhou, H. *J. Am. Chem. Soc.* **2014**, *136*, 13983-13986.

Kubota, R.; Tashiro, S.; Shiro, M.; Shionoya, M. *Nat. Chem.* **2014**, *6*, 913.

Strutt, N. L.; Fairen-Jimenez, D.; Iehl, J.; Lalonde, M. B.; Snurr, R. Q.; Farha, O. K.; Hupp, J. T.; Stoddart, J. F. *J. Am. Chem. Soc.* **2012**, *134*, 17436-17439.

Chen, T.; Schneemann, A.; Fischer, R. A.; Cohen, S. M. *Dalton Trans.* **2016**, *45*, 3063.

Mikhalyova, E. A.; Kolotilov, S. V.; Zeller, M.; Thompson, L. K.; Addison, A. W.; Pavlishchuk, V. V.; Hunter, A. D. *Dalton Trans.* **2011**, *40*, 10989.

Zhang, X.; Fan, L.; Sun, Z.; Zhang, W.; Fan, W.; Sun, L.; Zhao, X. *Cryst. Eng. Comm.* **2013**, *15*, 4910.

Allen, W. E.; Gale, P. A.; Brown, C. T.; Lynch, V. M.; Sessler, J. L. *J. Am. Chem. Soc.* **1996**, *118*, 12471-12472.

Torrisi, A.; Mellot-Draznieks, C.; Bell, R. G. *J. Chem. Phys.* **2010**, *132*, 044705.

Fernandez, C. A.; Liu, J.; Thallapally, P. K.; Strachan, D. M. *J. Am. Chem. Soc.* **2012**, *134*, 9046.

Chen, Q.; Chang, Z.; Song, W. –C.; Song, H.; Song, H. -B.; Hu, T. -L.; Bu, X. -H. *Angew. Chem., Int. Ed.* **2013**, *52*, 11550.

Fairen-Jimenez, D.; Moggach, S. A.; Wharmby, M. T.; Wright, P. A.; Parsons, S.; Duren, T. *J. Am. Chem. Soc.* **2011**, *133*, 8900.

Nijem, N.; Wu, H.; Canepa, P.; Marti, A.; Balkus, K. J.; Thonhauser, T.; Li, J.; Chabal, Y. J. *J. Am. Chem. Soc.* **2012**, *134*, 15201.

Waggoner, N. W.; Saccoccia, B.; Ibarra, I. A.; Lynch, V. M.; Wood, P. T.; Humphrey, S. M. *Inorg. Chem.* **2014**, *53*, 12674-12676.

Balonov, M.; et al. *Radiological Conditions in the Dnieper River Basin*; Radiological Assessment Reports Series; International Atomic Energy Agency: Vienna, 2006.

Schwochau, K. *Top. Curr. Chem.* **1984**, *124*, 91.

Gorden, A. E. V.; Xu, J.; Raymond, K. N. *Chem. Rev.* **2003**, *103*, 4207-4282.

Pearson, R. G. *J. Am. Chem. Soc.* **1963**, *85*, 3533.

Cram, D. J.; Lehn, J. M. *J. Am. Chem. Soc.* **1985**, *107*, 3657.

Hay, B. P.; Hancock, R. D. *Coord. Chem. Rev.* **2001**, *212*, 61.

Szigethy, G.; Raymond, K. N. *J. Am. Chem. Soc.* **2011**, *133*, 7942-7956.

Watson, L. A.; Hay, B. P. *Inorg. Chem.* **2011**, *50*, 2599-2605.

Beer, S.; Berryman, O. B.; Ajami, D.; Rebek, J. *Chem. Sci.* **2010**, *1*, 43-47.

Sather, A. C.; Berryman, O. B.; Rebek, J. *J. Am. Chem. Soc.* **2010**, *132*, 13572-13574.

Sather, A. C.; Berryman, O. B.; Moore, C. E.; Rebek, J. *Chem. Commun.* **2013**, *49*, 6379-6381.

Cinneide, S. O.; Scanlan, J. P.; Hynes, M. J. *Inorg. Nucl. Chem.* **1975**, *37*, 1013.

Qiu, J.; Burns, P. C. *Chem. Rev.* **2013**, *113*, 1097–1120.

Burns, P. C.; Kubatko, K.-A.; Sigmon, G.; Fryer, B. J.; Gagnon, J. E.; Antonio, M. R.; Soderholm, L. *Angew. Chem., Int. Ed.* **2005**, *44*, 2135–2139.

Qiu, J.; Ling, J.; Jouffret, L.; Thomas, R.; Szymanowski, J. E. S.; Burns, P. C. *Chem. Sci.* **2014**, *5*, 303–310.

Wang, K.; Chen, J. *Acc. Chem. Res.* **2011**, *44*, 531-540.

Pasquale, S.; Sattin, S.; Escudero-Adan, E. C.; Martinez-Belmonte, M.; Mendoza, J. *Nat. Commun.* **2012**, *3*, 785.

Thuery, P.; Harrowfield, J. *Cryst. Growth Des.* **2017**, *17*, 2881-2892.

McGrail, B. T.; Pianowski, L. S.; Burns, P. C. *J. Am. Chem. Soc.* **2014**, *136*, 4749-4800.

Thangavelu, S. G.; Cahill, C. L. *Inorg. Chem.* **2015**, *54*, 4208-4221.